MASS SPECTROMETRY BASED PROTEOMIC BIOMARKER SELECTION AND SAMPLE PREDICTION

by

JUNG HUN OH

Presented to the Faculty of the Graduate School of

The University of Texas at Arlington in Partial Fulfillment

of the Requirements

for the Degree of

DOCTOR OF PHILOSOPHY

THE UNIVERSITY OF TEXAS AT ARLINGTON

August 2008

To my wife Young Bun, my daughter Yuna,
my parents, my sisters and my wife's family

ACKNOWLEDGEMENTS

I would like to express my deepest gratitude to my advisor, Dr. Jean Gao, for her excellent guidance, patience and support to reach my goal. Through my doctoral work, she encouraged me to develop independent thinking and overall abilities in research. She continually stimulated my analytical thinking and greatly assisted me to develop new efficient algorithms.

I want to thank my exceptional doctoral committee, Dr. Nikola Stojanovic, Dr. Pawel Michalak, Dr. Leonidas Fegaras and Dr. Roger Walker, for their continual encouragement and advice. In comprehensive exam and defence, their suggestions and comments helped me improve my research and dissertation.

I wish to extend my warmest thanks to collaborators, Dr. Kevin Rosenblatt and Prem Gurnani, for allowing me to use their data sets and helping me to develop my background in mass spectrometry. Our good collaboration enabled us to publish several papers.

I am grateful to Biocomputing and Vision Lab members and my friends who were always willing to help and give their best suggestions through the good times and bad times.

Finally, I would like to thank my wife Young Bun and daughter Yuna for the constant love, support and encouragement. Especially, Young Bun is a good collaborator with

whom I can discuss about my research. We are very happy to complete our PhD degree together. I am also very grateful to my parents, sisters and my wife's family for their endless supports. This dissertation would not have been possible without their helps.

June 17, 2008

ABSTRACT

MASS SPECTROMETRY BASED PROTEOMIC BIOMARKER SELECTION AND SAMPLE PREDICTION

Jung Hun Oh, Ph.D.

The University of Texas at Arlington, 2008

Supervising Professor: Dr. Jean Gao

High-resolution MALDI-TOF (matrix-assisted laser desorption/ionization time-of-flight) mass spectrometry has recently shown promise as a screening tool for detecting discriminatory peptide/protein patterns. The major computational obstacle in finding such patterns is the large number of mass/charge peaks (features, biomarkers, data points) in a spectrum. To tackle this problem, we have developed methods for data preprocessing and biomarker selection. The preprocessing consists of binning, baseline correction, and normalization. An algorithm, Extended Markov Blanket (EMB), is developed for biomarker detection, which combines redundant feature removal and discriminant feature selection. The biomarker selection couples with support vector machine (SVM) to achieve sample prediction from high-resolution proteomic profiles.

Disease progresses in several stages. Therefore, there exist biomarkers corresponding to each stage. To deal with such a multi-class problem, we propose a classification and a feature selection method. The proposed classification method consists of two schemes: error-correcting output coding (ECOC) and pairwise cou-

pling (PWC). In prediction for a test sample, aggregated results of both schemes are considered. In PWC scheme, important features for each pair of classes are found by using extended Markov blanket (EMB) feature selection.

To identify the molecular formulae of the biomarkers, we develop a *de novo* peptide sequencing method. *De novo* peptide sequencing that determines the amino acid sequence of a peptide via tandem mass spectrometry (MS/MS) has been increasingly used nowadays in proteomics for protein identification. Current *de novo* methods generally employ a graph theory, which usually produces a large number of candidate sequences and causes heavy computational cost while trying to determine a sequence with less ambiguity. We present a novel *de novo* sequencing algorithm that greatly reduces the number of candidate sequences. By utilizing certain properties of b- and y-ion series in MS/MS spectrum, we propose a reliable two-way parallel searching algorithm to filter out the peptide candidates that are further pruned by an intensity evidence based screening criterion.

LDA is a traditional statistical scheme for feature reduction which has been widely used in a diversity of application areas. In a case where the dimensionality exceeds the sample size, however, the classical LDA faces a problem known as singularity. Since the dimensionality of the mass spectrometry data is considerably huge, the singularity problem necessarily happens. Another drawback of the classical LDA is its linear property with which LDA fails for nonlinear problems. To solve the problem, nonlinear based LDA methods have been proposed. However, they suffer from high cost in running. We propose a new fast kernel discriminant analysis (FKDA).

TABLE OF CONTENTS

LIST OF FIGURES

LIST OF TABLES

CHAPTER 1

PROTEOMIC BIOMARKER DETECTION BASED ON EXTENDED MARKOV BLANKET

1.1 Introduction

To study the heterogeneity of diverse protein molecules during disease process, proteomics has been recognized as a major technology to simultaneously screen for multiple biomarkers from patient specimen [1], [2]. Due to the perfusion of blood to each organ and tissue, serum proteomic pattern may reflect the abnormality or pathologic state of various diseases [3]. Patient serum protein profiling has been reported as a promising tool to achieve early disease detection, in which the procedure is simple, inexpensive, and minimally invasive [4], [5].

Among different serum profiling technologies, low resolution surface-enhanced laser desorption/ionization time-of-flight (SELDI-TOF) mass spectrometry has been used to detect protein patterns of normal, premalignant and malignant cells found in breast [2], prostate [6], [7], ovarian [8], and lung cancers [9]. High-mass protein products are identified by the low-resolution SELDI-TOF. However, low-molecular weight (LMW) end of the proteomic spectrum (proteins and peptides below 40,000 Dalton) contains an abundance of potential biomarkers [10], [11] and can not be detected by such technology. Therefore, high-resolution mass spectrometry is desired to detect the LMW molecules for better protein pattern identification.

Toward the goal of LMW biomarker detection, high-resolution MALDI-TOF (matrix-assisted laser desorption/ionization time-of-flight) mass spectrometry is capable of collecting data over a broad mass range (100 to $<$ 300,000 Dalton) in

a single acquisition and has less measurement error (mass shift). This technique results in higher accuracy because of the significantly large number of ion peaks. High-resolution MALDI-TOF mass spectrometry has increasingly been used to early disease diagnosis, monitoring disease progression and therapeutic effects of drugs. To discover and identify unique biomarker patterns hidden in the complex and high-dimensional mass spectra, robust computation algorithms have to be developed.

Numerous pattern recognition algorithms have been developed for low-resolution SELDI-TOF data analysis. Early research efforts used genetic algorithm (GA) and self-organizing map (SOM) to identify proteomic patterns to discriminate ovarian cancer samples from normal [6]. Candidate subsets containing 5 to 20 of 15,200 m/z (mass/charge) values were randomly selected. After examining the ability of subsets to distinguish samples, the m/z values contained in the highest rated sets were reshuffled to form new subset candidates. This process was performed iteratively until the discriminative feature set emerges. GA/k-nearest neighbors (GA/KNN) used in microarray expression analysis was also applied to the identification of ovarian cancer [12]. The top ten most discriminative m/z values below 500 were selected. Since such low m/z values are likely to contain ionized organic acid matrix from surface coatings and are generally discarded as noise, further experiments were conducted to omit such m/z values. Methods based on decision trees were successfully used in several studies such as prostate [7], [13] and ovarian cancer [14]. For the analysis of prostate cancer, the area under the ROC curve (AUC) was used as the early filtering, *i.e.*, peaks with an AUC < 0.62 were excluded from further data analysis. For ovarian cancer analysis, peak clustering was performed using the Biomarker Wizard software (Ciphergen Biosystems). Artificial neural network (ANN) known as a powerful tool for the analysis of complex data containing a high level of background noise was employed for molecular ion identification from SELDI-TOF mass spectrometry data

[15]. It was showed that this technique facilitates rapid identification of validated biomarkers.

For high-resolution mass spectrometry (MS) data, traditional machine learning algorithm may break down with high-dimensional input. Very limited research has been carried out to explore the computational challenges. Among current research endeavors, majority of the work has been focused on classifier design and there is a lot to be investigated on feature dimensionality reduction due to the high dimension nature of MALDI-TOF data. Ressom *et al.* designed a computational method that combines particle swarm optimization with SVM (Support Vector Machine) to distinguish liver cancer patients from healthy individuals in SELDI-QqTOF spectra [16]. Particle swarm optimization and ant colony optimization are interesting swarm intelligence techniques which have been successfully applied to a number of optimization problems. A comparative study of several well-known classification algorithms, such as linear discriminant analysis (LDA), k-nearest neighbor (KNN), random forest (RF), bagging, boosting, and support vector machine (SVM), has been carried out for ovarian cancer diagnosis [17]. MALDI-TOF mass spectrometry was used to obtain the dataset. It was demonstrated that RF approach leads to an overall higher accuracy rate as well as a more stable assessment for classification errors.

In this paper, we use high-resolution MALDI-TOF mass spectrometry for biomarker profiling to predict recurrent ovarian cancer. Ovarian cancer is commonly diagnosed at stage III or IV with a low five-year survival rate [18]. Primary therapy of ovarian cancer includes surgical cytoreduction followed by chemotherapy with a platinum agent. Three-quarters of the patients will eventually suffer a relapse within a few months or several years later [19]. If cancer does not recur and disease remits for six months or more since completion of primary chemotherapy, the cancer is considered "platinum-sensitive." On the other hand, if cancer relapses

within less than six months of completing the primary therapy, the cancer is considered "platinum-resistant" and is diagnosed as "early relapse" [20]. Patients with platinum-sensitive disease are usually treated again with the primary chemotherapy used before, while patients with recurrent platinum-resistance cancer are usually not responsive to standard therapy. Therefore many new secondary-chemotherapy drugs have been developed in recent years for re-treatment of these cases. Unfortunately, recurrent ovarian cancer is relatively difficult to be diagnosed. And there is currently no reliable technique for predicting early relapse in ovarian cancer. Hence, new methods such as MALDI-TOF are urgently needed to help physicians and gynecological oncologists to predict the early relapse and to give targeted therapy to patients at high risk of recurrent ovarian cancer.

One computational challenging in analyzing MALDI-TOF data is the high-dimension of ion peaks (a.k.a. features). To handle the large number of peaks in high-resolution MALDI-TOF data [21], we have developed a multi-step feature selection algorithm. Our framework starts with a preprocessing step composed of binning, baseline correction, and normalization. Then a new feature subset selection algorithm, *Extended Markov Blanket Filtering*, is presented. Markov blanket is an information-theory-based method for feature subset selection. It eliminates features having little or no information beyond what is subsumed by the remaining features [22], [23]. Instead of exhaustive search, heuristic Markov blanket is efficient and theoretically optimal. Our method finds two feature subsets relevant to each feature: low and high correlated feature subsets. The high correlated feature subset is used in Markov blanket and contributes to the removal of redundant features. On the other hand, the low correlated feature subset is utilized to assign a feature a weight to represent the extent that the feature contributes sample classification. The per-

formance of our method is demonstrated by comparison with other common-used feature selection methods.

1.2 Materials

1.2.1 Serum Samples

Human sera were collected from 113 patients undergoing gynecologic oncology surgery at the University of Texas Southwestern Medical Center from year 2000 to present using an institutional review board (IRB) approved protocol. Every serum was aliquoted and frozen at -80°C.

1.2.2 Sample Preparation on Chips

Serum samples were processed by using ProXPRESSION™ Biomarker Enrichment Kits (Perkin Elmer). Briefly, this system uses a Cibachron blue (CB) dye affinity-chromatography-based technology that is designed to capture high-abundance carrier proteins (such as albumin) in blood and then enrich for the peptide and protein fragments bound to the carrier proteins. CB filtration plates were purchased from PerkinElmer. ZipPlates™ and the vacuum manifold were purchased from Millipore. Millipore also provided custom-fitting adapters for direct spotting of samples on single-use MALDIchip™ Target plates (PerkinElmer). Serum samples were processed with CB filtration plates. CB filtration plates were washed 3 times with 400 μL of Sample Binding Buffer (SBB). A 15-μL portion of each serum sample was diluted with 150 μL of SBB. Each diluted sample was then loaded on a column and 7.5 mmHg of vacuum was applied. The column was washed with 400 μL of SBB, and the biomarkers were eluted with 200 μL of Sample Elution Buffer (Perkin Elmer) using the vacuum manifold. The elution step was repeated once more, and the two-elution volumes were co-eluted in the same 96 well-format, 1 ml capacity plate.

Eluted biomarkers were concentrated and desalted on ZipPlate and applied directly to MALDIchip targets by vacuum elution. The entire elution volume from each CB well was loaded into 1 well of a ZipPlate, and the sample bound by applying vacuum (12.5 mmHg). The biomarkers were eluted directly by vacuum onto disposable MALDIchip targets. The ZipPlates were lifted from the MALDIchip Target plate, leaving small droplets on the plate, indicating successful sample transfer. Samples are allowed to air dry at room temperature, which leads to the formation of matrix crystals. Mass spectra were acquired using a prOTOF$^{\mathbf{TM}}$ 2000 matrix-assisted laser desorption/ionization orthogonal time-of-flight (MALDI O-TOF) MS interfaced with TOFWorks$^{\mathbf{TM}}$ software (PerkinElmer/SCIEX). Because of the orthogonal design, a single external mass calibrant was used to achieve better than 10-ppm mass accuracy over an entire sample plate (up to 96 samples). In this study, a 2-point external calibration of the prOTOF instrument was performed before acquiring the spectra in a batch mode from 96 samples.

1.3 Background

1.3.1 Markov Blanket (MB) Feature Selection

Markov blanket filtering is an instance of backward feature elimination algorithm [22], [23]. Let $\mathbf{F}$ be a set of features with size r defined as $\mathbf{F} = (F_1, \cdots, F_r)$ and $\mathbf{M} \subseteq \mathbf{F}$ be a set of features which does not contain F_i. Feature set $\mathbf{M}$ is called Markov blanket for F_i if F_i is conditionally independent of $\mathbf{F} - \mathbf{M} - \{F_i\}$ given $\mathbf{M}$. Therefore, the information contained in feature F_i can be covered by its Markov blanket. However, since the full size Markov blanket may not be available, an approximate one that subsumes the feature information has to be sought. One Markov blanket $\mathbf{M}_i$ for F_i can be defined as the one having m highest Pearson correlations

with F_i. In general, to reduce computational overhead and to avoid fragmenting the training samples, small value m is used.

To evaluate the closeness between F_i and its Markov blanket $\mathbf{M}_i$, the following expected cross-entropy is estimated:

$$\triangle(F_i|\mathbf{M}_i) = \sum_{\mathbf{f}_{\mathbf{M}_i}, f_i} P(\mathbf{M}_i = \mathbf{f}_{\mathbf{M}_i}, F_i = f_i) \times D(P(c|\mathbf{M}_i = \mathbf{f}_{\mathbf{M}_i}, F_i = f_i)||P(c|\mathbf{M}_i = \mathbf{f}_{\mathbf{M}_i})), \quad (1.1)$$

where $\mathbf{f}_{\mathbf{M}i}$ and f_i are feature values to $\mathbf{M}_i$ and F_i, respectively, c is class label, and $D(.||.)$ represents cross-entropy. For any distributions μ and σ, the cross-entropy of μ to σ is $D(\mu||\sigma) = \sum_{x\in\Omega} \mu(x)\mathbf{log}\frac{\mu(x)}{\sigma(x)}$ that measures the extent of the difference which is made by using σ instead of μ. In Eq. (1.1), $\triangle(F_i|\mathbf{M}_i) = 0$ means that $\mathbf{M}_i$ is a perfect Markov blanket for F_i, therefore F_i does not provide any information about class labels beyond that subsumed by its Markov blanket $\mathbf{M}_i$. However, since this case is less likely to happen, we look for a set $\mathbf{M}_i$ such that $\triangle(F_i|\mathbf{M}_i)$ is small. The lower $\triangle(F_i|\mathbf{M}_i)$ means that the approximate Markov blanket of F_i is strongly correlated to F_i. The feature F_i with the lowest $\triangle(F_i|\mathbf{M}_i)$ value in the remaining features is considered to be the most redundant, and should be eliminated first.

To decide the Markov blanket of each feature, intensity values after the preprocessing task are used in the calculation of Pearson correlation coefficient. (Details for the preprocessing will be provided in Section 1.4.) For computational convenience, the discretized binary values are used in the calculation of the expected cross-entropy $\triangle(F_i|\mathbf{M}_i)$ [24]. In discretization of feature A value, suppose that there is a given set S of all samples and a partition boundary T by which S is partitioned into two subsets S_1 and S_2. Let $P(c_i, S_j)$ be the proportions of samples in subset S_j that belong to class c_i. Then the class information entropy of the partition is defined by:

$$E(A, T, S) = \frac{|S_1|}{|S|}Ent(S_1) + \frac{|S_2|}{|S|}Ent(S_2), \quad (1.2)$$

where $Ent(S_j) = -\sum_{i=1}^{k} P(c_i, S_j)\mathbf{log}(P(c_i, S_j))$ is the class entropy for subset S_j, k is the number of classes and $|\cdot|$ represents the number of samples in the subset. The cut point T_A for which $E(A, T, S)$ is minimal among all the candidate cut points is selected for a binary discretization for feature A [25]. Finally, the expected cross-entropy $\triangle(F_i|\mathbf{M}_i)$ can be calculated as:

$$\triangle(F_i|\mathbf{M}_i) \;=\; \sum_{j=1}^{n} P_j(\mathbf{M}_i, F_i) \times \sum_{l=1}^{k} P_j(c_l|\mathbf{M}_i, F_i)\mathbf{log}\Big(\frac{P_j(c_l|\mathbf{M}_i, F_i)}{P_j(c_l|\mathbf{M}_i)}\Big), \quad (1.3)$$

where n is the number of samples [26].

1.3.2 Support Vector Machines (SVMs)

SVMs are kernel based learning algorithms to solve two-class classification problems [27]. An optimal hyperplane is sought to separate a given set of binary labeled training data by maximizing the margin between the two classes. To do so, SVMs map the training data $\mathbf{x}$ into a higher dimensional space via a mapping function $\Phi(\mathbf{x})$ and construct a decision function as:

$$f(\mathbf{x}) = \langle \mathbf{w}, \Phi(\mathbf{x}) \rangle + b, \quad (1.4)$$

where $\mathbf{w}$ is a weight vector and b is a scalar.

Suppose there are n training samples $\{(\mathbf{x}_i, y_i), 1 \leq i \leq n\}$ where $\mathbf{x}_i$ is the i^{th} training sample consisting of an r-dimensional feature vector and $y_i \in \{$-1, 1$\}$ is the class label of $\mathbf{x}_i$. The problem of finding the optimal hyperplane can be formulated as the following quadratic programming problem

$$\min_{\alpha_i} \frac{1}{2} \sum_{i=1}^{n} \sum_{j=1}^{n} \alpha_i \alpha_j y_i y_j K(\mathbf{x}_i, \mathbf{x}_j) - \sum_{i=1}^{n} \alpha_i, \quad (1.5)$$

subject to

$$0 \leq \alpha_i \leq C, \qquad \sum_{i=1}^{n} \alpha_i y_i = 0, \tag{1.6}$$

where $K(\mathbf{x}_i, \mathbf{x}_j)$ is a kernel function, α is a Lagrange multiplier and C is a user defined soft-margin constant. In linear SVM, we compute the weight vector as:

$$\mathbf{w} = \sum_{i=1}^{n} \alpha_i^* y_i \mathbf{x}_i, \tag{1.7}$$

where α_i^* is solution to Eq. (1.5).

1.3.3 SVM-Recursive Feature Elimination (SVM-RFE)

SVM-RFE proposed by Guyon *et al.* is a backward feature elimination algorithm based on SVM [28]. At each iteration, weights for all existing features are obtained by using Eq. (1.7) and a feature corresponding to a smallest absolute weight is eliminated. This procedure continues until only one feature remains so that in the end all features are ranked.

1.4 Preprocessing

All samples used in this study were analyzed by MALDI-TOF mass spectrometry which is as accurate as 10-ppm (parts per million) mass accuracy with a single external mass calibrant. We extracted m/z values in the range between 1k and 10k Da (Dalton) from each spectrum of 726,343 m/z peaks. Since such a huge dimensionality causes considerable cost burden in feature selection and classification problem, most literatures using MALDI-TOF data perform a preprocessing work with the raw spectra data. We have designed a series of preprocessing steps to reduce input signal dimensionality and to remove noise of the raw spectra.

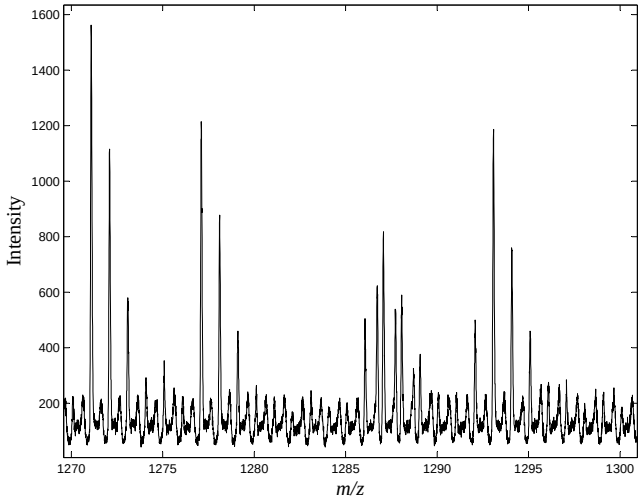

(a)

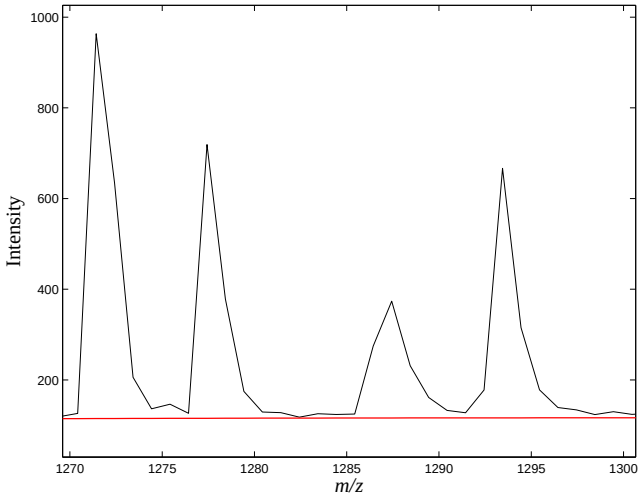

(b)

Figure 1.1. An example that shows a spectrum after binning. A few peaks that seem to be monoisotope and its isotopes are converted into a new peak in the same m/z range. Red line indicates the baseline. (a) raw spectrum; (b) binned spectrum.

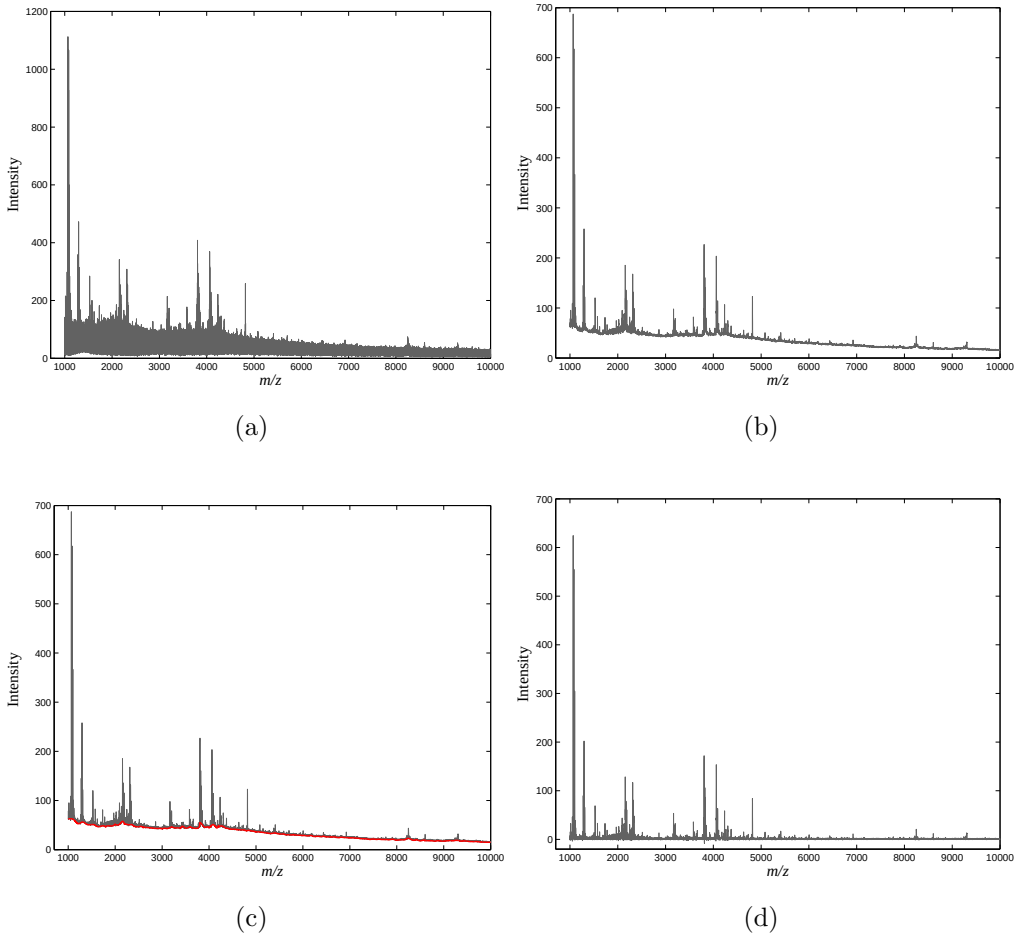

Figure 1.2. MALDI-TOF mass spectrum in the range between 1k and 10 kDa: (a) raw spectrum. (b) binned spectrum. (c) regressed baseline (red line). (d) spectrum after baseline correction.

1.4.1 Binning

In the first step of data preprocessing, binning is performed to divide the m/z axis into intervals of desired length. Prior to the task, we need to decide a starting m/z where the dividing begins. Moving from the lowest m/z of the spectrum to the right along the m/z axis, a point at which intensity changes from decreasing to increasing becomes the starting m/z. Let the starting point be SP. From the SP, we proceed to the right with a step of 100 Da and search for the minimum

intensity within a given small m/z clearance from $SP + 100$ m/z. Let the position of the minimum intensity be EP and the range between SP and EP be a window. Then, the window is divided by 100 yielding 100 bins so that the size of each bin is approximately 1 Da and the window consists of 100 bins. In each bin, peaks whose intensities are less than 10% of the maximum intensity of the bin, which tend to be noise, are removed. A mean value of all the remaining intensities in each bin is placed at the middle position of the bin indicating the representative intensity. In the similar way, we continue to proceed to the direction of increasing m/z values to find the next window starting from the EP of the first window, which becomes the new SP of the second window. This procedure is repeated until the end of the spectrum. The preprocessing step is individually performed for each spectrum. Without loss of generality, the first spectrum after preprocessing serves as the reference, by which all the bin and window positions of other spectra will be aligned with. Fig. 1.1 demonstrates a zoomed-in local segment of the spectrum before and after binning.

1.4.2 Baseline Correction

Baseline in mass spectrometry data is caused by the chemical noise in the matrix. For baseline correction, a window is divided into 10 groups with each group consisting of 10 bins. A minimum intensity and its m/z ratio are found in each group. Therefore, there exist 10 pairs of intensity and m/z ratio in each window. We estimate the baseline by fitting a fourth order polynomial to the 10 pairs of intensity and m/z ratio. The baseline correction is performed for each window. Finally, the overall regressed baseline is subtracted from the binned spectrum.

1.4.3 Normalization

Furthermore, we choose to normalize the baseline corrected spectrum because the amount of proteins in blood sample changes from patient to patient and even to the same patient with samples drawn at different times. Each baseline corrected m/z value is normalized by the total ion current of the spectrum. The total ion current is the summed intensity over all m/z values. Due to the very small normalized intensity value, all the intensities are multiplied by 10,000 for computational convenience. The consecutive steps of the preprocessing are shown in Fig. 1.2. It can be seen that the significant peaks are retained with smoothed and de-noised effects.

1.5 Methodology

1.5.1 Extended Markov Blanket

In this section, we will present a new feature selection algorithm called *extended Markov blanket*. Our algorithm considers reducing redundant features while selecting the most discriminant ones. To be more specific, for a feature F_i remained after preprocessing, two feature subsets are considered: the high correlated feature subset (HCFS) and the low correlated feature subset (LCFS) composed of the least correlated d features for F_i. HCFS feature subset is used to remove redundant features as in the classical Markov blanket feature selection. Our contribution comes from utilizing LCFS to estimate the classification capability of each feature during the Markov blanket process. This is derived from the fact that mutually low correlated features, in general, lead to good classification performance.

We will now describe how the extended Markov blanket algorithm works out for feature selection. We choose 10-fold cross validation for performance evaluation where all samples are randomly split into 10 exclusive folds. For each of the ten

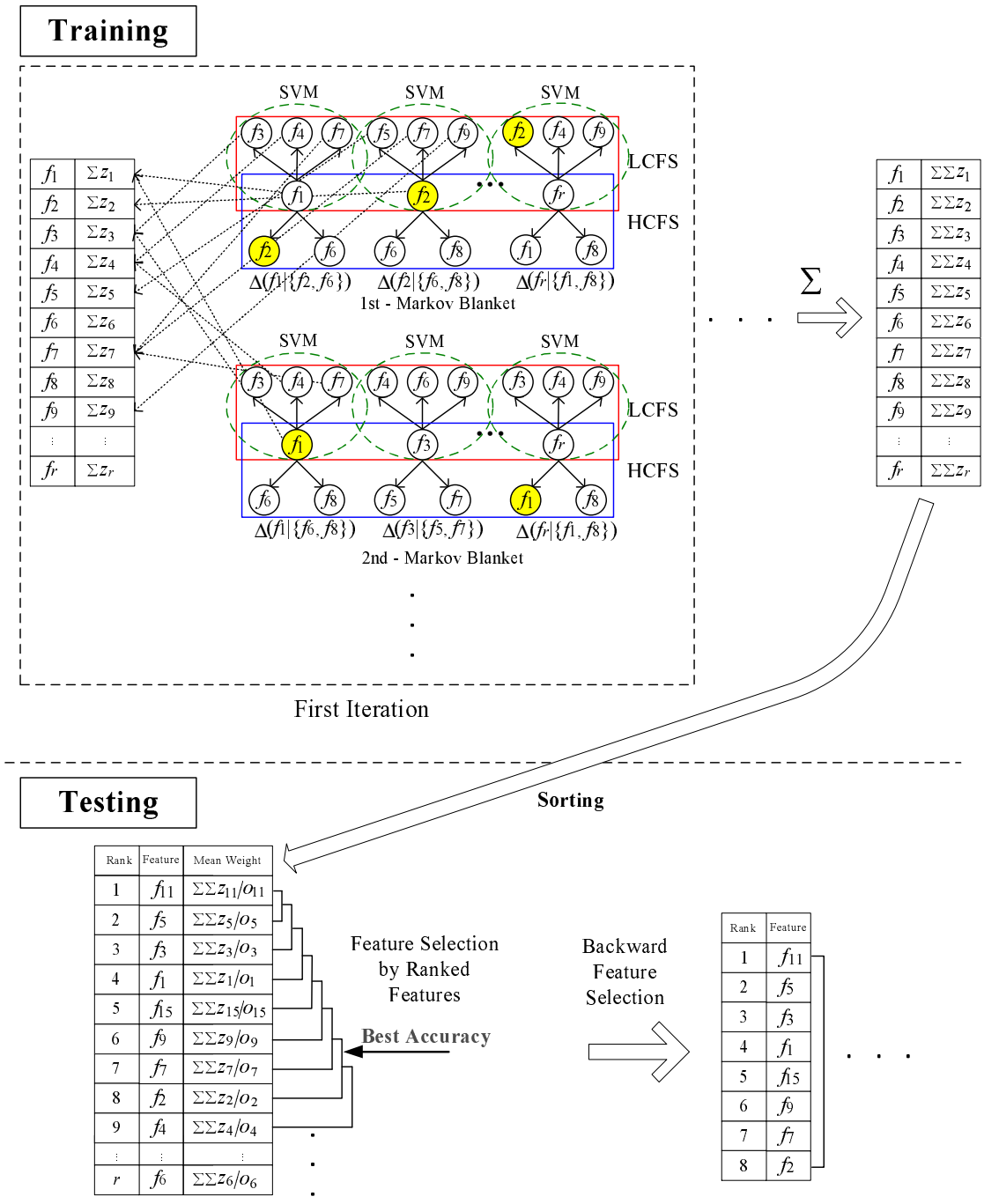

Figure 1.3. Diagram for Extended Markov Blanket algorithm. In the first Markov blanket run of the first iteration, the expected cross-entropy $\triangle(f_2|\{f_6, f_8\})$ for feature f_2 is the smallest value. Therefore, f_2 is removed from both LCFS and HCFS for all features. LCFS and HCFS of survival features are then rebuilt.

experiments, typically a single fold is retained as a validation data, and the remaining nine folds are used as train data. In our implementation, we divide the train data into sub-train and sub-test data in the ratio of 80%:20%. For each feature F_i, we perform Markov blanket algorithm with its HCFS obtained from the train data to compute the expected cross-entropy value, $\triangle(F_i|\mathbf{M}_i)$. On the other hand, using LCFS and feature F_i, we run the linear SVM algorithm where the sub-train and sub-test data are used for training and testing, respectively, to obtain an roughly estimated accuracy, denoted as β. Then, we compute the normalized weight for each feature in the LCFS using the following function:

$$z_k = \begin{cases} \frac{|w_k|}{\sum_{j=1}^{d+1} |w_j|} \times \beta \times \delta & \text{if } 0.5 < \beta, \\ \left(1 - \frac{|w_k|}{\sum_{j=1}^{d+1} |w_j|}\right) \times (0.5 - \beta) \times \delta & \text{otherwise} \end{cases} \tag{1.8}$$

where

$$\delta = \begin{cases} 1 & \text{if } 0.5 < \beta, \\ -1 & \text{otherwise} \end{cases}$$

and β is the accuracy from sub-test samples in the linear SVM, k is the index for features in LCFS including feature F_i, $|w_k|$ is the absolute SVM weight obtained using Eq. (1.7), and d is the size of LCFS chosen as 10, 20, or 30. After computing $|w_k|$ for all features in the LCFS, each $|w_k|$ is normalized by the summed absolute SVM weights of all the features in the LCFS and the weight of feature F_i.

In SVM-RFE (SVM-Recursive Feature Elimination) method by Guyon *et al.*, features with the smallest absolute SVM weights are eliminated at each iteration for feature selection [28]. Adversely, we assume that features with large absolute SVM weights are important in terms of classification power. Not surprisingly to observe, although the normalized SVM weight of certain feature in Eq. (1.8) may be high in an

LCFS, the classification accuracy of the linear SVM performed with the limited LCFS may be low due to the partial discriminant capacity of one LCFS. Therefore, not only the normalized SVM weight for each feature but also the accuracy with its LCFS are important factors to estimate feature weight. This leads to the multiplication of the normalized SVM weight by the accuracy obtained after the SVM. If the accuracy is greater than 50%, the proposed weight becomes positive by multiplying 1 as a value of δ. Otherwise, we treat it as a penalty using -1 as the δ.

After computing the proposed weights and expected cross-entropy $\triangle(F_i|\mathbf{M}_i)$ values for all features as introduced above, certain feature with the smallest $\triangle(F_i|\mathbf{M}_i)$ value is removed according to Markov blanket rule. Then, the HCFS and LCFS for all but the removed feature are rebuilt. As an example shown in Fig. 1.3, feature F_2 with value as f_2 was the one with the smallest cross-entropy and was removed first. Consequently feature f_1 that had f_2 and f_6 as members of HCFS now is updated as features f_6 and f_8. In fact, only those subsets that contain the removed feature will be affected and modified. Again, we compute the $\triangle(F_i|\mathbf{M}_i)$ values and the proposed weights for survival features. The feature weights will be accumulated during the Markov blanket feature removal process. The whole procedure keeps going on until the predefined feature number is reached.

1.5.2 Feature Pruning by Backward Feature Selection

The aforementioned feature removal was repeated 100 times for 10-fold cross validations. We compute a mean weight value for each feature after the 100 iterations by dividing each feature's accumulated weight by the occurrence counting O_i of feature F_i in all LCFS (Fig. 1.3). All the features are then ranked according to the mean weights. Then, we perform linear SVM using the first top ranked feature then the top two and so forth up to the top 60 features. From a feature subset with the

best accuracy, we start the standard backward feature elimination algorithm to find a compact feature subset. The backward feature selection approach removes one feature at a time from the current feature set. Each time a feature without which the accuracy is improved will be excluded. The backward feature selection method continues until one feature remains. The overall steps of Extended Markov Blanket can be seen from Fig. 1.3.

1.6 Experimental Results

We implemented the preprocessing part using Matlab and the proposed algorithm using JAVA based on LIBSVM [29]. Serum samples were collected from 113 ovarian cancer patients who had undergone a surgical operation: 48 for platinum-resistant and 65 for platinum-sensitive.

1.6.1 Preprocessing Results

After the binning preprocessing for the high-resolution MALDI-TOF serum profiles, the number of features, *i.e.*, mass-to-charge ratio peaks, was reduced from 726,343 to 8,900. Despite the considerable reduction of dimensionality, the size of 8,900 features still makes considerable computation burden for afterward feature selection and classification problem. In order to further filter the high-dimensional number of features, we adopted a two-sample t-test to assess the degree of separation between two classes for single features. With the significance level of 5% at each of the m/z values in all spectra after preprocessing, the number of features was reduced to 1,338. Then, Extend Markov Blanket was applied to the reduced 1,338 features.

Table 1.1. Top ranked 60 features. Weight indicates normalized feature weight. Accuracy, sensitivity and specificity show the performance when different number of top ranked features are used.

No	*M/Z*	Weight	Accuracy	Sensitivity	Specificity	No	*M/Z*	Weight	Accuracy	Sensitivity	Specificity
1	1994.8493	100.00	0.6480	0.1625	0.9717	31	3089.4179	39.18	0.6910	0.6087	0.7458
2	1992.8479	95.36	0.6475	0.1650	0.9692	32	1206.4049	39.18	0.6960	0.6375	0.7350
3	1575.5422	90.21	0.6910	0.3100	0.9450	33	5001.5661	38.66	0.7220	0.6675	0.7583
4	1690.6383	89.69	0.7205	0.4212	0.9200	34	1440.4985	32.47	0.7320	0.6838	0.7642
5	1577.5430	85.05	0.7145	0.4212	0.9100	35	3231.4611	29.90	0.7385	0.6813	0.7767
6	2573.1582	79.90	0.7285	0.5500	0.8475	36	1576.5426	29.38	0.7350	0.6800	0.7717
7	2106.8983	76.29	0.7245	0.5388	0.8483	37	2297.0062	28.87	0.7230	0.6638	0.7625
8	1777.7205	71.65	0.7035	0.5075	0.8342	38	2842.2901	28.35	0.7200	0.6600	0.7600
9	1554.5333	67.53	0.7025	0.5163	0.8267	39	3232.4618	27.32	0.7170	0.6612	0.7542
10	1553.5329	66.49	0.6880	0.5013	0.8125	40	2298.0063	25.26	0.7080	0.6463	0.7492
11	2252.0007	65.46	0.6875	0.5113	0.8050	41	2871.2989	23.71	0.7230	0.6675	0.7600
12	2196.9908	64.43	0.6880	0.5325	0.7917	42	8282.1306	23.20	0.7205	0.6738	0.7517
13	1616.5681	63.40	0.6785	0.5250	0.7808	43	4224.0366	21.65	0.7180	0.6688	0.7508
14	1463.5031	60.31	0.6745	0.5225	0.7758	44	5085.5824	14.43	0.7200	0.6712	0.7525
15	2572.1574	59.79	0.6765	0.5237	0.7783	45	4165.0030	11.86	0.7140	0.6613	0.7492
16	1008.3059	59.28	0.6720	0.5413	0.7592	46	1742.6875	11.86	0.7155	0.6500	0.7592
17	2050.8725	58.25	0.6630	0.5100	0.7650	47	8283.1316	10.31	0.7135	0.6575	0.7508
18	1131.3802	56.70	0.6675	0.5238	0.7633	48	1740.6856	9.28	0.7535	0.7025	0.7875
19	2322.0129	55.15	0.6700	0.5363	0.7592	49	2149.9425	8.25	0.7560	0.6950	0.7967
20	1793.7357	48.97	0.6615	0.5338	0.7467	50	4772.4132	7.73	0.7535	0.6913	0.7950
21	1688.6364	47.42	0.6810	0.5275	0.7833	51	3597.6778	5.67	0.7420	0.6725	0.7883
22	2147.9404	45.88	0.6690	0.5100	0.7750	52	1913.7935	4.64	0.7350	0.6688	0.7792
23	4084.9432	45.88	0.6530	0.5113	0.7475	53	1009.3066	4.12	0.7515	0.6963	0.7883
24	2148.9415	45.36	0.6440	0.5138	0.7308	54	4152.9948	3.61	0.7635	0.6975	0.8075
25	1915.7949	43.81	0.6390	0.5125	0.7233	55	1914.7942	3.09	0.7620	0.7000	0.8033
26	8284.1325	43.81	0.6395	0.5225	0.7175	56	1057.3399	3.09	0.8085	0.7925	0.8192
27	2275.0035	43.30	0.6345	0.5250	0.7075	57	8878.4549	2.06	0.8125	0.7938	0.8250
28	2962.3593	42.78	0.6600	0.5600	0.7267	58	1741.6865	2.06	0.8195	0.8013	0.8317
29	3147.4299	41.75	0.6725	0.5950	0.7242	59	2755.2383	1.03	0.8195	0.8000	0.8325
30	2195.9898	41.75	0.6695	0.5862	0.7250	60	2076.8826	1.03	0.8175	0.7825	0.8408

1.6.2 Biomarker Selection and Classification Validation

The size of LCFS used in extended Markov blanket is 10. Using 20 and 30 features yielded similar results. For Markov blanket, size of 2 was used. Table. 1.1 lists the top ranked 60 features, their relative weights, and the corresponding m/z values. Classification performance using different number of top ranked features is also listed. In this study, accuracy refers to the total number of correctly classified platinum-sensitive and platinum-resistant samples. Sensitivity is defined as the percentage of platinum-resistant samples that are correctly classified, while specificity refers to the percentage of platinum-sensitive samples that are correctly classified.

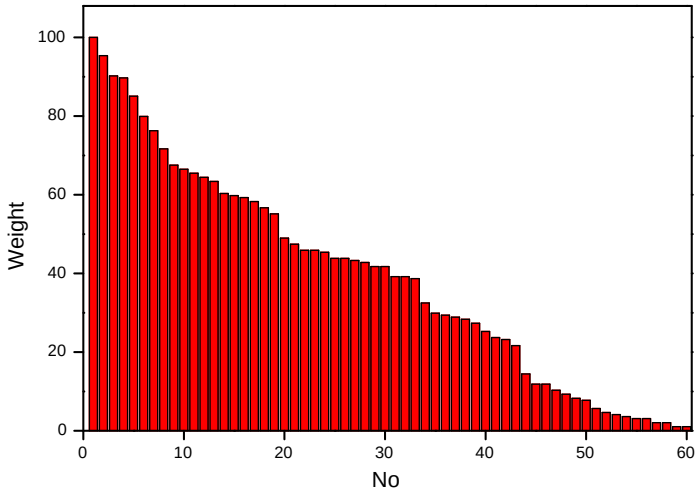

Figure 1.4. Relative weights of the top 60 ranked biomarkers.

We can see the best performance is obtained when the top 58 ranked features were used with 81.95% accuracy, 80.13% sensitivity and 83.17% specificity. Fig. 1.4 shows the visual graph of different feature weights.

To further improve the sample prediction performance and obtain a compact biomarker set, the backward feature elimination algorithm was performed. The algorithm starts with the current selected 58 features and removes one at a time without which the best accuracy using the remaining features is obtained. In Table 1.2, the bottom row shows the performance when the first feature, which happens to be feature with m/z of 1575.5422 and rank of 3, was removed. From the table we can see, the next removed feature is the one ranked 17. The order of removed features and relevant performances are displayed from bottom to top in Table 1.2. From the table row, we can see Extended Markov blanket obtained overall best performance of 96.75% accuracy, 96.63% sensitivity and 96.83% specificity with 20 features.

The sample classification can be visualized in Fig. 1.5 when different number of features was used in the backward feature pruning process. As shown in Fig. 1.5, with four features, extended Markov blanket achieved 78.7% accuracy, 79.37% sensitivity

Table 1.2. Feature removal by backward feature selection. The order of removed features is shown from bottom up.

No	*M/Z*	Accuracy	Sensitivity	Specificity
16	1008.3059	0.5830	0.0625	0.9300
35	3231.4611	0.7080	0.6025	0.7783
41	2871.2989	0.7310	0.7113	0.7442
23	4084.9432	0.7870	0.7938	0.7825
55	1914.7942	0.8320	0.8388	0.8275
48	1740.6856	0.8530	0.8713	0.8408
19	2322.0129	0.8535	0.8363	0.8650
14	1463.5031	0.8700	0.8150	0.9067
1	1994.8493	0.8720	0.8188	0.9075
53	1009.3066	0.8880	0.8500	0.9133
57	8878.4549	0.9065	0.8725	0.9292
33	5001.5661	0.9100	0.9025	0.9150
49	2149.9425	0.8990	0.8825	0.9100
37	2297.0062	0.9180	0.9163	0.9192
34	1440.4985	0.9480	0.9438	0.9508
15	2572.1574	0.9560	0.9663	0.9492
30	2195.9898	0.9555	0.9625	0.9508
36	1576.5426	0.9580	0.9588	0.9575
39	3232.4618	0.9660	0.9688	0.9642
51	3597.6778	0.9675	0.9663	0.9683
29	3147.4299	0.9635	0.9763	0.9550
25	1915.7949	0.9570	0.9675	0.9500
52	1913.7935	0.9505	0.9575	0.9458
2	1992.8479	0.9430	0.9538	0.9358
44	5085.5824	0.9530	0.9563	0.9508
7	2106.8983	0.9500	0.9613	0.9425
32	1206.4049	0.9460	0.9350	0.9533
42	8282.1306	0.9525	0.9550	0.9508
4	1690.6383	0.9580	0.9575	0.9583
8	1777.7205	0.9530	0.9538	0.9525
38	2842.2901	0.9660	0.9713	0.9625
24	2148.9415	0.9555	0.9525	0.9575
26	8284.1325	0.9565	0.9563	0.9567
18	1131.3802	0.9610	0.9788	0.9492
58	1741.6865	0.9625	0.9663	0.9600
46	1742.6875	0.9625	0.9550	0.9675
56	1057.3399	0.9550	0.9575	0.9533
28	2962.3593	0.9620	0.9575	0.9650
50	4772.4132	0.9510	0.9600	0.9450
12	2196.9908	0.9465	0.9500	0.9442
43	4224.0366	0.9575	0.9688	0.9500
22	2147.9404	0.9470	0.9625	0.9367
10	1553.5329	0.9400	0.9500	0.9333
47	8283.1316	0.9410	0.9425	0.9400
20	1793.7357	0.9415	0.9488	0.9367
27	2275.0035	0.9230	0.9200	0.9250
40	2298.0063	0.9275	0.9200	0.9325
6	2573.1582	0.9090	0.9013	0.9142
11	2252.0007	0.9190	0.9088	0.9258
54	4152.9948	0.9085	0.9125	0.9058
9	1554.5333	0.8995	0.8963	0.9017
13	1616.5681	0.8985	0.8950	0.9008
45	4165.0030	0.8780	0.8775	0.8783
21	1688.6364	0.8730	0.8713	0.8742
5	1577.5430	0.8585	0.8513	0.8633
31	3089.4179	0.8510	0.8375	0.8600
17	2050.8725	0.8435	0.8263	0.8550

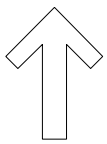

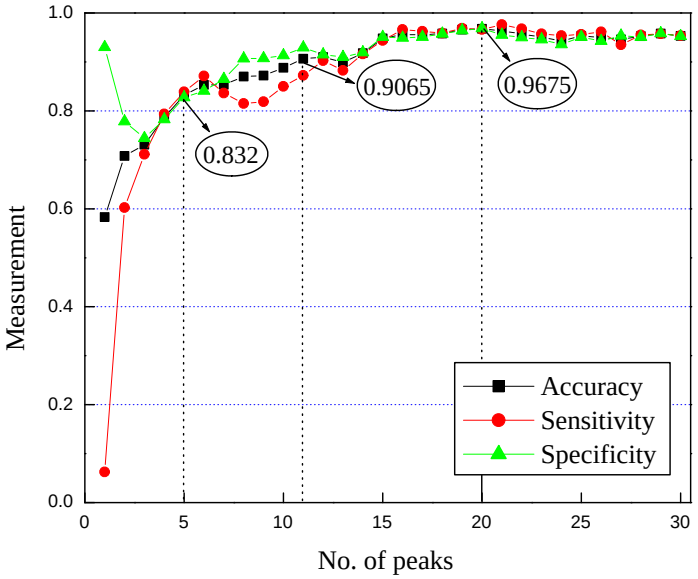

Figure 1.5. Performance measurements of Extended Markov blanket algorithm. The x-axis represents the number of peaks (features) used. 83.2% and 90.65% accuracies were obtained with 5 and 11 features, respectively. With 20 features, the best accuracy of 96.75% was achieved.

and 78.25% specificity. This result, though not the best one out of our method, is better in accuracy measurement than other feature selection algorithms which is to be presented in the next subsection. Another example of performance measurement is 90.65% accuracy, 87.25% sensitivity and 92.92% specificity with 11 features.

To see how different the intensity of m/z ratios between platinum-resistant and platinum-sensitive samples is, we plotted the average intensity graphs and box plots of the two-class samples for each of the 20 features that were used to obtain the best accuracy in the extended Markov blanket. As can be seen in Fig. 1.6, there is a significant difference between platinum-resistant and platinum-sensitive samples for these selected possible protein/peptide markers.

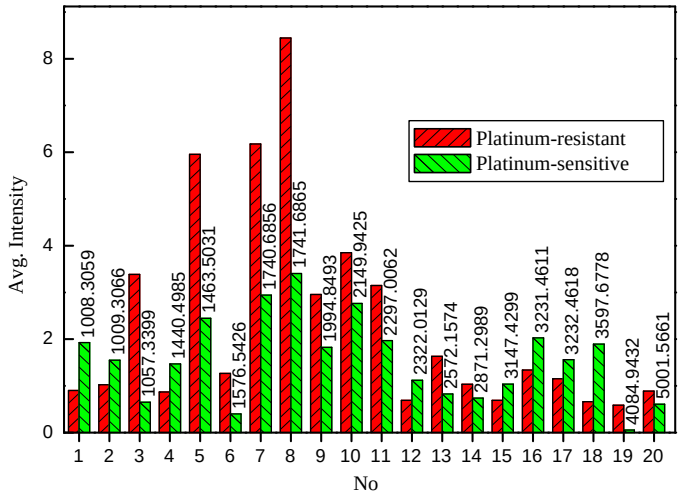

(a)

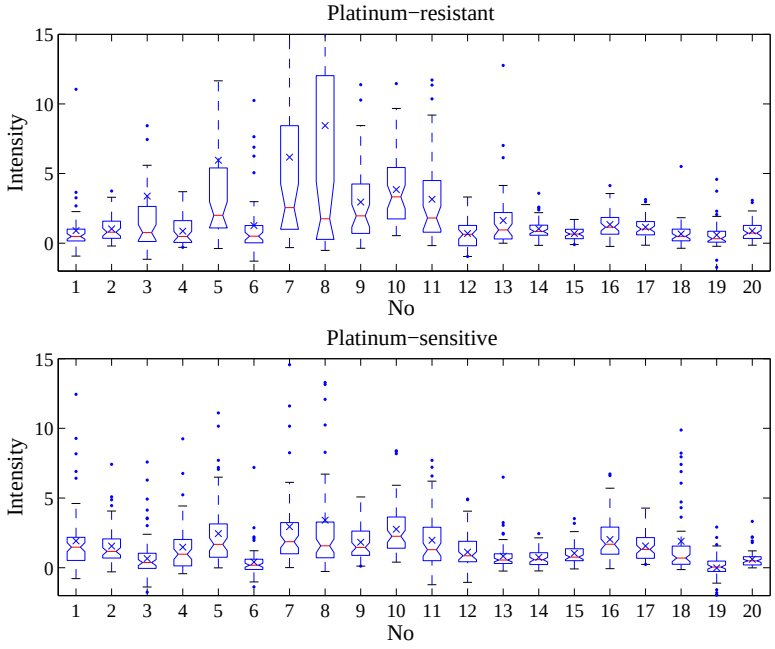

(b)

Figure 1.6. Average intensity of platinum-resistant and platinum-sensitive samples. (a) comparison of average intensity of platinum-resistant and platinum-sensitive samples in each of 20 features which were used to obtain the best accuracy in extended Markov blanket algorithm. The values over bars represent m/z. (b) box plot of the 20 features in platinum-resistant and platinum-sensitive cases.

Table 1.3. Performance comparison with other feature selection algorithms such as information gain, relief-F and χ^2-statistic. All algorithms used SVM as a classifier with 10-fold cross validation. MB = Markov blanket

	Extended MB	Information Gain	Relief-F	χ^2-Statistic
Accuracy(%)	96.75	77.10	72.10	75.25
Sensitivity(%)	96.63	51.87	59.00	71.50
Specificity(%)	96.83	93.92	80.83	77.75
No. of peaks	20	21	5	18

1.6.3 Comparison with Other Algorithms

To validate the performance of our algorithm, we carried out comparison experiments with other algorithms: information gain, relief-F and χ^2 feature selection methods. Table 1.3 presented the best results from individual algorithms. These algorithms were implemented based on codes provided by WEKA package [30]. After running the feature selection algorithms, features were ranked according to the scores from each algorithm. Then, we performed the linear SVM using the 10-fold cross validation from the top one to the top 60 ranked features. Next, backward feature elimination algorithm was used to find the final compact feature list as introduced in Section 1.5.2. As can be seen in Table 1.3, our proposed approach gives overall better performance than other algorithms. We can see in terms of sensitivity and specificity, satisfactory performance was obtained using our proposed method while other methods achieved relatively somewhat good specificity, but poor performance in sensitivity.

Table 1.4. Comparison of the individually top 60 features (peaks) found in different algorithms. For each feature found in extended Markov blanket algorithm, features within 3Da in other algorithms are shown. MB = Markov blanket

Extended MB	Information Gain	Relief-F	χ^2-Statistic
1008.3059 1009.3066	1008.3059		1008.3059
1553.5329 1554.5333	1553.5329	1551.5321 1552.5325 1553.5329	1552.5325 1553.5329
1740.6856 1741.6865 1742.6875		1743.6884	
1992.8479 1994.8493		1992.8479 1993.8486 1994.8493	1994.8493
2050.8725		2048.8718 2049.8722 2050.8725	
2147.9404 2148.9415 2149.9425	2148.9415		
3147.4299	3148.4301 3149.4303		3148.4301 3149.4303
3597.6778	3598.6779		
5001.5661		5002.5666 5004.5670	5002.5666
8282.1306 8283.1316 8284.1325	8280.1286		8280.1286

1.7 Conclusions and Discussions

Computational data analysis is critical for biomarker selection from high-resolution mass spectrometry data where the number of candidates can easily go beyond one million. In this paper we presented a preprocessing method and a new feature selection algorithm for high-resolution MALDI-TOF data. Our algorithm was applied to clinical recurrent ovarian cancer study to find biomarkers causing platinum-sensitive and platinum-resistant. Experimental results showed that our proposed algorithm yields better performance in overall sensitivity and specificity

compared to other feature selection methods. Prediction of early recurrence in ovarian cancer will help ontologists give targeted therapy to ovarian cancer patients who are usually not responsive to standard therapy. Our algorithm shows the sets of different biomarker patterns and the corresponding prediction results. This information will provide insight and assistive information for alternative treatment and drug design.

In future work, we plan to carry out protein sequencing to identify the molecular formulae for the selected biomarkers found in this study. To reduce experimental cost during sequencing, we will compare the selected biomarkers obtained from different algorithms and start with the most common ones. Currently we investigated the top 60 features which were used in each algorithm of this study. Table 1.4 shows features present within 3Da in other algorithms for each feature found by extended Markov blanket. For example, biomarker with m/z of 1553.5329 can be found by all four different feature selection methods. This indicates the reliability of the marker and this peptide should be among the ones to be first sequenced. We also plan to apply our algorithm to other studies such as prostate cancer and preterm delivery.

CHAPTER 2

DIAGNOSIS OF EARLY RELAPSE IN OVARIAN CANCER USING SELDI-TOF MASS SPECTROMETRY DATA

2.1 Introduction

Ovarian cancer is commonly diagnosed at stage III or IV with a low 5-year survival rate. Primary therapy of ovarian cancer includes surgical cytoreduction followed by chemotherapy with a platinum agent. Ovarian cancer commonly recurs at the rate of 75% within a few months or several years later [19]. If cancer does not recur and disease remits for 6 months or more since completion of primary chemotherapy, the cancer is considered platinum-sensitive. On the other hand, if cancer relapses within less than 6 months of completing primary therapy, or grows during primary therapy, the cancer is considered platinum-resistant. Platinum-sensitive patients are usually treated again with primary chemotherapy used before, while patients with recurrent platinum-resistance cancer are usually not responsive to standard therapy. Therefore many new secondary-chemotherapy drugs have been found in recent years for re-treatment of them. Unfortunately, recurrent ovarian cancer is relatively difficult to be diagnosed. There is currently no reliable technique for predicting early relapse in ovarian cancer. Hence, new methods in this area are urgently needed to help physicians and gynecological oncologists give targeted therapy to patients with recurrent ovarian cancer.

Recently, surface-enhanced laser desorption/ionization time-of-flight (SELDI-TOF) mass spectrometry has been used successfully to detect protein patterns of several cancers for early disease diagnosis. In addition to being a platform for biomarker

discover, SDLDI-TOF system can be applied for toxicology screening and monitoring of disease progression and therapeutic effects of drugs. An advantage of SELDI-TOF over electrospray ionization (ESI) is a higher tolerance for salts that makes this technique better suited to the examination of biological samples such as serum.

In this paper, we propose a new feature subset selection algorithm, SVM-Markov blanket/recursive feature elimination (SVM-MB/RFE) combining SVM-RFE with Markov blanket filtering. Markov blanket is a feature subset selection method which eliminates features having little or no information beyond that subsumed by the remaining features [23]. Major obstacles in analyzing SELDI-TOF mass spectrometry data are a large number of peaks and mass error [21], [31]. We have developed an efficient software in order to overcome such problems, which consists of feature pruning, binning, normalization and feature selection. In this paper, we demonstrate the better ability of our method over other algorithms through the comparison of performance.

2.2 SVM-Markov Blanket/Recursive Feature Elimination

2.2.1 Preprocessing

In the preprocessing task, we employe t-test as a method to asses the degree of separation between two classes. By using the result, we want to filter the huge number of features (m/z ratios) of mass spectrometry data to reduce computational burden in the next stage of our algorithm. The test is performed at each m/z ratio while yielding its t-test statistic value,

$$t_i = \frac{\mu_i^+ - \mu_i^-}{\sqrt{\frac{(\sigma_i^+)^2}{n^+} + \frac{(\sigma_i^-)^2}{n^-}}} \tag{2.1}$$

where + and − stand for two class labels; μ_i^+ and μ_i^- are the means of the i^{th} feature; σ_i^+ and σ_i^- are the corresponding standard deviations; n^+ and n^- represent the number of samples contained in each class [32]. At each m/z ratio, the larger the test statistic in absolute value, the stronger the evidence that there is a difference between the two classes so that we can use the m/z ratio as a candidate feature to classify samples. In this experiment, we used the significance level of 0.05 as a criterion for filtering peaks.

Since one m/z and its neighbors are likely to come out from the same molecule and to be strongly correlated each other, the binning work is required. Mass difference between peak i and peak $i+1$ is calculated for each peak using the following formula,

$$\beta = \frac{m/z(i+1) - m/z(i)}{m/z(i)} \tag{2.2}$$

where $m/z(i)$ and $m/z(i+1)$ are m/z values of peak i and $i+1$, respectively. If β is less than a given threshold, two peaks are considered as belonging to the same bin. In this study, we perform 5-fold cross validation experiments changing the β value and select the one with which we obtain the best accuracy as the β value.

Usually through normalization, we can expect the better performance of classification algorithm. By doing so, values in each m/z ratio are converted such that the transformed values lie between 0 and 1. Let I_i denote the raw intensity at the i^{th} m/z position and I_{min} and I_{max} denote the smallest and largest intensity, respectively. Then, the normalized intensity NI_i is calculated by

$$NI_i = \frac{I_i - I_{min}}{I_{max} - I_{min}}. \tag{2.3}$$

Table 2.1. Serum sample information.

	Resistant	Sensitive
# training samples	33	45
# test samples	15	20
# total samples	48	65

2.2.2 Scoring function

We propose a new scoring function combining SVM-RFE weight with Markov blanket scoring value which both are instances of backward feature elimination algorithm. By applying a new score combined from the expected cross-entropy value $\triangle(F_i|\mathbf{M}_i)$ of Markov blanket and the weight value w_i^2 of SVM-RFE, we hope that Markov blanket helps SVM-RFE select more relevant features by removing redundant and irrelevant features. We use the following score to eliminate a feature at every iteration of SVM-MB/RFE,

$$C_i = \frac{\triangle(F_i|\mathbf{M}_i)}{\max_j\{\triangle(F_j|\mathbf{M}_j)\}} + \frac{(w_i)^2}{\max_j\{(w_j)^2\}} \tag{2.4}$$

where C_i indicates the final score assigned to F_i, which lies between 0 and 2. To have the same range for all the features, the weight value and the expected cross-entropy value are divided by their maximum values.

2.3 Experimental Results

We implemented SVM-MB/RFE algorithm using C++ code. A total of 160 serum samples were run on an IMAC30 ProteinChip$^{\mathbf{TM}}$ and CM10 ProteinChip$^{\mathbf{TM}}$ arrays from Ciphergen Biosystems. Of them, 113 serum samples (48 platinum-

Table 2.2. Change of the number of peaks.

	initial	500 *m/z* <	after t-test	after binning
# peaks	27000	22687	641	58

resistant, 65 platinum-sensitive) as an initially preliminary study were analyzed by SELDI-TOF mass spectrometry. The raw m/z and intensity were exported to an excel file using Biomarker Wizard software (Ciphergen Biosystems). Those samples were randomly divided into 33 and 45 as a training set, respectively, from platinum-resistant and platinum-sensitive samples, and the reminder as a test set. Table 2.1 shows the information of serum samples used in this study. In our study, the SVM soft margin parameter was set to $C = 1$.

Each serum sample consists of 27000 m/z ratios. Since m/z values below 500 are likely to reflect the surface coatings and not serum proteins, we removed such m/z values from our samples before the beginning of work [12], [33]. In each sample, the number of peaks whose m/z values are above 500 is 22687. Next, after t-test for feature pruning, the number of peaks was reduced up to 641. Finally, by the binning task which choose the highest peak in each bin, 58 peaks were obtained. We performed 5-fold cross validation changing β and chose $\beta = 1.0$ as a criterion for binning because the best performance was obtained when the β value was used. Fig. 2.1 and Table 2.2 represent the change of the number of peaks.

Since we are interested in small peak subsets, we investigated the performance of three algorithms such as SVM-MB/RFE, SVM-RFE and Markov blanket with small peak subsets first using the top peak then the top two peaks and so forth up to the top 30 peaks according to the ranked features for each algorithm. This experiment was repeated 50 times, and the means and standard deviations of accuracy,

sensitivity and specificity were evaluated. Since the large size of Markov blanket may cause fragmentation of training samples and the results to degrade, we chose the small value as the size of Markov blanket, *i.e.*, $k = 1$ and 2. Fig. 2.2 represents the results of experiments showing accuracy (a), sensitivity (b) and specificity (c) when $k = 1$, and accuracy (d), sensitivity (e) and specificity (f) when $k = 2$. Here, sensitivity is the percent of platinum-resistant samples that are correctly classified as the platinum-resistant. Specificity is the percent of platinum-sensitive samples that are correctly classified as the platinum-sensitive. As can be seen, SVM-MB/RFE outperformed other methods. Accuracy and sensitivity have the similar tendency as the number of peaks increases, while specificity has a valley shape. We investigated that how frequent the candidate peaks of 58 took part in forming 30 peaks subset during 50 runs. 46 peaks were used at least one time. 17 peaks were used in every iteration. Table 2.3 represents measurements comparison when 30 peaks subset was used. Fig. 2.3 shows the frequency along with the t-test value of each peak. Note that although no. 6 and 43 (765.260 and 5683.916 m/z) have a relatively high t-test value as 3.039 and 3.412, respectively, they participated just 3 and 9 times, respectively. On the other hand, no 13 (985.589 m/z) was used in the every run although the t-test value is as low as 1.926. And we observed that the accuracy when $k = 2$ is better than when $k = 1$.

2.4 Conclusion

We proposed a new supervised feature selection method (SVM-MB/RFE) to identify markers for detecting early relapse of ovarian cancer. In the preprocessing task of SVM-MB/RFE, the number of features was reduced up to 58 from 27000 of the raw data. By using a new score ranking combined from the expected cross-entropy value of Markov blanket and the weight value of SVM-RFE, SVM-MB/RFE

Table 2.3. Measurements comparison when $k = 1$ and $k = 2$ in SVM-MB/RFE. The number in parenthesis is the standard deviation.

k	Measurement	SVM-MB/RFE	SVM-RFE	MB
$k = 1$	Accuray (%)	83.7(6.0)	81.4(5.9)	79.0(5.7)
	Senstivity (%)	71.6(10.8)	68.5(12.3)	62.3(10.5)
	Specificity (%)	92.8(6.9)	91.1(7.4)	91.6(6.0)
$k = 2$	Accuray (%)	85.8(5.0)	82.6(5.3)	79.2(4.7)
	Senstivity (%)	73.5(9.5)	69.3(10.2)	65.9(11.1)
	Specificity (%)	95.1(5.0)	92.5(5.6)	89.2(7.0)

outperformed other methods. We demonstrated that although features have low t-test values, it is worth to see if they can be used as candidate features. In general, the small size of Markov blanket is used to avoid the fragmentation of training set. We compared the performance when $k = 1$ and 2, and showed that the accuracy when $k = 2$ is better than when $k = 1$ in SVM-MB/RFE. This project is in progress. Next, we will classify the full serum samples of ovarian cancer which includes a control dataset by implementing the multiple SVM-MB/RFE. The discovery of accurate biomarkers for identifying early recurrence of ovarian cancer will help ontologists give targeted therapy to ovarian cancer patients.

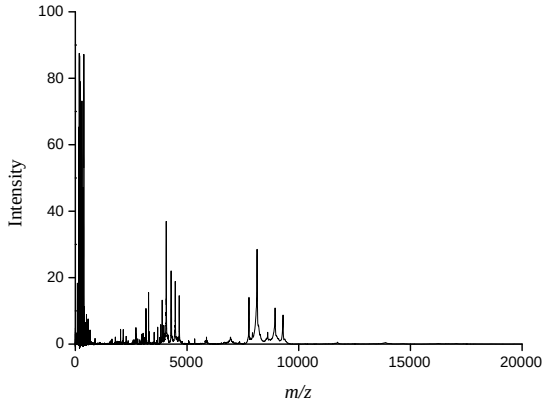

(a)

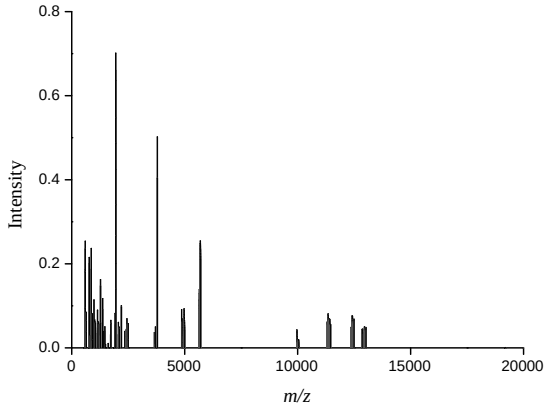

(b)

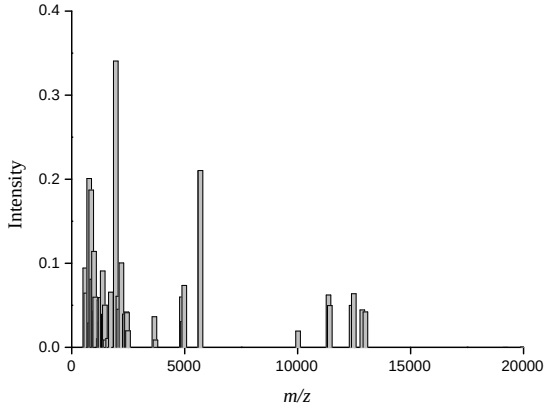

(c)

Figure 2.1. Example that shows the change of the number of peaks in one sample. (a) raw peaks (27000), (b) peaks after t-test (641), (c) peaks after binning (58).

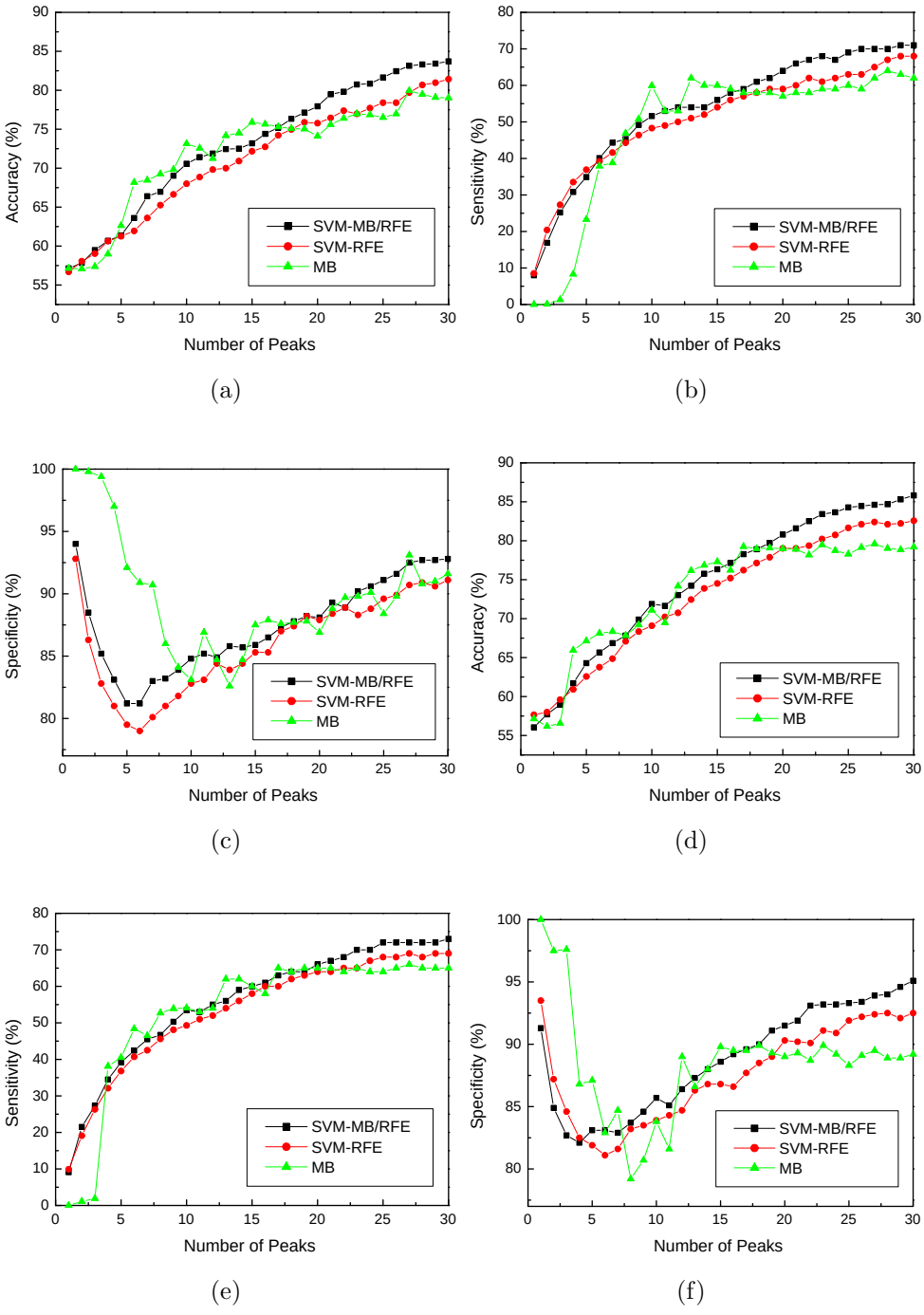

Figure 2.2. Average measurements changing the size of feature subset (a) accuracy when $k = 1$, (b) sensitivity when $k = 1$, (c) specificity when $k = 1$, (d) accuracy when $k = 2$, (e) sensitivity when $k = 2$, (f) specificity when $k = 2$.

No	*m/z*	frequency	t-test value	No	*m/z*	frequency	t-test value
1	538.115	42	2.657	24	1439.987	9	1.967
2	599.249	19	2.552	25	1467.177	6	2.196
3	641.756	18	2.202	26	1495.840	50	2.652
4	738.831	50	2.334	27	1613.690	3	2.195
5	756.015	50	2.347	28	1668.505	16	2.331
6	765.260	3	3.039	29	1732.524	50	2.913
7	773.979	1	2.275	30	1862.826	49	2.315
8	786.563	34	2.378	31	1918.018	1	2.645
9	815.623	1	2.053	32	1950.779	39	2.460
10	862.975	4	2.147	33	2064.532	41	1.986
11	909.771	31	2.317	34	2101.403	50	2.578
12	929.156	8	2.051	35	2198.208	31	2.522
13	985.579	50	1.962	36	2351.324	35	2.252
14	1023.450	38	2.417	37	2421.550	50	2.773
15	1040.963	50	2.068	38	2445.361	50	3.392
16	1063.064	37	2.057	39	2490.714	32	2.130
17	1132.880	50	3.029	40	3753.111	45	2.206
18	1194.392	50	2.342	41	4923.713	44	2.944
19	1201.287	50	2.209	42	4981.335	50	2.504
20	1225.759	50	2.050	43	5683.916	9	3.412
21	1260.511	1	2.045	44	12863.914	49	2.160
22	1370.018	4	2.175	45	19196.391	50	3.319
23	1419.366	50	2.370	46	19976.675	50	2.979

(a)

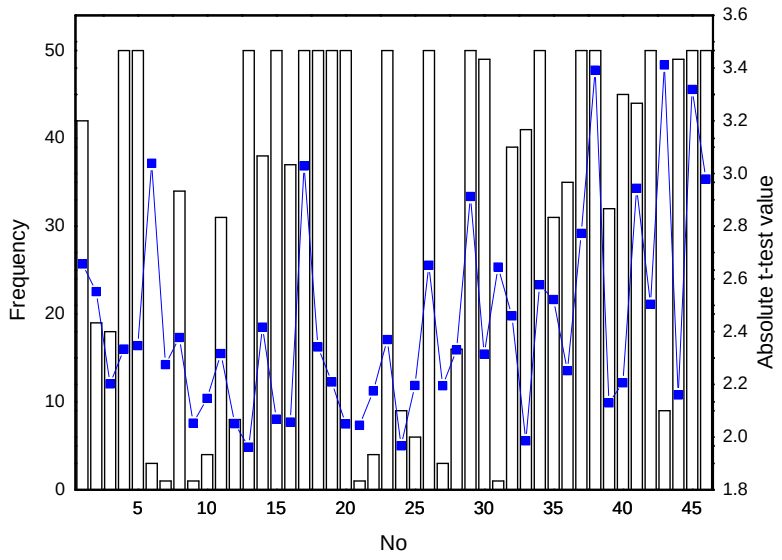

(b)

Figure 2.3. Frequency of the 58 candidate peaks and t-test values. (a) table that shows how often the 58 candidate peaks take part in forming 30 peaks subset along with their t-test values, (b) comparison graph with regard to the frequency and t-test value.

CHAPTER 3

MULTI-STAGE DISEASE CLASSIFICATION BASED ON BI-CLASSIFICATION STRATEGY

3.1 Introduction

For high-resolution mass spectrometry (MS) data, traditional machine learning algorithms may break down with high-dimensional input (mass-to-charge ratios, features, biomarkers). Very limited research has been carried out to explore the computational challenges. Yu *et al.* developed two approaches using different preprocessing and classification methods to analyze high-resolution SELDI-TOF (surface-enhanced laser desorption ionization time-of-flight) MS ovarian data [34], [35]. In the first study, a feature dimension reduction method consisting of a four-step preprocessing was proposed followed by a standard Support Vector Machine (SVM) for classification [34]. In the second paper [35], Bayesian neural network models were used for sample classification. Sequential feature selection was carried out by using bootstrap technique based on the two-sample Kolmogrov-Smirnov test (KS-test). Ressom *et al.* have designed a computational method that combines particle swarm optimization with support vector machine to distinguish liver cancer patients from healthy individuals in SELDI-QqTOF spectra [16]. Recently, this group proposed to combine ant colony optimization (ACO) with SVM to distinguish hepatocellular carcinoma patients from cirrhosis patients via MALDI-TOF mass spectra [36]. Particle swarm optimization and ant colony optimization are interesting swarm intelligence techniques that have been successfully applied to a number of optimization problems. A comparative study of several well-known classification algorithms, such as

linear discriminant analysis (LDA), k-nearest neighbor (KNN), random forest (RF), bagging, boosting, and SVM, has been carried out for ovarian cancer diagnosis [17]. It was demonstrated that RF approach leads to an overall higher accuracy rate as well as a more stable assessment in terms of classification errors. As a summary for current literature on high-resolution MS data analysis, the work, feature selection and classification, has been focused on binary class samples. However, medical data sets typically contain multiple classes. Therefore, feature selection as well as sample prediction for multi-categories are necessary.

Multi-category classification involves assigning an unknown sample into one of the k classes ($k > 2$) [37], [38]. There are two main strategies to tackle the multi-class problems [39]. The first method considers all classes at once by constructing a decision function, which may require high cost and complexity. In the second method, the multi-class problems are broken down into a set of binary classification problems, which is more computationally tractable [40]. There exist several methods to reduce multi-class problems to binary class problems. These include one-against-the-rest, one-against-one, and error-correcting output coding (ECOC). ECOC has shown the generalization capability in multi-sample classification.

ECOC was inspired from communication theory, where misclassifications wrongly guessed by classifiers can be corrected. In the ECOC multi-class classification problem, there are several factors to affect the performance of the algorithm. Investigations have been carried out on the selection of coding matrix [41], [42], [43], [39] and optimization of the decoding function [44], [45], [46]. In the study of coding matrix design, Dietterich and Bakiri provided methods for constructing error-correcting codes in which the coding method varies depending on the number of classes included in the problem [41]. Also the robustness of ECOC in handling small sample size and with respect to the assignment of codewords was also investigated in this work.

Crammer and Singer investigated problem-dependent discrete and continuous codes where they proved that finding an optimal discrete matrix is unfeasible and proposed a relaxation of output codes by using continuous values [42]. Pujol *et al.* introduced a heuristic coding method based on the mutual information between classes in each column to achieve maximum discrimination [43]. Ie *et al.* proposed a multi-category classification method based on ECOC for assigning a sequence of amino acids to one of the known protein structures [39]. The coding matrix is directly related to the structural hierarchy such as fold and superfamily detectors. Decoding rule plays an important role in ECOC classification [44], [45], [46]. Smith and Windeatt reviewed existing decoding rules which are based on distance, probability estimation and pattern space transformation, and proposed a likelihood decoding rule [44]. Passerini *et al.* introduced a new decoding function based on class conditional probabilities that represent the closeness between codewords and the vector formed by the outputs of the classifiers [45]. Kuncheva and Whitaker proposed to use diversity measures rather than the standard minimum Hamming distance to evaluate the quality of an error-correcting code and suggested an evolutionary algorithm to construct the code [46]. Methods combining boosting and ECOC have been studied to take the performance advantages of boosting [47], [48].

In this paper, we develop an ensemble based multi-class learning algorithm by integrating a new ECOC scheme and one-against-one pairwise coupling (PWC) scheme. The motivation is to take advantage of each multi-class classification strategy to achieve the most reliable sample prediction. Our contributions come from defining a performance-based weighting function for binary classifiers (dichotomies) in ECOC and a robust decoding function incorporating individual sample property and the overall dichotomy performance. A unique set of biomarkers to distinguishing each pair of categories (classes) is discovered by a new feature selection method,

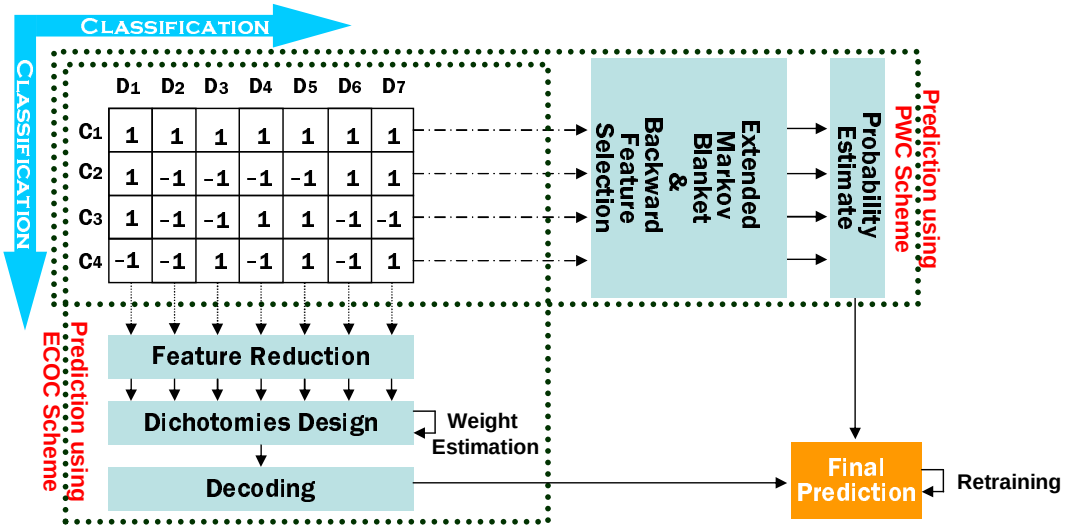

Figure 3.1. Framework of the proposed algorithm.

Extended Markov Blanket. Fig. 3.1 shows the framework of the proposed biomarker selection and sample category prediction.

The MALDI-TOF data set used in this study is opened by Ressom *et al.*. It consists of hepatocellular carcinoma (HCC) patients, cirrhosis patients, and healthy individuals [36]. Among the three-class data set, Ressom *et al.* used hepatocellular carcinoma (HCC) and cirrhosis spectra for two category sample classification leaving healthy spectra for peak screening and outlier detection. In this study, however, we used all three-class spectra for multi-category sample classification and biomarker selection for each class.

3.2 Methods

3.2.1 Data Preprocessing

The binned spectra of MALDI-TOF MS for liver cancer study were binned with the size of 100 ppm (parts-per-million) and in total yielding 23,846 bins. Preprocessing by baseline correction and normalization was applied to the binned spectra

prior to the next stage pattern finding. For baseline correction, we follow the same method, spline approximation, as what was done by Ressom *et al.* [36]. After that, each spectrum is normalized by dividing the baseline corrected spectrum by its total ion current (the summed intensity over all *m/z* values in the baseline corrected spectrum). Because of the small normalized intensity value, all the intensities are multiplied by 10,000 for computational convenience. Ressom *et al.* generated windows by combining bins after preprocessing. In this study, however, we used the binned data itself to find biomarker candidates in narrow mass regions. To reduce computational burden caused by using peaks in all the bins, we rank peaks by a feature ranking method based on the ratio of between-group to within-group peak differences and select the tractable size of features in our algorithm. The feature ranking method was proposed by Dudoit *et al.* for feature selection in multi-class problems [49]. For certain *m/z* peak j, the ratio is:

$$\mathbf{BW}(j) = \frac{\sum_i \sum_k I(y_i = k)(\overline{x}_{kj} - \overline{x}_{.j})^2}{\sum_i \sum_k I(y_i = k)(x_{ij} - \overline{x}_{kj})^2}, \tag{3.1}$$

where $I(\cdot)$ is the indicator function, $\overline{x}_{kj}$ denotes the average intensity of peak j across samples belonging to class k, $\overline{x}_{.j}$ is the average intensity of peak j across all samples, x_{ij} is the intensity of sample i at peak j, and y_i is the class label for sample i. The larger the ratio, the more likely *m/z* peak j will be relevant to the class separation. In the next section, we will describe the basic algorithms used in our biomarker selection and classifier design.

3.2.2 A Redesigned ECOC Scheme for Multi-Class Classification

ECOC is a classification method that breaks a k-class prediction problem into several binary classifications. In the ECOC framework, each class is assigned a unique codeword of length h composed of 1 and -1 (Fig. 3.1), forming a $k \times h$ coding matrix.

Typically, the rows of the matrix are codewords assigned to the corresponding class c_i and the columns D_j represent binary classifiers which partition the samples into two subsets labeled according to the coding matrix. Based on the class partitions, the matrix produces h binary classifiers called dichotomies. For a test sample, a code of length h is obtained as a result of the outputs of the h binary functions. This code is compared with each of the k codewords defined in the coding matrix, and the sample is assigned to a class with the closest codeword using certain distance measure. In doing so, the classification process can be seen as a decoding operation.

Good error-correcting codes should meet two main criteria: row and column separations. Row separation represents that each codeword should be well separated from the others. Column separation indicates that the columns should be uncorrelated with each other and is achieved by maximizing the distance between one column and each of the other columns. The minimum Hamming distance is used to measure the quality of an error-correcting code between any pair of codewords.

In the generic ECOC multi-class classification problem, there are several factors affecting the performance of the algorithm. As previously introduced, investigations have been carried out on the designing of coding matrix and option of the decoding function. We develop a new ECOC framework from three aspects: a weighting strategy for different dichotomies, feature dimensionality reduction, and performance-based decoding function.

3.2.2.1 Weighting strategy

In standard ECOC framework, the influence of all the dichotomies during classification of an unknown sample is equally treated. However, the importance of each dichotomy is different in terms of generating decision boundaries for the training samples. Therefore, we define a weighting function which is similar to the one used

in boosting algorithms as shown in Eq. (3.12). The weight value of each dichotomy is computed by using the error rate estimated for the dichotomy with the validation data set. Therefore, the weight value represents how confident the dichotomy is. In Eq. (3.12), v_i and e_i are the weight value and the error rate of the i-th dichotomy. In the case where the accuracy of the dichotomy is greater than 50%, the weight value becomes positive; otherwise, a negative value is returned,

$$v_i = 0.5\mathbf{log}(\frac{1-e_i}{e_i}). \tag{3.2}$$

Throughout the study, we choose 10-fold cross validation (CV) where all samples are randomly split into 10 exclusive folds. Without loss of generality, SVM is used as the dichotomy function. For each of the ten experiments (iterations), typically nine folds are used as train data, and the remaining one fold is applied as test data. In our implementation, to estimate the accuracy of each dichotomy function, we further divide the nine fold train data into 10 folds, *i.e.*, sub-10-fold. In each iteration of the sub-10-fold, nine folds become sub-train and one fold for sub-test. An averaged error rate resulting from sub-test data is put into Eq. (3.12) to obtain the weight value. This estimation is separately performed for each dichotomy.

3.2.2.2 Feature reduction

In the training of dichotomies, due to the high dimensionality of mass profile even after the preprocessing, irrelevant features might still exist. Therefore, using all features will degrade the ability of dichotomies and increase computational cost. Here, we employ a feature reduction algorithm based on information gain to remove irrelevant features in each dichotomy.

Let S be the set of instances from k classes, $c_1, c_2, \ldots, c_k$ and $P(c_i, S)$ be the fraction of the instances in S that belong to c_i. The entropy of the class distribution in S is as follows:

$$I(S) = -\sum_{i=1}^{k} P(c_i, S)\mathbf{log}P(c_i, S). \tag{3.3}$$

Suppose feature F_i has m distinct values, $f_i^1, f_i^2, \ldots, f_i^m$. Let S_j be the set of instances whose value on attribute F_i is f_i^j. Then, the information gain of instance set S based on attribute F_i is calculated as

$$\begin{aligned} Gain(F_i) &= I(S) - I(S|F_i), & (3.4)\\ &= I(S) - \sum_{j=1}^{m} P(F_i = f_i^j) I(S_j), & (3.5)\\ &= I(S) - \sum_{j=1}^{m} \frac{|S_j|}{|S|} \times I(S_j). & (3.6) \end{aligned}$$

The information gain reflects the reduction in uncertainty about the overall class entropy when certain feature F_i is given. In other words, features with zero information gain indicate the inability to reduce such uncertainty and should be removed during the training of dichotomy function.

3.2.2.3 Decoding function

Based on the binary class predictions from the ensemble dichotomies, an output code is generated for the test sample. To assign the final class label to the test sample, a decoding function is required. The decoding function measures the closeness between the output code and the codewords in the coding matrix M. A new decoding function reflecting the importance of individual dichotomies is defined as:

$$d_j = \sum_{i=1}^{h} \mathbf{exp}(-v_i x_i y_i^j), \tag{3.7}$$

where d_j is the distance between the test sample and the j-th class, v_i is the importance of the $i-$th dichotomy, x_i is the i-th bit of the output code for the test sample

and y_i^j is the i-th bit of the codeword for the j-th class in the M matrix. A test sample is assigned to the class which has the minimum distance,

$$c_e = argmin_{1 \leq j \leq k} d_j. \tag{3.8}$$

3.2.3 Pairwise Coupling (PWC) Scheme

Though ECOC multi-class sample prediction performs well in most cases, the major limitation of this framework is that it is hard to be used for subspace feature selection. As a result, biomarkers contributing to certain phenotype category can not be estimated within this framework. Therefore, we incorporate another binary classification scheme, pairwise one-against-one classifier, which will provide us the capability to find discriminant biomarkers to distinguish phenotype differences between one class and another.

Here we are not applying one-against-the-rest binary classifiers. This selection comes from the legitimate biomedical interpretation. As an example, if choosing one-against-the-rest, we need to find biomakers to distinguish cirrhosis patients from the rest which is the combined samples of normal and hepatocellular carcinoma (HCC). Lumping the different stage samples like HCC and normal which may be very different from each other at molecular level could obscure biomarkers that truly distinguish patients from cirrhosis. On the other hand, one-against-one comparisons may point out differences between classes of patients that should not be lumped together, such as normal and HCC. Furthermore, with the number of class k in biomedicine usually less than 10, the computation issue raised by one-against-one binary classification will not be a concern.

The number of all possible binary classifiers using one-against-one classification is $k(k-1)/2$. A common way to determine a final class for the test sample is

voting. However in many cases, it is essential that multi-class classification should be a confidence measure, such as posterior probability [50]. In this study, we use a probability measure based on pairwise coupling (PWC) scheme to leverage binary prediction results. The probability for a test sample belonging to class i is calculated from combining $k(k-1)/2$ two-class probabilities [51]:

$$p_i = \frac{1}{\sum_{j=1,j\neq i}^{k} \frac{1}{\mu_{ij}} - (k-2)}, \tag{3.9}$$

where $\mu_{ij} = P(y = i|y = i \textbf{ or } j, \mathbf{x})$ corresponding to the posterior probability from the binary classifier.

Since standard SVM does not provide a way to measure the posterior probabilities, this is obtained using a parametric sigmoid model proposed by Platt [52]. For a SVM binary classification, the posterior probability is obtained as:

$$P(y = 1|x) = \frac{1}{1 + \textbf{exp}(A \times f(x) + B)}, \tag{3.10}$$

where $y = 1$ is the class label for binary class sample x. The parameters A and B are determined by the maximum likelihood estimation from the training set.

A test sample in PWC scheme is assigned to a class which has the maximum probability,

$$c_p = argmax_{1\leq i\leq k} p_i. \tag{3.11}$$

3.2.4 Extended Markov Blanket Feature Selection

Here, we describe the extended Markov blanket algorithm mentioned in 1.5.1 again. To discover the discriminant biomarkers among multi-classes, we propose a new wrapper-based feature selection algorithm called *extended Markov blanket* (EMB). This feature selection process is embedded in the pairwise coupling (PWC) multi-class classification scheme. The original Markov blanket is a filter-based feature selection method. Our algorithm considers reducing redundant features while

selecting the most discriminant ones. With the feature subset selected by extended Markov blanket, we run a linear SVM to calculate probabilities for the pair of classes.

To be more specific, for feature F_i remained after preprocessing, two feature subsets are considered: the high correlated feature subset (HCFS) and the low correlated feature subset (LCFS) composed of the least correlated d features for F_i. HCFS feature subset is used to remove redundant features as in the classical Markov blanket feature selection. Our contribution comes from utilizing LCFS to estimate the classification capability of each feature during the Markov blanket process. This is derived from the fact that mutually low correlated features, in general, lead to good classification performance.

We will now describe how the extended Markov blanket algorithm works out for feature selection. 10-fold cross validation data split is the same as previously introduced in section 3.2.2.1. For each feature F_i, we perform Markov blanket algorithm with its HCFS obtained from the train data to compute the expected cross-entropy value, $\triangle(F_i|\mathbf{M}_i)$. On the other hand, using LCFS and feature F_i, we run the linear SVM algorithm where the sub-train and sub-test data are used for training and testing, respectively, to obtain a roughly estimated accuracy, denoted as β. Then, we compute the normalized weight for each feature in the LCFS using the following function:

$$W_k = \begin{cases} \frac{|w_k|}{\sum_{j=1}^{d+1} |w_j|} \times \beta \times \delta, & \text{for } \gamma \leq \beta \ , \\ \left(1 - \frac{|w_k|}{\sum_{j=1}^{d+1} |w_j|}\right) \times (\gamma - \beta) \times \delta, & \text{for } \gamma > \beta \ , \end{cases} \tag{3.12}$$

where

$$\delta = \begin{cases} 1, & \text{for } \gamma \leq \beta \\ -1, & \text{for } \gamma > \beta \end{cases} \tag{3.13}$$

and β is the accuracy from sub-test samples in the linear SVM, k is the index for features in LCFS including feature F_i, $|w_k|$ is the absolute SVM weight obtained

using Eq. (1.7), d is the size of LCFS chosen as 10, 20, or 30, and γ is a heuristic performance threshold typically specified as 0.5. After computing $|w_k|$ for all features in the LCFS, each $|w_k|$ is normalized by the summed absolute SVM weights of all the features in the LCFS and that of feature F_i.

In contrast to SVM-RFE where features with the smallest absolute weights are removed, we assume that features with large absolute SVM weights are important in terms of classification power. Not surprisingly to observe, although the normalized SVM weight of certain feature in Eq. (1.7) may be high in an LCFS, the classification accuracy of the linear SVM performed with the limited LCFS may be low due to the partial discriminant capacity of one LCFS. Therefore, not only the normalized SVM weight for each feature but also the accuracy with its LCFS are important factors to estimate feature weight. This leads to the multiplication of the normalized SVM weight by the accuracy obtained after the SVM. Through a few experiments, we found that $\gamma = 0.5$ assures a good performance. If the accuracy is greater than 50%, the proposed weight becomes positive by multiplying 1 as a value of δ. Otherwise, we treat it as a penalty using -1 as δ value.

After computing the proposed weights and expected cross-entropy $\triangle(F_i|\mathbf{M}_i)$ values for all features as introduced above, certain feature with the smallest $\triangle(F_i|\mathbf{M}_i)$ value is removed according to Markov blanket rule. Then, the HCFS and LCFS for all but the removed feature are rebuilt. In fact, only those subsets that contain the removed feature will be affected and modified. Again, we compute the $\triangle(F_i|\mathbf{M}_i)$ values and the proposed weights for survived features. The feature weights will be accumulated during the Markov blanket feature removal process. The whole procedure keeps going until the predefined feature number is reached.

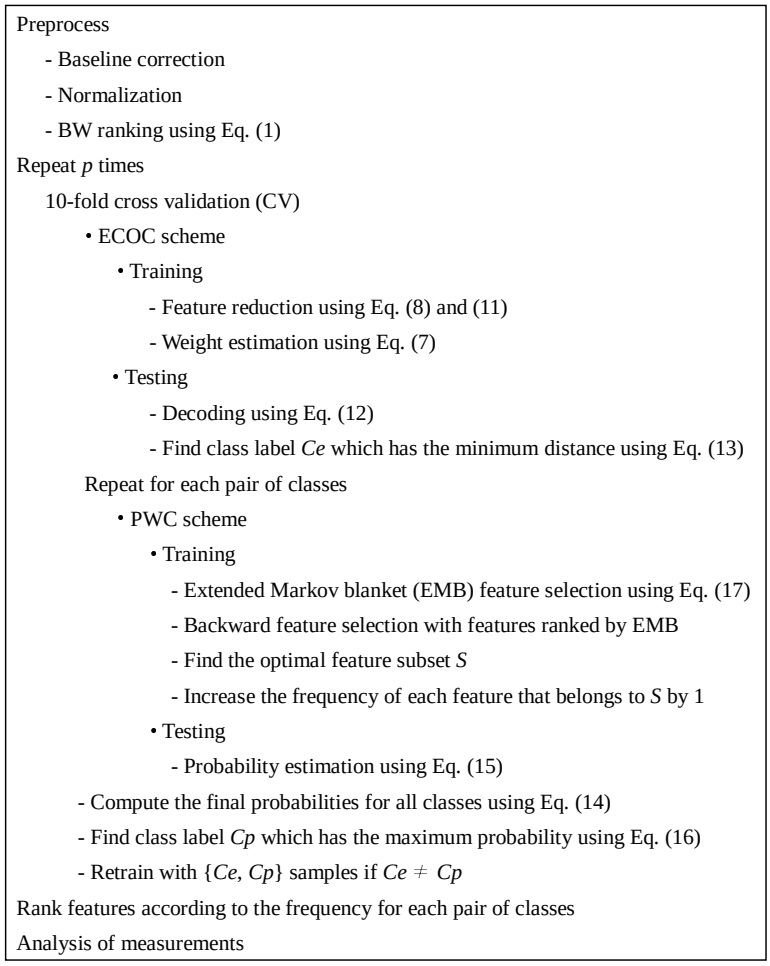

Figure 3.2. Flowchart of the algorithm ($p = 20$ in this study).

3.2.5 Feature Pruning by Backward Feature Selection

After each iteration of 10-fold CV (20 times of 10-fold CV were applied, totalled 200 iterations), a mean weight value for each feature is calculated using the accumulated weight divided by the occurrence counting in all LCFS. All the features are then ranked according to the mean weights. Then, a backward feature elimination method with the top 60 features is performed by using a linear SVM to find a compact feature subset during each 10-fold CV iteration. The backward feature selection approach removes one feature at a time from the current feature set. Each

time a feature without which the accuracy is improved will be excluded. This process continues until one feature remains. Features with which the best accuracy is obtained form an optimal feature subset for the pair of classes. With the optimal feature subset, one-against-one binary classifier for certain pair of classes is built. This method is performed for exhaustive pairs of classes.

After finishing all the iterations of 10-fold CV training, we count how many times a single feature is included in individual optimal feature subsets for each pair of classes. A final feature set is sorted according to the frequency. The higher the frequency, the more reliable a feature is. Fig. 3.2 shows the overall operation flow of the proposed framework.

3.2.6 Retraining

In section 3.2.4 and 3.2.5, a method to find important features for each pair of classes was presented. The final sample prediction will be determined by outputs of ECOC and PWC schemes. If two resultant class labels are the same ($c_e = c_p$), the test sample is assigned to the identical class; otherwise ($c_e \neq c_p$), a retraining will be performed using samples that only belong to classes c_e and c_p excluding other class samples. Therefore, the retraining comes to be a binary classification problem. In retraining, we use the feature subset which is found for the two classes c_e and c_p by Extended Markov Blanket. As a consequence of the binary classification, the final class is determined for the test sample.

3.3 Experiments

Liver cancer data opened by Ressom *et al.* consists of 201 spectra, hepatocellular carcinoma (78), cirrhosis (51) and health (72). In this paper, all the samples were used to find biomarkers in such a multi-stage liver cancer. We implemented the

Table 3.1. The means and standard deviations (in parenthesis) of accuracies in liver cancer data set.

Methods	Accuracy \ No. of peaks	100	200	300	400	500
Proposed Method	Overall	81.94(1.54)	86.92(1.79)	**88.71(1.85)**	87.61(1.78)	84.93(1.95)
	Cirrhosis	80.39(2.07)	80.98(3.82)	86.86(1.86)	87.25(3.10)	86.67(2.58)
	HCC	86.54(1.93)	90.26(2.28)	89.62(2.13)	88.08(2.27)	85.13(2.28)
	Health	78.06(2.91)	87.50(2.78)	89.03(2.89)	87.36(3.17)	83.47(3.43)
ECOC	Overall	78.75(2.25)	81.34(1.74)	79.90(2.07)	79.45(2.36)	77.16(1.34)
	Cirrhosis	79.22(3.36)	78.24(4.66)	79.61(5.16)	79.22(2.80)	74.51(3.46)
	HCC	83.97(2.58)	83.46(2.05)	81.67(4.10)	82.44(3.63)	81.03(2.08)
	Health	72.78(5.08)	81.25(3.54)	78.19(3.76)	76.39(4.19)	74.86(2.66)
Random Forest	Overall	78.86(1.63)	81.29(1.22)	80.45(1.83)	83.28(1.37)	82.89(1.56)
	Cirrhosis	71.37(4.15)	76.08(2.41)	74.71(4.18)	76.27(4.28)	78.04(3.04)
	HCC	83.72(3.92)	85.64(2.25)	85.38(2.20)	87.82(1.84)	88.08(1.71)
	Health	78.89(2.25)	80.28(2.68)	79.17(2.85)	83.33(2.85)	80.69(3.30)
Naive Bayes	Overall	79.01(0.51)	81.94(0.41)	82.69(0.51)	83.73(0.62)	84.03(0.64)
	Cirrhosis	80.59(1.72)	82.75(1.80)	83.53(1.01)	83.14(1.01)	82.94(0.95)
	HCC	88.33(0.41)	89.87(0.73)	87.31(0.73)	87.31(0.41)	87.31(0.41)
	Health	67.78(1.10)	72.78(1.49)	77.08(1.50)	80.28(1.94)	81.25(2.10)
J48	Overall	71.09(3.19)	71.74(3.38)	73.28(2.86)	73.23(2.95)	73.08(3.50)
	Cirrhosis	65.49(5.93)	65.29(3.70)	66.08(5.47)	64.90(4.75)	65.88(4.99)
	HCC	76.54(5.54)	77.69(3.69)	78.85(2.03)	78.33(3.80)	76.54(4.15)
	Health	69.17(3.63)	69.86(6.07)	72.36(4.56)	73.61(3.82)	74.44(4.64)

proposed algorithm based on LIBSVM [29] and WEKA library [30]. A linear SVM was adopted in retraining and in both ECOC scheme and PWC scheme. For ECOC scheme, a random coding strategy was used in which values of {+1, -1} were selected uniformly at random to generate codes.

According to the BW ratios after preprocessing, we ranked the 23,846 binned peaks (features) and performed experiments with the top 100, then the top 200 and so forth up to the top 500 peaks. The performance of our method was compared with other classification algorithms such as standard ECOC, Random Forest, Naive Bayes, and J48. In all experiments, 10-fold cross validation was applied.

Table 3.1 shows the experimental results in terms of accuracy means and standard deviations. The individual accuracy for each class is the ratio of correctly labelled samples over the real ones while the overall accuracy is with respect to the total correctly labelled samples for all the classes. The proposed method shows the

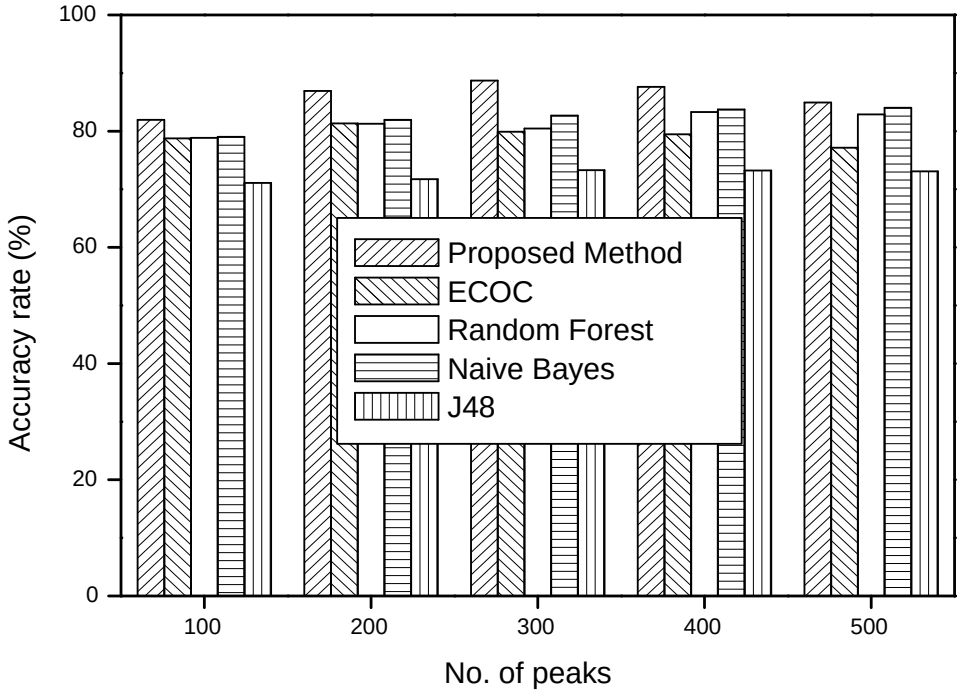

Figure 3.3. Comparison of overall classification accuracies.

best accuracy of 88.71% when the experiments were done with the top 300 peaks ranked by BW ratios. The corresponding accuracies for cirrhosis, HCC, and health are 86.86%, 89.62%, and 89.03%, respectively. As a comparison, J48 achieved the least satisfactory performance in all the trials. Fig. 3.3 visually represents the overall classification accuracies from different classifiers.

In PWC scheme, for each pair of classes (cirrhosis vs health, cirrhosis vs HCC, and health vs HCC) we count how many times each peak is included in the optimal feature subset after the backward feature elimination (See sections 3.2.4 and 3.2.5). Peaks with high frequencies are more reliable than randomly observed biomarkers. In the situation of best overall accuracy when 300 peaks were chosen, the frequencies of all optimal feature sets after backward feature elimination were counted. Fig. 3.5 drafts the normalized frequency of the top 60 peaks selected by our method in cirrho-

Ranking	Cirrhosis vs Health	Cirrhosis vs HCC	Health vs HCC
1	1326.4894	1865.4808	3201.7317
2	1961.9057	1797.0038	3202.0519
3	2307.1390	2390.0313	2373.1230
4	1961.7096	1865.6674	2389.7923
5	2372.1740	2365.5415	2535.5320
6	1327.1527	2391.4656	2536.0392
7	2362.9410	1961.7096	2373.3603
8	2389.5533	2365.3050	3202.3721
9	1327.2855	2390.9874	2535.0250
10	1325.5612	1710.3930	2535.7856
11	1325.6938	2390.2703	2372.1740
12	1451.1138	2390.5093	1452.5656
13	2306.6776	2373.3603	2535.2785
14	1796.6444	2365.0685	2534.2646
15	1796.8241	2373.5976	2372.4112
16	2389.7923	2363.6499	2536.2928
17	1962.1019	2390.7483	2534.0112
18	1957.5945	1796.8241	3216.1712
19	2389.3144	2365.7780	2373.5976
20	1718.7941	1961.9057	5900.6426

(a)

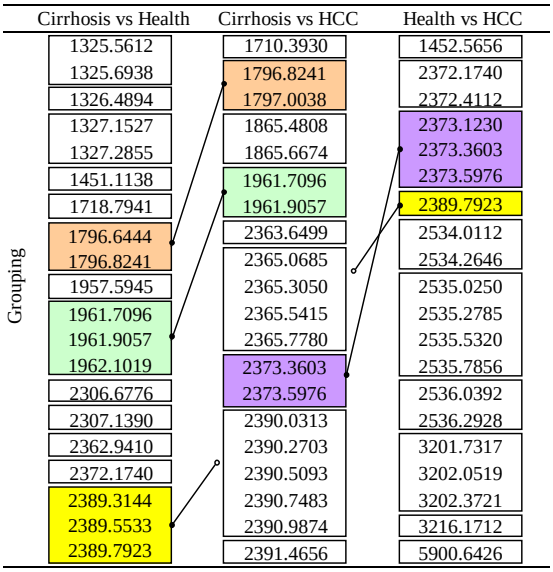

(b)

Figure 3.4. The top 20 peaks out of 300 peaks and grouping of peaks. (a) The m/z values for the top 20 observed peaks out of 300 peaks obtained by BW ratios. (b) Grouping of peaks within 0.3 Da from (a).

sis vs health, cirrhosis vs HCC, and health vs HCC experiments where the highest frequency was scaled to 100. Among the 60 peaks, the top 20 peaks, sorted by the frequency, were listed in Fig. 3.4(a). Furthermore, we grouped the 20 peaks within 3 Da as shown in Fig. 3.4(b). Note that some peaks were commonly selected: 1796.8241, 1961.7096, 1961.9057 in cirrhosis vs health and cirrhosis vs HCC; 2373.3603 and 2373.5976 in cirrhosis vs HCC and health vs HCC; and 2389.7923 in cirrhosis vs health and health vs HCC. This further proves that not a single biomarker but a group of them contributes to the expressions of different phenotypes. We compared peaks selected by our method with those found in cirrhosis vs HCC experiments by Ressom *et al.*. We observed that 1865.4808 and 1797.0038 m/z corresponding to rank 1 and 2 by our algorithm belong to m/z windows 1864.0-1870.2 and 1793.1-

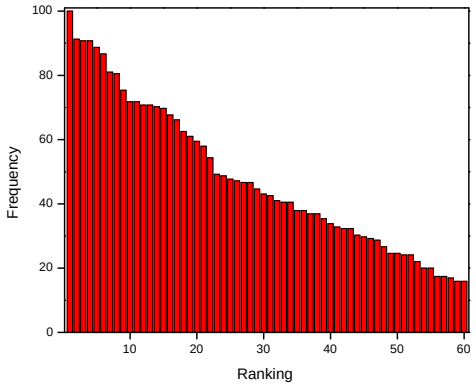

(a)

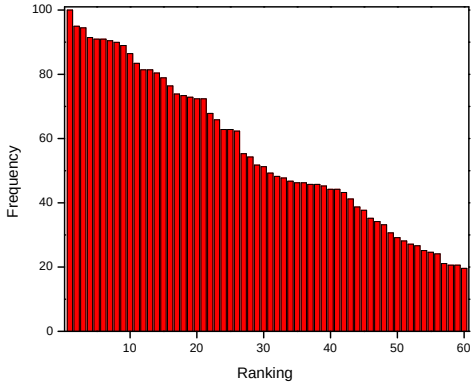

(b)

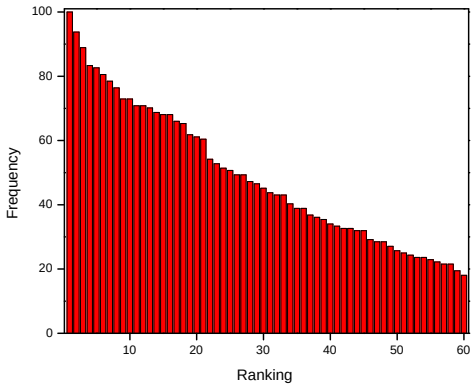

(c)

Figure 3.5. Frequency for the optimal feature sets from the top 300 peaks based on BW ratios. (a) Cirrhosis vs Health, (b) Cirrhosis vs HCC, (c) Health vs HCC.

1797.0, respectively, which were selected by ACO-SVM. In particular, 1865.4808 m/z is top-ranked in our algorithm as well as in both methods of weighting factor and ACO-SVM by Ressom *et al.*.

Fig. 3.6 represents the average intensity for peaks in Fig. 3.4(a). We should note that in each pair of classes more severe stage of the disease shows higher intensity distribution. This may imply more protein secretion relevant to the disease. In particular, there are a few peaks which have significant intensity difference in cirrhosis vs HCC and health vs HCC: peaks ranking 2, 9, 15, and 20 corresponding to 1797.0038, 2390.9874, 2373.5976, and 1961.9057 in cirrhosis vs HCC; peaks ranking 6, 9, 10, 13, and 19 corresponding to 2536.0392, 2535.0250, 2535.7856, 2535.2785, and 2373.5976 in health vs HCC. Note that three peaks 2535.0250, 2535.7856, and 2535.2785 among five high intensity peaks in health vs HCC were grouped as seen in Fig. 3.4(b). Also, peak 2373.5976 was commonly found in cirrhosis vs HCC (ranking 15)and health vs HCC (ranking 19) experiments, with much higher average intensity in HCC. In cirrhosis vs HCC, however, the top-ranked peak 1865.4808 not only in our algorithm but in both methods by Ressom *et al.* does not show a considerable difference of intensity. This further evinces that the importance of possible biomarkers is not only purely determined by its absolute volume but also by its correlation or coregulation with other biomarkers.

For next stage of biomarker identification, finding exact m/z values is critical to sequencing candidate selection, as small mass difference may lead to different protein candidates. Since our biomaker candidates fall into single bins whose size is usually less than 1 Dalton as opposed to a large window size spanning several daltons, the proposed approach offers narrow range to choose the sequencing candidates.

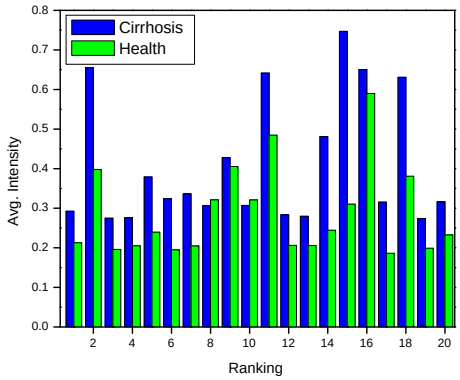

(a)

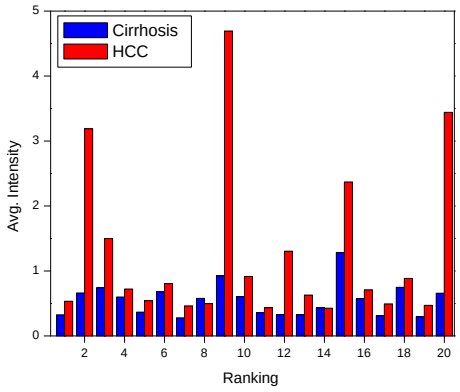

(b)

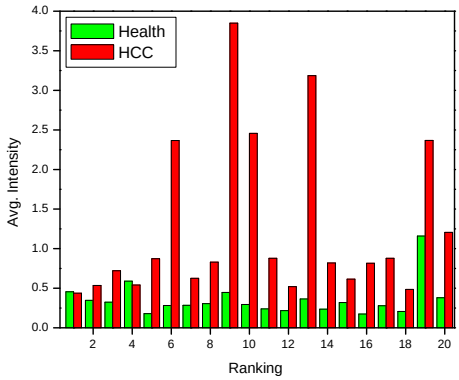

(c)

Figure 3.6. Average intensities for the top 20 peaks observed by the proposed method (corresponding to peaks listed in Fig. 3.4). (a) Cirrhosis vs Health, (b) Cirrhosis vs HCC, (c) Health vs HCC.

3.4 Conclusion

Disease progresses in several stages. It is important to diagnose the exact current stage of patients in order to provide proper treatments. Therefore, diagnosing of multi-stage diseases and finding of biomarkers corresponding to each stage are imperative. The work presented in this paper echoes the necessity. We proposed a new multi-class sample classification scheme with simultaneous feature selection. The classification framework is formed by the integration of a redesigned error-correcting output code (ECOC) scheme and a pairwise coupling (PWC) scheme with each scheme producing its best prediction. If the two predictions are the same, the identical class label is assigned for a test sample; otherwise, a retraining is carried out only with the two-class samples excluding samples from other classes. Also, we proposed a feature selection method, Extended Markov Blanket (EMB), within the multi-class classification framework. EMB chooses features by considering two aspects of biomarkers: redundancy and relevance. The reliability of features is also taken into consideration based on the appearance frequency. A final optimal feature set is discovered for pairwise categories. Experimental results using multi-stage liver cancer data demonstrated the performance of the proposed work. Comparison study using different multi-classification approaches was also presented. Distinct biomarker patterns were found in different stages of the disease between pair-wise categories.

CHAPTER 4

TWO-WAY SEARCH FOR BIOMARKER IDENTIFICATION

4.1 Introduction

Tandem mass spectrometry (MS/MS) is a mass spectrometry that has more than one analyzer. It has been recognized as one of the most powerful tools in proteomics for protein identification [53], [54], [55], [56]. Prior to an MS/MS experiment, proteins are digested into peptides by ionization process such as electrospray ionization (ESI) or matrix-assisted laser desorption ionization (MALDI). Tandem mass spectrometer usually has two analyzers. The first analyzer selects ions of a particular charged peptide called *precursor* or *parent peptide* according to the mass-charge ratio (m/z). The selected peptide ions are fragmented by a process known as collision-induced dissociation (CID). Once fragmented ions pass through the second analyzer, they are detected by an ion detector which is connected with a data system where mass-charge ratios are stored together with their relative abundances to generate the MS/MS spectrum.

The fragmentation of a precursor peptide bond is determined by the properties of the peptide and the energy of CID. Fig. 4.1 illustrates how a peptide with four amino acids can be cleft into different fragmentations [57], [58]. There are three different types of bonds in a peptide, *i.e.*, CH-CO, CO-NH and NH-CH bonds. Each bond breakage produces two pieces. Therefore, there are six likely types of fragment ions for each amino acid residue: the N-terminal a, b, c fragments and C-terminal x, y, z fragments. The most common cleavage happens at CO-NH bonds by low-energy

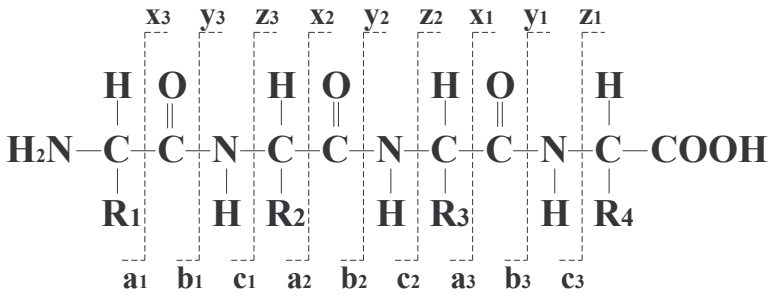

Figure 4.1. Structure of a peptide consisting of four amino acids linked by the C-N bonds. Six different types of fragment ions are produced by CID, *i.e.*, a, b, c type fragment ions with N-terminal and x, y, z type fragment ions with C-terminal.

CID, which makes b- and y-ions dominant fragment types. For a peptide consisting of n amino acids, the possible number of fragment ions is $6(n-1)$.

Though the m/z ratios of fragment ions provide informative information for protein identification, no knowledge about the cleavage positions or charge of fragments is provided. In addition, contamination and inaccuracy of instrument may generate fake m/z ratio peaks. Consequently successful identification of protein structure still remains a challenging task. Current endeavors to unambiguous peptide identification can be generalized into two classes: *database search algorithms* and *de novo sequencing algorithms*. In the first, one seeks to determine the peptide sequence by the best match by comparing the experiment spectrum with the theoretical spectrum generated from a candidate peptide list which is obtained from a protein database [56], [58], [59], [60], [61], [62]. The early popular SEQUEST computes the cross correlation value (Xcorr) between the experimental MS/MS spectrum and the hypothetical spectra generated from candidate peptides in the database with the same mass [60]. The candidate peptide producing the highest Xcorr value comes to be the first hit. However, a drawback of this algorithm is that its scoring function is not based on a rigorous probability manner. ProteinProspector is composed of several tools for mining sequence databases in conjunction with mass spectrometry

experiments [63]. It takes into account the impact of mass measurement accuracy on protein identification experiment. Mascot computes the probability based scoring to obtain the significance of the observed match between the experimental data and mass values calculated from a candidate peptide [64]. SCOPE calculates the probability density function based on a two-step model, *i.e.*, the probability of a particular fragmentation pattern of a peptide and the probability that the observed spectrum is generated by the fragmentation pattern of the peptide [59]. It is assumed that fragments are independent in order to make its complex probability problem computable. ProbID makes use of the Bayesian approach as the basis for the probabilistic score function [56]. It calculates the final posterior probability by considering several contributing factors. Despite the simple approach, the performance of this algorithm is comparable to industry-standard software. Lu and Chen propose a suffix tree based approach to identify peptide sequence [61]. The construction and search of suffix tree are performed within the reasonable time. To rank candidate peptide sequences, a SEQUEST-like scoring function is used. Fu *et al.* introduce a scoring algorithm by considering the correlative information among fragment ions to improve the peptide identification accuracy [58]. The Kernel Spectral Dot Product (KSDP) extended from SDP is used as a scoring method. The success of all these algorithms depends largely on the completeness of database and the robustness of the scoring metrics, and can not be used for the identification of proteins from unknown genomes.

On the other hand, *de novo* algorithms rely heavily on the MS/MS spectrum for the determination of peptide sequence, and often do not use a database. SHERENGA constructs an optimal path scoring in the spectrum graph, and automatically learns fragment types and intensity thresholds from test spectra [53]. Lutefisk converts an experimental spectrum into a spectrum graph of their corresponding b type ion masses to make a sequence graph [65]. To identify variants of known proteins in

database, sequence candidates obtained from Lutefisk can be used as input. PEAKS uses the dynamic programming to compute 10000 sequences with the highest scores [55]. It shows not only the confidence level of each output sequence but also the confidence level of each amino acid in the sequence. For each mass, this method first computes the reward and penalty. The reward is given, if there is a peak close to the mass, otherwise penalty. This algorithm tries to find a sequence such that its y and b ions maximize the total rewards at their mass values. Yan *et al.* propose a novel graph approach to solve the problem of separating b-ions from y-ions, in which two types of edges are considered: a type-1 edge connects two peaks possibly of the same ion types and a type-2 edge connects two peaks possibly of different ion types [66]. This algorithm does not deal with the PTM (Post-Translational Modification) problem. Jarman *et al.* present a partial peptide identification based on a model of random sequence probability and the evidence defined as the instances of consecutive subsequences [67]. In this paper, the sequence hierarchy is used to represent a family of candidate partial peptides. Recently, Frank and Pevzner presented a new peptide sequencing algorithm using a probabilistic network for a scoring scheme that assigns a relevance score to peptide prefix masses [68]. The probabilistic network represents three different types of relations such as correlations between fragment ions, the positional influence of the cleavage site and the influence of flanking amino acids to the cleavage site. These factors help to improve the accuracy of the peptide sequencing algorithm. Majority of *de novo* algorithms employs a graph theory through which the experimental spectrum is transformed into a spectrum graph. Each peak in the spectrum is converted into several nodes representing different ion types. Two nodes are connected by an edge if the mass of an amino acid is approximately equal to the difference between the two nodes. For the final resulting directed acyclic graph (DAG), each path from start node to end node corresponds to a candidate sequence.

Regardless of the different mechanisms, a lot of research focus has been put on effective scoring metrics which is doubtlessly essential for unambiguous peptide identification. However, robust selection of peptide candidates can not only improve the computation, but also can eliminate false positives. In this paper, we will present an effective and efficient two-way *de novo* searching algorithm to reduce the number of candidate sequences dramatically by utilizing the properties of MS/MS spectrum and the confidence measurement based on the intensity values of spectrum. To make a spectrum graph, the decision of start and end position is very important. We also introduce the new positioning method. Experimental results demonstrate the performance and efficacy of our novel approach and the positioning method is correct for precursor charge +1 and +2.

This paper is organized as follows. In Section 4.2, we give a detailed description of our algorithm which embodies properties of MS/MS spectrum, relation between the precursor m/z and mass of peptide, normality test, and an elaboration of our two-way searching algorithm. Then in Section 4.3, we test our algorithm on public data, and finally we close our paper by conclusion and future work.

4.2 Algorithms

4.2.1 Random peptide sequence denotation

We will first introduce several peptide notations before moving on to the proposed algorithms. Let Σ be the alphabet set which consists of 20 amino acids. And each amino acid has a distinctive mass which is represented by $m(a)$, $a \in \Sigma$. By denoting the product of Σ_1 and Σ_2 as $\Sigma_1 \times \Sigma_2 = \{ab \mid a \in \Sigma_1 \text{ and } b \in \Sigma_2\}$, the following expressions $\Sigma^1 = \Sigma$, $\Sigma^2 = \Sigma \times \Sigma$, and $\Sigma^n = \Sigma \times \Sigma^{n-1}$ are possible. Σ^n means a set that includes all possible sequences with length n, whose number of

elements $|\Sigma^n|$ is 20^n. So the set Σ^+ consisting of all possible sequences with different lengths made by 20 amino acids can be written as

$$\Sigma^+ = \Sigma^1 \cup \Sigma^2 \cup \cdots \cup \Sigma^n \cup \cdots = \bigcup_{i=1}^{\infty} \Sigma^i. \tag{4.1}$$

Obviously $\Sigma = \{\text{A, C, } \ldots, \text{ Y}\}$, and the power expressions of Σ indicating peptides with different lengths are defined recursively as $\Sigma^1 = \{\text{A, C, } \ldots, \text{ Y}\}$, $\Sigma^2 = \{\text{AA, AC, } \ldots, \text{ AY, CA, CC, } \ldots, \text{ CY, YA, YC, } \ldots, \text{ YY}\}$, etc.. The union of all possible peptides is $\Sigma^+ = \{\text{A, C, } \ldots, \text{ Y, AA, AC, } \ldots, \text{ YY, AAA, AAC, } \ldots, \text{ YYY, } \ldots\}$.

A parent peptide $P = p_1 p_2 \ldots p_n$ is a sequence of amino acids, which consists of n amino acids. And the mass of peptide P is $m(P) = \sum_{i=1}^{n} m(p_i)$ where $P \in \Sigma^n$ and the mass of each amino acid is $m(p_i)$. Let T be an element of Σ^+, *i.e.*, $T \in \Sigma^+$. If the mass of T is approximately equal to that of the target peptide P, *i.e.*, $|m(T) - m(P)| < \epsilon$, T will be one candidate sequence with respect to the parent peptide. ϵ is the tolerant error the mass spectrometer has.

4.2.2 Properties of MS/MS spectrum

The actual mass of peptide P can be written as $18+m(P)$. Number 18 comes from two extra hydrogen atoms and one extra oxygen atom at the C- and N-terminals where the mass of one hydrogen atom is approximately 1 Da (Dalton) and the mass of one oxygen atom is approximately 16 Da. The mass of b-ion with i amino acids, represented by b_i, can be computed as

$$b_i = 1 + m(p_1) + \cdots + m(p_i) = 1 + \sum_{j=1}^{i} m(p_j) \tag{4.2}$$

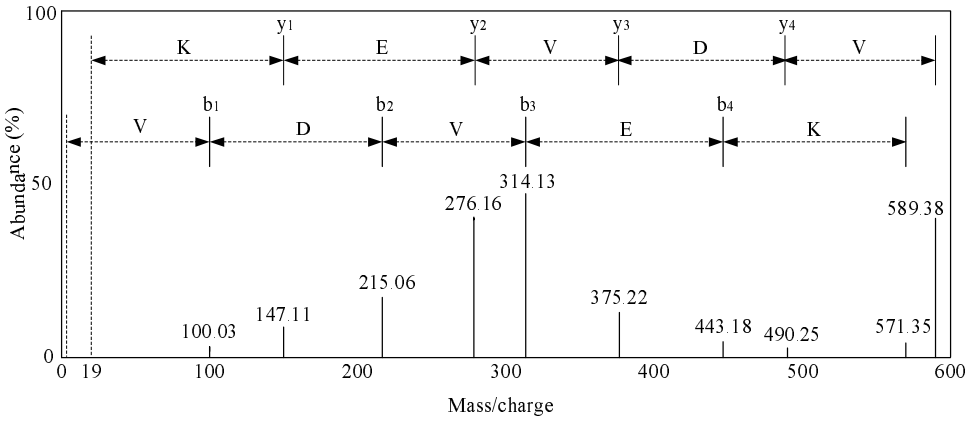

Figure 4.2. Hypothetical MS/MS spectrum and amino acid sequences.

where mass 1 comes from one hydrogen atom attached to the b-ion type fragments. Similarly, the mass of y-ion with i amino acids, denoted by y_i, can be calculated by

$$y_i = 19 + m(p_{n-i+1}) + \cdots + m(p_n) = 19 + \sum_{j=n-i+1}^{n} m(p_j) \tag{4.3}$$

where mass 19 is due to three hydrogen atoms and one oxygen atom linked to the y-ion type fragments.

The difference of m/z ratio of two adjacent singly-charged b- or y-ions is the exact mass of one residue. However, in real MS/MS spectra, an ion may be charged with different values (+1, +2, ...), which make several different peaks. In addition, there is no information about the fragment ion type (b, y, ...) and fragmenting position. For a tandem mass spectrometry, we suppose that each fragment ion has a unique mass-charge ratio and each amino acid is fragmented. Therefore, the m/z value of an ion is equal to the mass of the ion. Before introducing our Two-way Searching Algorithm in Section 4.2.5, following two properties will be presented:

Property One: If the mass-charge ratio of precursor is given, then the positions of start and end nodes for both b- and y-ion series are known. (More details will be

provided in Section 4.2.3).

Proof: Start nodes are always at 1 m/z for b-ion series and 19 m/z for y-ion series in the spectrum because of the extra attachments as explained above. And the end nodes of b- and y-ion series will happen at $m(P) + 1$ m/z and $m(P) + 19$ m/z, respectively by Eq. (4.2) and (4.3). Therefore, the m/z positions of b_1, y_1, b_{n-1}, and y_{n-1} can be expressed as $b_1 = 1 + m(p_1)$, $y_1 = 19 + m(p_n)$, $b_{n-1} = m(P) + 1 - m(p_n)$, and $y_{n-1} = m(P) + 19 - m(p_1)$ respectively.

Furthermore, let $S = \{(S_i, I_i) \mid 1 \leq i \leq k\}$ be an MS/MS spectrum ordered by m/z values where S_i and I_i denote the position and intensity of the i-th peak, and k is the number of peaks. Then the position of b_i in the spectrum is determined by the m/z value with the largest intensity I_j within the tolerant error.

$$b_i = \underbrace{\text{argmax}}_{S_j}\{I_j \mid |S_j - b_{i-1} - m(a)| < \epsilon\} \tag{4.4}$$

where $a \in \Sigma$. The same rule is applied to y_i position locating.

Property Two: There exists a pair-wise relationship between peaks in the b- and y-ion series. That is, the sequence identified in the b-ion series is the same as that identified in the y-ion series in the reversed order.

Proof: We can derive the equation $b_i + y_{n-i} = 20 + m(P)$ from Eq. (4.2) and (4.3). Therefore, b_i and y_i can be expressed as $b_i = 20 + m(P) - y_{n-i}$ and $y_i = 20 + m(P) - b_{n-i}$, respectively. This means that the sequence of b-ion series is the same as that of y-ion series in the reverse order. Fig. 4.2 shows the two properties of an MS/MS spectrum.

Table 4.1. Upper tail percentage points for Anderson-Darling statistic A^*.

α	0.2	0.15	0.1	0.05	0.025	0.01	0.005
A^*_α	0.509	0.561	0.631	0.752	0.873	1.035	1.159

4.2.3 Relation between the precursor m/z and mass of peptide

To simultaneously identify peptide from both the start and end nodes, knowledge of the positions of these nodes is important. Since the end nodes of b- and y-ion series happen at $m(P) + 1$ m/z and $m(P) + 19$ m/z, information about the mass of the target peptide sequence is required which can be obtained based on the precursor information. Let the m/z of precursor be P^z, where z is the charge of the ion. When $z = 1$, the positions of end node of b- and y-ion series are $P^1 - 18$ and P^1, because of $P^1 - 19 \approx m(P)$.

For $z \geq 2$ the above equation can not be used any more. Through experiment, the following equation is formed based on some heuristic δ value:

$$P^2 \times 2 - \delta - 19 \approx m(P) \tag{4.5}$$

where $0.9 \leq \delta \leq 1.0$. Therefore, for P^2 the positions of end node of b- and y-ion series are $P^2 \times 2 - \delta - 18$ and $P^2 \times 2 - \delta$, respectively. The position of start node in P^2 is the same as that of P^1. We used $\delta = 0.95$ in our experiment and showed δ can be used as the pertinent adjusted value.

4.2.4 Normality Test

One assumption we used in our *de novo* peptide sequencing is that the measured mass-charge ratio can be modelled as a normal distribution as other researchers have done [59], [63]. We performed a goodness of fit test to confirm whether we can use

Table 4.2. Normality test for distribution of measured mass-charge ratios.

i	$X_{(i)}$	$(X_{(i)} - \mu)/\sigma$	$F(Z_{(i)})$	$\ln(F(Z_{(i)}))+ \ln(1 - F(Z_{(r+1-i)}))$
1	0.006	-1.168	0.121	-5.314
2	0.009	-1.119	0.132	-12.626
3	0.028	-0.844	0.199	-17.774
4	0.037	-0.715	0.237	-16.947
5	0.043	-0.634	0.263	-19.084
6	0.089	0.029	0.512	-15.255
7	0.094	0.110	0.544	-11.885
8	0.109	0.321	0.626	-11.097
9	0.161	1.065	0.857	-6.411
10	0.171	1.210	0.887	-4.958
11	0.208	1.744	0.959	-3.588

the normal distribution as analysis model for our experiment data set or not. There are several approaches for assessing the underlying distribution of a data set. Among them, Anderson-Darling (AD) test which belongs to a class of distance test is known as a more powerful test than other distance tests. AD test shows a good performance in small samples as well as large samples. When the number of measured mass-charge ratios with respect to the center one within the tolerant error is sparse, AD test is more appropriate because of applying the cumulative distribution function(CDF) of the data set.

To test the normality, we define hypotheses:

H_0 : The distribution for the data set is a normal distribution.

H_1 : The distribution for the data set is a non-normal distribution.

Let X be a random sample $X = (X_{(1)}, X_{(2)}, \ldots, X_{(r)})$ sorted in the ascending order with sample size r. The standardized value is $Z_{(i)} = (X_{(i)} - \mu)/\sigma$ where μ and σ denote mean and variance for the sample data. The AD normality test calculates the following function:

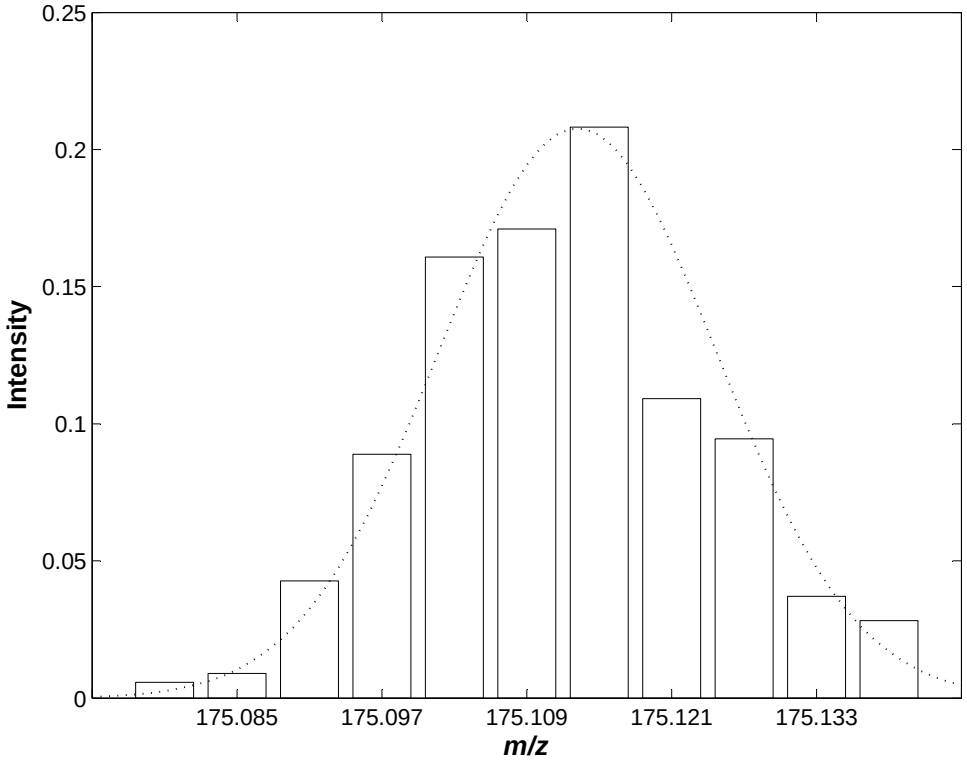

Figure 4.3. Measured mass-charge ratios (solid line bar) and normal distribution (dotted curve).

$$AD = -\frac{1}{r}\{\sum_{i=1}^{r}(2i-1)\ln F[Z_{(i)}](1-F[Z_{(r+1-i)}])\} - r \tag{4.6}$$

where F is the standard normal cumulative probability and ln is the natural logarithm (base e). Eq. (4.6) is modified by computing

$$A^* = AD(1 + \frac{0.75}{r} + \frac{2.25}{r^2}). \tag{4.7}$$

If A^* exceeds the selected critical values given in Table 4.1, we will reject the null hypothesis at the $100\alpha\%$ level.

As an example for peptide YLYELAR shown in Fig. 4.3, we normalize the intensities of all peaks such that the highest peak has one and extract those with more than 1 % (0.00208) of maximum intensity (0.208). So we obtain the sample data

(0.006, 0.009, 0.043, 0.089, 0.161, 0.171, 0.208, 0.109, 0.094, 0.037, 0.028). Mean and variance of these intensities are $\mu = 0.087$ and $\sigma = 0.069$. We obtained $AD = 0.358$ and $A^* = 0.389$ through the procedure shown in Table 4.2. At level of significance 0.1, $A^* = 0.389 \leq \alpha = 0.631$. Therefore, we can assume normality for distribution of measured mass-charge ratios. Fig. 4.3 represents the distribution of measured mass-charge ratios and normal distribution. In general, if the p-value is 0.1 or more, we can assume normality.

We found most measured mass-charge ratios are self-centered normal distribution. Therefore the application of normal distribution as the fundamental frame in the following scoring function is legitimate.

4.2.5 Two-way searching algorithm

4.2.5.1 Peptide candidate initial filtering by two-way searching

Our new two-way searching algorithm for MS/MS peptide sequencing begins with both start and end position localizations. In our approach, the positions of start and end nodes for b-ion and y-ion are determined in advance in the MS/MS spectrum, *i.e.*, at 1 and $m(P)+1$ m/z for b-ion series, and at 19 and $m(P)+19$ m/z for y-ion series as shown in Fig. 4.2. During our two-way parallel searching, these four initial nodes will extend simultaneously by scanning the whole spectrum, where start nodes for b- and y-ion series proceed simultaneously in the forward direction, and end nodes in the backward direction at the same time. This procedure keeps going until some requirements are met. We denote the direction from low m/z to high m/z as the forward direction and from high m/z to low m/z as the reverse direction.

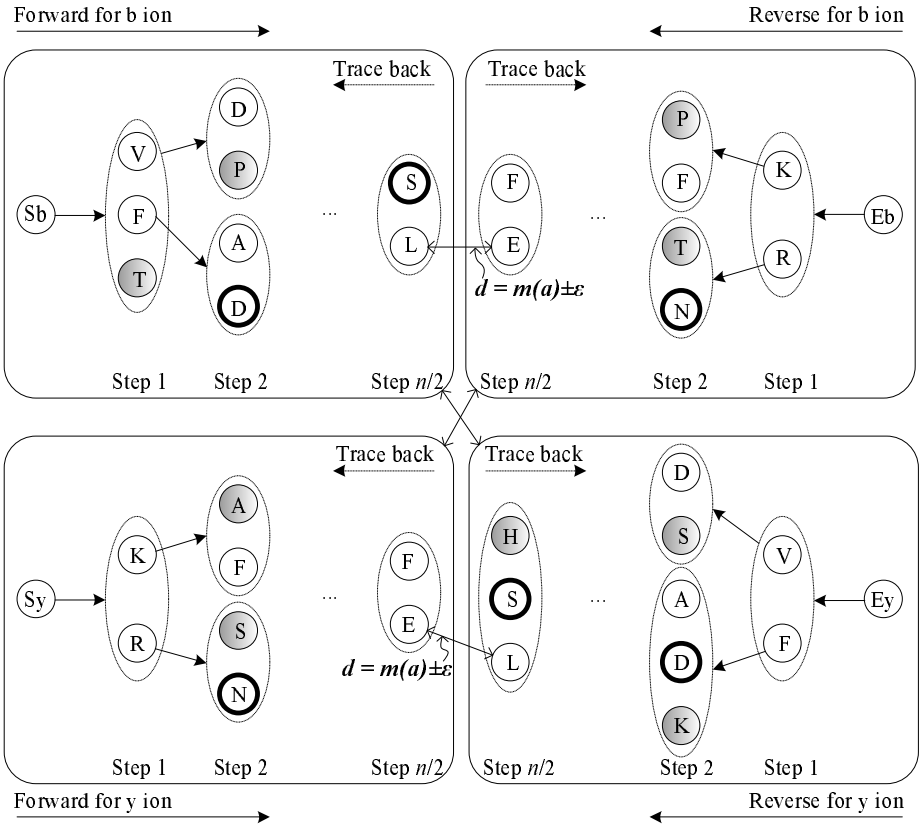

Figure 4.4. Two-way searching algorithm. Sb and Eb represent the start and end nodes of b-ion series, respectively. Sy and Ey represent the start and end nodes of y-ion series, respectively. Amino acid sets Fb and Ry always have the same amino acids. Same to sets Rb and Fy. Amino acids with gray color are deleted in the comparison procedure and amino acids with thick boundaries are removed in the further pruning procedure.

Four amino acid sets generated in the process of graph extension are denoted as Fb (forward for b-ion), Rb (reverse for b-ion), Fy (forward for y-ion), and Ry (reverse for y-ion) as shown in Fig. 4.4. At every extension of the graph, the candidate amino acids of Fb are compared with those of Ry. The common amino acids are kept and new nodes are added in positions corresponding to the m/z values. And the amino acids which are not in common are eliminated to reduce the computational burden. Likewise, the amino acids of Rb are compared with those of Fy simultaneously.

In stead of exhaustively checking all possible paths, we reduce the number of nodes in the spectrum graph effectively through such a method. Consequently it reduces the number of candidate sequences and computational cost to determine a sequence with the best score. After the successive progress, when the nodes of Fb meet those of Rb within the error range, *i.e.*, $|b_i - b_j| < \epsilon$, $bi \in Fb$, and $bj \in Rb$, we merge two nodes into one and trace back in the two-way direction while storing the amino acids.

Finally, the two partial amino acids are concatenated into one complete sequence which will be used as one candidate sequence. It is also possible that these processes confront with a distance, which corresponds to one amino acid between Fb and Rb nodes, *i.e.*, $|bi - bj - m(a)| < \epsilon$, $bi \in Fb$, $bj \in Rb$, and $a \in \Sigma$. If nodes of both sides cross over, the nodes disappear from the graph. The number of steps to obtain amino acid sequences of the same length as the target peptide is $\lceil n/2 \rceil$. The same rule is applied to Fy and Ry. Fig. 4.4 shows a diagram representing our algorithm.

Since the b- and y-ions may lose a water or ammonia molecule, it is necessary to employ all the related ion types for the series. Ions b, b - H_2O, and b - NH_3 for b-ion series are considered in the forward and reverse direction, which are the most frequent N-terminal ions, and y, y - H_2O, and y - NH_3 for y-ion series. In addition, we consider the a-ion which is also a dominant ion. After the initial filtering, we have a reduced amino acid candidate pool. Next we will introduce further pruning of candidate amino acids by a scoring function to determine the best sequence.

4.2.5.2 Scoring function for final candidate screening

By utilizing the piece-wise local region intensity values of MS/MS, we define an evidence based scoring function for screening out the best optimal peptide candidate.

Based on the normality test verification introduced in Section 4.2.4, we can let I_{bi} be the Gaussian sum of all peak intensities close to b_i within a tolerant error ϵ:

$$I_{bi} = \sum_{b_i+\epsilon}^{b_i-\epsilon} \frac{I_j}{I_M} \exp(-(S_j - b_i)^2/2\sigma^2) \tag{4.8}$$

where I_M is the highest intensity in the whole spectrum and I_j is the individual peak intensity of the local region. In the procedure of normalization, intensities of all peaks are divided by the highest intensity. Standard deviation σ represents to which extent the peak positions in the experimental spectrum deviate from the theoretical ones. Without loss of generality based on the normality test, we can assume the peak having the highest intensity in the whole spectrum is most likely to be a real fragment and neighbor peaks close to the peak will form the normal distribution. Standard deviation σ can be heuristically determined by

$$\sigma_{min} = \underbrace{\text{argmin}}_{\sigma} \sum_{b_i+\epsilon}^{b_i-\epsilon} (\exp(-(S_j - S_M)^2/2\sigma^2) - \frac{I_j}{I_M}) \tag{4.9}$$

where S_M is the m/z value corresponding to the highest intensity I_M.

Let x be the mass of b-ion, then the masses of a-ion, b - H_2O, and b - NH_3 are $x - 28$, $x - 18$, and $x - 17$, respectively, *i.e.*, differences $\triangle = \{$-28, -18, -17$\}$. Given the b_i we define

$$I_{bi\ -\ NH_3} = \sum \frac{I_j}{I_M} \exp(-(S_j - S_{b_i-NH_3})^2/2\sigma^2) \tag{4.10}$$

where $S_{b_i-NH_3} = \underbrace{\text{argmax}}_{S_j}\{I_j \mid |b_i - S_j - 17| < \epsilon\}$.
Likewise, we can compute $I_{b_i-H_2O}$, I_{b_i-a}, I_{y_i}, $I_{y_i-H_2O}$ and $I_{y_i-NH_3}$. The total intensity of ions related to b_i is

$$I_{Tbi} = I_{bi} + I_{bi-NH_3} + I_{bi-H_2O} + I_{bi-a}. \tag{4.11}$$

And I_{Tyi} is expressed as follows

$$I_{Tyi} = I_{yi} + I_{yi-NH_3} + I_{yi-H_2O}. \tag{4.12}$$

The total intensity of b-ion series in the forward direction is

$$I_{Fb} = \sum_{i=1}^{n/2} I_{Tbi} \tag{4.13}$$

where n is the number of steps to obtain the peptide sequence. The total intensity of b-ion series in the reverse direction is

$$I_{Rb} = \sum_{i=(n/2)+1}^{n-1} I_{Tbi}. \tag{4.14}$$

Similarly, we can compute I_{Ry} and I_{Fy}. A legitimate intensity scoring function is obtained by summing the four direction total intensities and the top scoring sequence among all candidate sequences becomes the best candidate:

$$Scoring = I_{Fb} + I_{Rb} + I_{Fy} + I_{Ry}. \tag{4.15}$$

This scoring function is reasonable because many of the noise peaks have a low intensity value. By incorporating abundance difference of b- and y-ions, *i.e.*, y-ions are usually more ample than b-ions, we may apply different weights to the total summing intensity of b-ion series and the total summing intensity of y-ion series. Then, the scoring function can be modified as

$$Scoring = \lambda(I_{Fb} + I_{Rb}) + (1 - \lambda)(I_{Fy} + I_{Ry}). \tag{4.16}$$

Obviously λ is set as less than or equal to 0.5.

Before the scoring function is applied, for further pruning of candidate pool, we define a screening criterion from the calculation of total intensities I_{Tbi} and $I_{Ty(n-i)}$

Table 4.3. Experimental results of peptide sequencing with $\beta = 35\%$ ($\beta = 20\%$ for 678.3 m/z) in our method. For comparison, Lutefisk was performed. We cannot distinguish between the isobaric amino acid pairs leucine (L) and isoleucine (I), and glutamine (Q) and lysine (K) as with most *de novo* methods where m(I)=m(L)=113.16 Da, m(Q)=128.13 Da, m(K)=128.17 Da. The value shown in brackets represents an approximate mass of the remaining amino acid residues.

Spectrum	z	Correct sequence	Two-way searching algorithm		Lutefisk	
			Sequence	Rank	Sequence	Rank
634.4	1	IFVQK	**LFVQK**	1	**LFVQK**	1
678.3	1	YIPGTK	**YLPGTK**	1	**YLPGTK**	1
779.4	1	MIFAGIK	**MLFAGLK**	2	[244.12]**FAGLK**	1
927.4	1	YLYEIAR	**YLYELAR**	1	[276.11]**YE**[184.08]**R**	1
584.8	2	TGPNLHGLFGR	**TGPNLHGLFGR**	3	[409.25]**R**	1
689.9	2	HGTVVLTALGGILK	**HGTVVLTALGGLLK**	3	[194.08][WY]**K**	2
728.8	2	TGQAPGFSYTDANK	**TGQAPGFS**PQQP**NK**	1	AQGT[HS]**K**	3
792.9	2	KTGQAPGFSYTDAN	**KTG**AG**AP**AMAPQG**DAN**	1	[209.58]NH**ANK**	3
943.0	2	YLEFISDAIIHVLHSK	**YLEFL**ALTT**LHVLHSK**	3	[222.56]**HVLH**[215.12]	1

of ions in the i-th step of graph extension where $|b_j - b_{j-1}| \approx |y_{n-j+1} - y_{n-j}| \approx m(a)$ with $b_{-1} = \mathrm{S_b}$, $y_n = \mathrm{Ey}$ and $1 \leq j \leq i$. This screening criterion is used at every step of node extension of the spectrum graph. Suppose there exist q candidate amino acids in the i-th step after eliminating amino acids which are not in common between Fb and Ry. Let I_i be a set whose elements indicate the sum of I_{Tbi} and $I_{Ty(n-i)}$ where b_i and y_{n-i} are a complementary ion pair.

$$I_i = \{{I_{Tbi}}^1 + {I_{Ty(n-i)}}^1, \ldots, {I_{Tbi}}^q + {I_{Ty(n-i)}}^q\} \tag{4.17}$$

The elements in set I_i are sorted in ascending order, and the first $\beta\%$ amino acids are removed from Fb and Ry. The same rule is applied to every step of Fy and Rb.

4.3 Experimental Results

The two-way peptide sequencing algorithm was implemented by using C++ codes. We employed nine data sets whose ground truths were given, among which

Table 4.4. The number of candidates and rankings as the screening ratio changes. The numerator indicates the ranking of the correct sequence our algorithm made, and the denominator represents the total number of candidate sequences. 0% means no screen is adopted.

Spectrum	0%	10%	20%	30%	40%	50%	60%
634.4	1/91	1/27	1/21	1/19	1/14	1/12	0/6
678.3	1/1	1/1	1/1	0/0	0/0	0/0	0/0
779.4	2/173	2/152	2/93	2/64	2/10	2/6	2/6
927.4	1/5197	1/819	1/360	1/239	1/195	1/126	1/24

four data sets with precursor charge +1 and five data sets of +2. These data sets were obtained from QSTAR instrument. In this study, we used $\epsilon = 0.3$ and $\lambda = 0.5$.

Table 4.3 shows results of our algorithm with $\beta = 35\%$ ($\beta = 20\%$ for spectrum 678.3 m/z) as a screening criterion on $\delta = 0.95$. To show the result which is most optimal to benchmark, instead of listing the most optimal identified peptide, *i.e.*, the one with highest scoring value or with ranking 1, we show the sequence which is within ranking 3 range. We compared results of the proposed method with those of Lutefisk [65]. Lutefisk converts an experimental spectrum into a sequence graph where partial sequences are examined. To reduce candidates, after finding complete sequences, sequences that appear to have been derived from alternating b-type and y-type ions and that are derived mostly from the low-mass fragments are discarded. Finally, Lutefisk yields at most 50 candidates. Users can set the parameter. When we set the parameter as the maximum value, 50, 45, 50 and 50 candidates were made in 634.4, 678.3, 779.4 and 927.4 m/z, respectively.

For precursor charge +2, we found that there exists an equation $P^2 \times 2 - \delta - 19 \approx m(P)$ where $0.9 \leq \delta \leq 1.0$. We used $\delta = 0.95$ to determine the position of end node in the graph extension. This value is greater than our tolerant error 0.3. Therefore

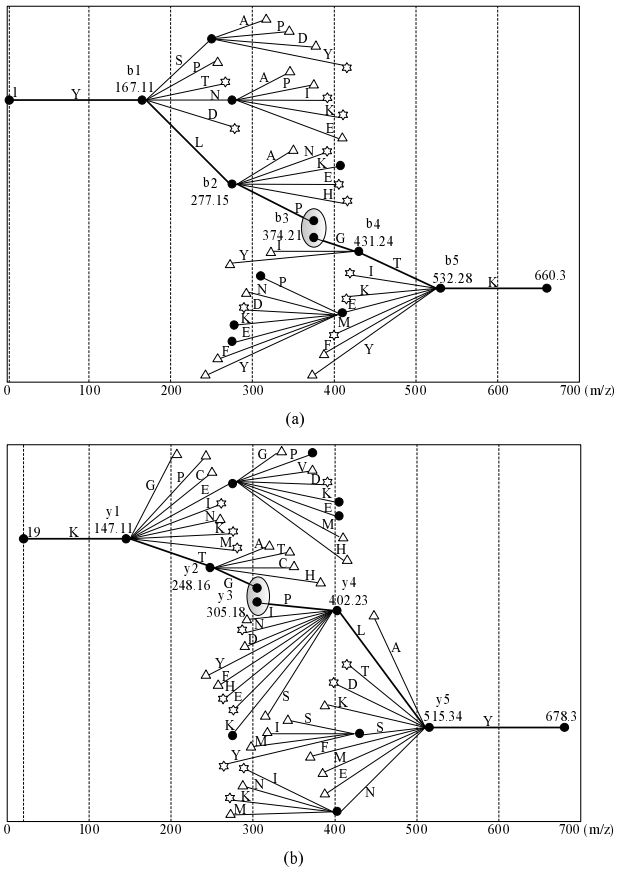

Figure 4.5. Example of peptide sequence YIPGTK in the graph extension: (a)The sequence of b-ion series; (b) The sequence of y-ion series. Amino acids with triangle symbols are deleted in the procedure of comparison and amino acids with star symbols are removed from the candidate amino acid pool in the procedure of further pruning. Amino acids represented in black circles are reserved. Thick line presents the path of one candidate sequence.

if we use $P^2 \times 2 - 19 \approx m(P)$ as the position of end node as in other methods which proceed in the forward direction only, our algorithm will not provide good answers. Thus the positions of end node of b- and y-ion series are respectively $P^2 \times 2 - 0.95 - 18$ and $P^2 \times 2 - 0.95$. For example for spectrum 584.8 *m/z*, the end nodes of b- and y-ion series come to appear in the $584.8 \times 2 - 0.95 - 18 = 1150.65$ *m/z* and $584.8 \times 2 - 0.95 = 1168.65$ *m/z*. The position of start node in P^2 is the same as that of P^1. Our algorithm came up six sequences identical with ground truth.

Table 4.4 shows the number of candidates change as the screening criterion β varying from 0% to 60% for the charged +1 sequences. Although β changes, the rankings remain unchanged. For spectrum 678.3 *m/z*, since the number of candidates after initial two-way searching was reduced to only one as seen in Fig. 4.5, no screen was applied. With 10% further pruning at every step of graph extension, we can reduce the number of candidates significantly up to 70% and 84% for spectra 634.4 and 927.4 *m/z*, respectively. Therefore, by adopting a proper screening criterion to our algorithm, we can reduce the processing time effectively.

4.4 Conclusion

In this paper, we presented a novel *de novo* approach called two-way searching algorithm for determining the sequence of peptide. The main contribution of this paper lies in the greatly reduced number of peptide candidates. Based on the property that the same identification of peptide sequence will be resulted from b-ion or y-ion series, we obtained a list of peptide candidates by simultaneously searching from four different start and end positions and filtering out peptide sequences which violate this property. The initially filtered candidate pool is further pruned by incorporating a screening criterion based on the local region intensities of the spectrum. The final optimal best candidate is singled out based on the highest confidence defined as the global intensity from two-way search results. Contributions of this paper also come from the determination of the end nodes for b and y-ion series in the case of the charged +2 precursor. For the future work, we will improve our algorithm by introducing gap edges corresponding to the di- and tri-peptides in a spectrum graph. Also we will modify the scoring algorithm by using a probabilistic model to make the pruning more robust.

CHAPTER 5

FAST KERNEL DISCRIMINANT ANALYSIS FOR DIAGNOSIS OF ALZHEIMER DISEASE STAGE USING MASS SPECTRA

5.1 Introduction

Alzheimer's disease (AD) is characterized by progressive memory loss and other impaired abilities to carry out daily activities. AD is the most common form of dementia in people over age 65. The risk increases with age. It is estimated that as many as 4.5 million in the United States suffer from the disease. One of the causes of AD is genetic mutation which leads to accumulation of beta amyloid protein in the brain. Amyloid plaques and neurofibrillary tangles are considered signs of AD. Unfortunately, since the ultimate cause and treatment of AD are not known, it is urgent to identify biomarkers for the disease in order to accelerate drug and therapeutic development.

Matrix-assisted laser desorption/ionization (MALDI) and surface enhanced laser desorption/ionization (SELDI) time-of-flight (TOF) mass spectrometry have increasingly been used to early disease diagnosis, monitoring disease progression and therapeutic effects of drugs [69], [70]. Currently, MALDI TOF/TOF based platform has been used for quantitative proteomics analysis. In our recent study for neurodegenerative diseases such as AD and Parkinson's disease (PD), a set of candidate biomarkers were detected and validated using LC MALDI TOF/TOF based targeted quantitative proteomics platform [71].

LDA is a traditional statistical scheme for feature reduction which has been widely used in a diversity of application areas such as face recognition [72], [73],

microarray data classification [74] and text classification [75]. In a case where the dimensionality exceeds the sample size, however, the classical LDA faces a problem known as singularity [76]. Since the dimensionality of the mass spectrometry data is considerably huge, the singularity problem necessarily happens. Several methods were proposed to overcome the limitation. Li *et al.* proposed a new LDA method named generalized linear discriminant analysis (GLDA) which solves the singularity problem and is fast in the calculation of eigenvectors [77]. Ye *et al.* developed uncorrelated linear discriminant analysis (ULDA) based on generalized singular value decomposition (GSVD) which was tested with microarray datasets [74]. Another drawback of the classical LDA is its linear property with which LDA fails for nonlinear problems [78]. To solve the problem, nonlinear based LDA methods were proposed. The main idea is to map the input space into a high dimensional feature space. In the feature space, the classical LDA is performed. Baudat and Anouar proposed a nonlinear extension of the classical LDA called generalized discriminant analysis (GDA) where experimental data in the feature space is centered by shifting feature vectors by the global centroid vector [79]. Mika *et al.* developed a nonlinear extension of Fisher's linear discriminant analysis called kernel Fisher discriminant analysis (KFD). However, KFD was designed only for two class problems [80].

In this paper, we propose a new fast kernel discriminant analysis (FKDA) which is a nonlinear extension of GLDA. To tackle the large number of peaks and noise in high-resolution MALDI-TOF data, we have developed a multi-step feature selection algorithm. We apply FKDA to the classification of AD dataset analyzed by Lopez *et al.* which consists of three classes, mild cognitive impairment (MCI), AD and normal. However, they analyzed the dataset as a binary class problem combining MCI and AD [10]. In this study, we analyze the Alzheimer dataset as three classes.

5.2 Preprocessing

In this study, we use m/z values over the mass range 1k-10k Da (Dalton) in which a raw mass spectrum contains over 750,000 m/z values. To reduce the noise and dimensionality of the raw spectrum, we employ a three-step preprocessing procedure: (1) binning, (2) baseline correction and (3) normalization. Another objective in such preprocessing tasks is to improve the performance of identifying the disease.

In the first step, binning of raw mass spectra is performed. Starting from 1k Da, a bin size of 1 Da is used, which yields about 9000 bins. For the binned spectrum, the m/z ratio represents the left boundary of an interval. The binning not only makes the spectrum smooth but also aligns m/z values in all spectra so that it facilitates the analysis of mass spectrometry data. For baseline correction, we find a minimum intensity per every 10 bins, proceeding from low mass to high mass range. And then, the baseline is estimated by fitting a fourth order polynomial to 20 minimum intensities. The regressed baseline is subtracted from the binned spectrum. Furthermore, we choose to normalize the baseline corrected spectrum because the amount of proteins varies depending on serum samples. Each spectrum is normalized by dividing the baseline corrected spectrum by its total ion current (the summed intensity over all m/z values in the baseline corrected spectrum). Because of the very small normalized intensity value, all the intensities are multiplied by 1000 for computational convenience. As shown in Fig. 5.1 (d), our preprocessing task appears to be satisfactory because almost all significant peaks are retained.

5.3 Method

Classifiers based on discriminative learning try to find a decision boundary that maximizes separation between classes. SVM is a popular learning algorithm to

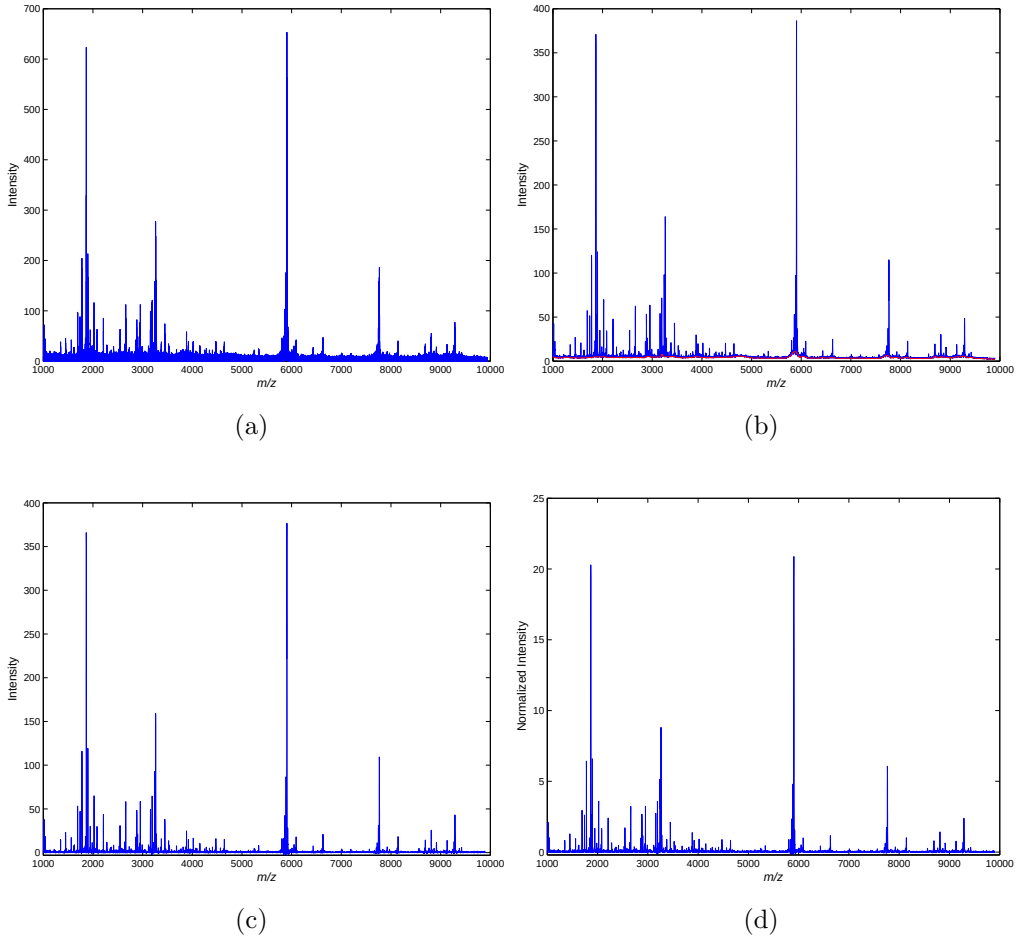

Figure 5.1. Mass spectrum of a sample in Alzheimer dataset over the mass range 1k-10k Da: (a) raw spectrum, (b) binned spectrum, (c) baseline corrected spectrum, (d) normalized spectrum. In (b), the red line indicates the baseline.

solve two-class classification problems [27], [38], [28], [37]. An optimal hyperplane that separates a given set of binary labeled training data is built by maximizing margin between two classes. LDA is very similar to SVM in the underlying idea. A distinct difference is that LDA looks for the decision boundary using all training samples, while SVM uses only support vectors that are close to the decision boundary. Also SVM was basically designed for two-class classification problems, while LDA has the ability to classify multi-class samples. However, the classical LDA

might fail in nonlinear problems due to its linearity property. Another issue is that in many real datasets where the dimensionality is larger than the number of samples the singularity problem arises. In this study, we propose a novel kernel based discriminant analysis algorithm for classifying multi-class samples that can overcome the singularity problem in the classical LDA with an efficient method.

A given data set of n samples, each of which consists of l features, is represented as $X = [\mathbf{x}_1, \cdots, \mathbf{x}_n] \in R^{l \times n}$. Suppose that the data set is clustered to c classes $[N_1, \cdots, N_c]$ where each class X_i has n_i samples, *i.e.*, $X = \bigcup_{i=1}^{c} N_c$ and $n = \sum_{i=1}^{c} n_i$. In nonlinear discriminant analysis, the input data space R^l is mapped into the higher feature space $F \subset R^m$ via a nonlinear mapping function Φ. Unfortunately, we cannot explicitly observe the data in the feature space F. An alternative method is to use the kernel function that defines the inner product in the feature space. More specifically, if the kernel function k satisfies Mercer's condition, there exists a mapping Φ such that

$$k(x, y) = \ < \Phi(x), \Phi(y) > . \tag{5.1}$$

The main idea of the nonlinear discriminant analysis is to solve the LDA problem in the feature space by maximizing the following Fisher criterion:

$$J^{\Phi}(\mathbf{W}) = \frac{\mathbf{W^T S_b^{\Phi} W}}{\mathbf{W^T S_t^{\Phi} W}} \tag{5.2}$$

where $\mathbf{W}$ is a linear transformation matrix; $\mathbf{S}_b^{\Phi}$ and $\mathbf{S}_t^{\Phi}$ are the between-class and total scatter matrices obtained in the feature space. Suppose that p_i, $\mathbf{m}_i^{\Phi}$, $\mathbf{m}^{\Phi}$ are a prior probability of the ith class, the mean vector of the training samples of the ith class, and the mean vector across all training samples in the feature space, respectively. Then, $\mathbf{S}_b^{\Phi}$ and $\mathbf{S}_t^{\Phi}$ are defined as follows:

$$\mathbf{S}_b^{\Phi} = \sum_{i=1}^{c} p_i (\mathbf{m}_i^{\Phi} - \mathbf{m}^{\Phi})(\mathbf{m}_i^{\Phi} - \mathbf{m}^{\Phi})^{\mathbf{T}}, \tag{5.3}$$

$$\mathbf{S}_t^{\Phi} = \frac{1}{n}\sum_{i=1}^{n}(\Phi(\mathbf{x}_i) - \mathbf{m}^{\Phi})(\Phi(\mathbf{x}_i) - \mathbf{m}^{\Phi})^{\mathbf{T}}, \tag{5.4}$$

where $p_i = \frac{n_i}{n}$, $\mathbf{m}_i^{\Phi} = \frac{1}{n_i}\sum_{j\in N_i}\Phi(\mathbf{x}_j)$, and $\mathbf{m}^{\Phi} = \frac{1}{n}\sum_{i=1}^{n}\Phi(\mathbf{x}_i)$. The scatter matrices $\mathbf{S}_b^{\Phi}$ and $\mathbf{S}_t^{\Phi}$ can be decomposed as

$$\mathbf{S}_b^{\Phi} = \mathbf{M}_b\mathbf{M}_b^{\mathbf{T}} \quad \text{and} \quad \mathbf{S}_t^{\Phi} = \mathbf{M}_t\mathbf{M}_t^{\mathbf{T}} \tag{5.5}$$

where

$$\begin{aligned}\mathbf{M}_b &= [\sqrt{p_1}(\mathbf{m}_1^{\Phi} - \mathbf{m}^{\Phi}), \ldots, \sqrt{p_c}(\mathbf{m}_c^{\Phi} - \mathbf{m}^{\Phi})] \in R^{m\times c},\\ \mathbf{M}_t &= \frac{1}{\sqrt{n}}[(\Phi(\mathbf{x}_1) - \mathbf{m}^{\Phi}), \ldots, (\Phi(\mathbf{x}_n) - \mathbf{m}^{\Phi})] \in R^{m\times n}.\end{aligned}$$

By solving the generalized eigenvalue equation, the optimal discriminant vector $\mathbf{W}$ corresponding to the eigenvector of the equation can be obtained

$$\mathbf{S}_b^{\Phi}\mathbf{W} = \mathbf{S}_t^{\Phi}\mathbf{W}\Lambda, \quad \mathbf{W} = [\mathbf{W}_1, \ldots, \mathbf{W}_{c-1}] \in R^{m\times(c-1)} \tag{5.6}$$

where $(\mathbf{S}_t^{\Phi})^{-1}\mathbf{S}_b^{\Phi}$ has at most $c-1$ non-zero eigenvalues ($m >> c$). It is possible to express the eigenvector as a linear combination of the observations in the feature space. Hence we have

$$\mathbf{W}_j = \sum_{i=1}^{n}\alpha_{ij}\Phi(\mathbf{x}_i) \tag{5.7}$$

and

$$\mathbf{W} = \left[\begin{array}{c}\sum_{i=1}^{n}\alpha_{i1}\Phi(\mathbf{x}_i), \cdots, \sum_{i=1}^{n}\alpha_{i(c-1)}\Phi(\mathbf{x}_i)\end{array}\right] = \mathbf{Q}\alpha \tag{5.8}$$

where $\alpha = [\alpha_1, \ldots, \alpha_n]^{\mathbf{T}}$ is a coefficient vector and $\mathbf{Q} = [\Phi(\mathbf{x}_1), \ldots, \Phi(\mathbf{x}_n)]$. We can also express α as

$$\alpha = [\alpha^1, \cdots, \alpha^{(c-1)}] = \left[\begin{array}{ccc}\alpha_{11} & \ldots & \alpha_{1(c-1)}\\ & \vdots & \\ \alpha_{n1} & \ldots & \alpha_{n(c-1)}\end{array}\right] \in R^{n\times(c-1)}. \tag{5.9}$$

Here, we multiply both sides of the eigenvalue equation in Eq. (5.6) by $\mathbf{Q^T}$. Then, Eq. (5.6) becomes

$$\mathbf{Q^T S_b^\Phi W} = \mathbf{Q^T S_t^\Phi W}\widetilde{\Lambda}. \tag{5.10}$$

Replacing $\mathbf{S_b^\Phi}$ and $\mathbf{S_t^\Phi}$ with $\mathbf{M}_b\mathbf{M_b^T}$ and $\mathbf{M}_t\mathbf{M_t^T}$, we obtain

$$\mathbf{Q^T M}_b\mathbf{M_b^T Q}\alpha = \mathbf{Q^T M}_t\mathbf{M_t^T Q}\alpha\widetilde{\Lambda}. \tag{5.11}$$

Let $\widetilde{\mathbf{M}}_b$ and $\widetilde{\mathbf{M}}_t$ denote $\widetilde{\mathbf{M}}_b = \mathbf{Q^T M}_b$ and $\widetilde{\mathbf{M}}_t = \mathbf{Q^T M}_t$, respectively. Then, $\widetilde{\mathbf{M}}_b$ and $\widetilde{\mathbf{M}}_t$ can be expressed with the kernel function instead of the mapping function:

$$\begin{aligned}
\widetilde{\mathbf{M}}_b &= \mathbf{Q^T M}_b \in R^{n\times c} \\
&= \begin{bmatrix} \Phi(\mathbf{x}_1)^\mathbf{T} \\ \vdots \\ \Phi(\mathbf{x}_n)^\mathbf{T} \end{bmatrix} [\sqrt{p_1}\Phi_b^1 \quad \dots \quad \sqrt{p_c}\Phi_b^c] \\
&= \begin{bmatrix} \sqrt{p_1}K_b^{11} & \dots & \sqrt{p_c}K_b^{c1} \\ & \vdots & \\ \sqrt{p_1}K_b^{1n} & \dots & \sqrt{p_c}K_b^{cn} \end{bmatrix},
\end{aligned} \tag{5.12}$$

where $\Phi_b^l = \frac{1}{n_l}\sum\limits_{j\in N_l}\Phi(\mathbf{x}_j) - \frac{1}{n}\sum\limits_{i=1}^{n}\Phi(\mathbf{x}_i)$ and $K_b^{lp} = \frac{1}{n_l}\sum\limits_{j\in N_l}k(\mathbf{x}_j,\mathbf{x}_p) - \frac{1}{n}\sum\limits_{i=1}^{n}k(\mathbf{x}_i,\mathbf{x}_p)$,

$$\begin{aligned}
\widetilde{\mathbf{M}}_t &= \mathbf{Q^T M}_t \in R^{n\times n} \\
&= \begin{bmatrix} \Phi(\mathbf{x}_1)^\mathbf{T} \\ \vdots \\ \Phi(\mathbf{x}_n)^\mathbf{T} \end{bmatrix} \frac{1}{\sqrt{n}}[\Phi_t^1 \quad \dots \quad \Phi_t^n] \\
&= \frac{1}{\sqrt{n}}\begin{bmatrix} K_t^{11} & \dots & K_t^{n1} \\ & \vdots & \\ K_t^{1n} & \dots & K_t^{nn} \end{bmatrix}
\end{aligned} \tag{5.13}$$

where $\Phi_t^l = \Phi(\mathbf{x}_l) - \frac{1}{n}\sum_{i=1}^{n}\Phi(\mathbf{x}_i)$ and $K_t^{lp} = k(\mathbf{x}_l, \mathbf{x}_p) - \frac{1}{n}\sum_{i=1}^{n} k(\mathbf{x}_i, \mathbf{x}_p)$.

Substituting $\widetilde{\mathbf{M}}_b$ and $\widetilde{\mathbf{M}}_t$ into Eq. (5.11), we have

$$\widetilde{\mathbf{M}}_b\widetilde{\mathbf{M}}_b^{\mathbf{T}}\alpha = \widetilde{\mathbf{M}}_t\widetilde{\mathbf{M}}_t^{\mathbf{T}}\alpha\widetilde{\Lambda}. \tag{5.14}$$

Let $\mathbf{H}_b$ and $\mathbf{H}_t$ denote $\mathbf{H}_b = \widetilde{\mathbf{M}}_b\widetilde{\mathbf{M}}_b^{\mathbf{T}}$ and $\mathbf{H}_t = \widetilde{\mathbf{M}}_t\widetilde{\mathbf{M}}_t^{\mathbf{T}}$, respectively. Therefore, Eq. (5.14) becomes

$$\mathbf{H}_b\alpha = \mathbf{H}_t\alpha\widetilde{\Lambda} \tag{5.15}$$

where α comes to the eigenvector of $\mathbf{H}_t^{-1}\mathbf{H}_b$ in the newly defined eigenvalue equation. However, since $\mathbf{H}_t$ is singular, we cannot directly calculate the inverse matrix of it. Instead, we use simply the pseudoinverse. Let $\mathbf{H}_t^+$ denote the pseudoinverse of $\mathbf{H}_t$. To obtain α, we should calculate $\mathbf{H}_t^+$ and the eigenvector of $\mathbf{H}_t^+\mathbf{H}_b$. Both $n \times n$ matrix calculations are required. Here, to save running time and memory required to calculate α, we develop an efficient algorithm.

In deed, $\mathbf{H}_t$ and $\mathbf{H}_b$ correspond to the total scatter matrix and between-scatter matrix in the n dimensional space where the data set is represented as follows :

$$\begin{bmatrix} k(\mathbf{x}_1, \mathbf{x}_1) & \dots & k(\mathbf{x}_1, \mathbf{x}_n) \\ & \vdots & \\ k(\mathbf{x}_n, \mathbf{x}_1) & \dots & k(\mathbf{x}_n, \mathbf{x}_n) \end{bmatrix}. \tag{5.16}$$

That is, each column in the data matrix can be viewed as a data point. Now we can deal with the data set in a very reduced data space, that is, the dimensionality is reduced from m to n ($m >> n$). By singular value decomposition (SVD), $\widetilde{\mathbf{M}}_t$ can be expressed as $\widetilde{\mathbf{M}}_t = \mathbf{U}\widehat{\Lambda}^{\frac{1}{2}}\mathbf{V}^{\mathbf{T}}$ where $\mathbf{U}$ and $\mathbf{V}$ are orthonormal column matrices and Λ is a diagonal matrix with positive or zero elements in decreasing order. Then, $\mathbf{H}_t = \widetilde{\mathbf{M}}_t\widetilde{\mathbf{M}}_t^{\mathbf{T}} = \mathbf{U}\widehat{\Lambda}^{\frac{1}{2}}\mathbf{V}^{\mathbf{T}}(\mathbf{U}\widehat{\Lambda}^{\frac{1}{2}}\mathbf{V}^{\mathbf{T}})^{\mathbf{T}} = \mathbf{U}\widehat{\Lambda}^{\frac{1}{2}}\mathbf{V}^{\mathbf{T}}\mathbf{V}\widehat{\Lambda}^{\frac{1}{2}}\mathbf{U}^{\mathbf{T}} = \mathbf{U}\widehat{\Lambda}\mathbf{U}^{\mathbf{T}}$. That is, $\mathbf{U}$ and $\widehat{\Lambda}$ are the eigenvector and the eigenvalue of $\mathbf{H}_t$, respectively.

Definition (**Moore − Penrose Inverse**) *Given a matrix* $\mathbf{A}$*, a matrix which satisfies the following four equations is called Moore − Penrose inverse of* $\mathbf{A}$*.*

(1) $(\mathbf{A}\mathbf{A}^+)^{\mathbf{T}} = \mathbf{A}\mathbf{A}^+$ (2) $(\mathbf{A}^+\mathbf{A})^{\mathbf{T}} = \mathbf{A}^+\mathbf{A}$

(3) $\mathbf{A}\mathbf{A}^+\mathbf{A} = \mathbf{A}$ (4) $\mathbf{A}^+\mathbf{A}\mathbf{A}^+ = \mathbf{A}^+$

Assume that the rank of $\mathbf{H}_t$ is r. Hence, $\mathbf{H}_t = \sum_{i=1}^{r} \lambda_i u_i u_i^{\mathbf{T}}$. Here, the Moore-Penrose inverse of $\mathbf{H}_t$ can be expressed as $\mathbf{H}_t^+ = \sum_{i=1}^{r} \frac{1}{\lambda_i} u_i u_i^{\mathbf{T}} = \mathbf{U}\widehat{\Lambda}^+\mathbf{U}^{\mathbf{T}}$. Since $\mathbf{H}_t$ is positive semidefinite, $\mathbf{H}_t^{\frac{1}{2}} = \mathbf{U}\widehat{\Lambda}^{\frac{1}{2}}\mathbf{U}^{\mathbf{T}}$. Therefore, the Moore-Penrose inverse of $\mathbf{H}_t^{\frac{1}{2}}$ is $\mathbf{H}_t^{+\frac{1}{2}} = \mathbf{U}\widehat{\Lambda}^{+\frac{1}{2}}\mathbf{U}^{\mathbf{T}}$.

Corollary *Covariance matrices are always positive semidefinite. If a matrix* $\mathbf{A}$ *is positive semidefinite and* $\mathbf{A} = \mathbf{U}\mathbf{\Lambda}\mathbf{U}^{\mathbf{T}}$ *where* $\mathbf{U}$ *and* $\mathbf{\Lambda}$ *are the eigenvector and eigenvalue of* $\mathbf{A}$*, then the following equation holds:*
$\mathbf{A}^{b/a} = \mathbf{U}\mathbf{\Lambda}^{b/a}\mathbf{U}^{\mathbf{T}}$ *where* $b/a > 0$*.*

Suppose that $\mathbf{S}_b$ and $\mathbf{S}_t$ are the between scatter matrix and total scatter matrix in the input space. Then, we use $\mathbf{S}_b = \mathbf{S}_b\mathbf{S}_t^+\mathbf{S}_t$ which was proven in [77]. Likewise, since $\mathbf{H}_b$ and $\mathbf{H}_t$ are the between scatter matrix and total scatter matrix in the n dimensional space, the following equation holds:

$$\mathbf{H}_b = \mathbf{H}_b\mathbf{H}_t^+\mathbf{H}_t. \tag{5.17}$$

Similarly, $\mathbf{H}_b = \mathbf{H}_t\mathbf{H}_t^+\mathbf{H}_b$. Then, Eq. (5.15) becomes

$$\mathbf{H}_b\mathbf{H}_t^+\mathbf{H}_t\alpha = \mathbf{H}_t\alpha\widetilde{\Lambda}. \tag{5.18}$$

Let $\mathbf{K}$ denote $\mathbf{K} = \mathbf{H}_t\alpha$. Therefore, α is

$$\alpha = \mathbf{H}_t^+\mathbf{K} = \mathbf{H}_t^{+\frac{1}{2}}(\mathbf{H}_t^{+\frac{1}{2}}\mathbf{K}) \tag{5.19}$$

because of

$$\begin{aligned} J(\mathbf{H}_t^+\mathbf{K}) &= J(\mathbf{H}_t^+\mathbf{H}_t\alpha) \\ &= \mathbf{tr}((\alpha^{\mathbf{T}}\mathbf{H}_t\mathbf{H}_t^+\mathbf{H}_t\mathbf{H}_t^+\mathbf{H}_t\alpha)^{-1}(\alpha^{\mathbf{T}}\mathbf{H}_t\mathbf{H}_t^+\mathbf{H}_b\mathbf{H}_t^+\mathbf{H}_t\alpha)) \\ &= \mathbf{tr}((\alpha^{\mathbf{T}}\mathbf{H}_t\mathbf{H}_t^+\mathbf{H}_t\alpha)^{-1}(\alpha^{\mathbf{T}}\mathbf{H}_b\mathbf{H}_t^+\mathbf{H}_t\alpha)) \\ &= \mathbf{tr}((\alpha^{\mathbf{T}}\mathbf{H}_t\alpha)^{-1}(\alpha^{\mathbf{T}}\mathbf{H}_b\alpha)) = J(\alpha) \end{aligned} \tag{5.20}$$

and $\mathbf{H}_t\mathbf{H}_t^+\mathbf{H}_t = \mathbf{H}_t$ by Moore-Penrose inverse.

From Eq. (5.18), we have

$$\mathbf{H}_b\mathbf{H}_t^+\mathbf{K} = \mathbf{K}\widetilde{\Lambda}. \tag{5.21}$$

Multiplying both sides of Eq. (5.21) by $\mathbf{H}_t^{+\frac{1}{2}}$, we have

$$\mathbf{H}_t^{+\frac{1}{2}}\mathbf{H}_b\mathbf{H}_t^{+\frac{1}{2}}(\mathbf{H}_t^{+\frac{1}{2}}\mathbf{K}) = (\mathbf{H}_t^{+\frac{1}{2}}\mathbf{K})\overline{\Lambda}. \tag{5.22}$$

We know $\mathbf{H}_t^{+\frac{1}{2}}\mathbf{H}_b\mathbf{H}_t^{+\frac{1}{2}} = (\mathbf{H}_t^{+\frac{1}{2}}\widetilde{\mathbf{M}}_b)(\mathbf{H}_t^{+\frac{1}{2}}\widetilde{\mathbf{M}}_b)^{\mathbf{T}}$ where $\mathbf{H}_t^{+\frac{1}{2}}$ is a symmetric matrix. Thus, $\mathbf{H}_t^{+\frac{1}{2}}\mathbf{K}$ can be obtained by solving singular value decomposition (SVD) of $\mathbf{H}_t^{+\frac{1}{2}}\widetilde{\mathbf{M}}_b \in R^{n\times c}$.

If we express a matrix $\mathbf{A}$ as $\mathbf{A} = \mathbf{U}\mathbf{\Lambda}^{\mathbf{1/2}}\mathbf{V}^{\mathbf{T}}$ via SVD, where $\mathbf{U}$ and $\mathbf{\Lambda}$ are orthonormal column matrices and $\mathbf{\Lambda}^{\mathbf{1/2}}$ is a diagonal matrix with positive or zero elements in decreasing order, then $\mathbf{A}\mathbf{A}^{\mathbf{T}} = \mathbf{U}\mathbf{\Lambda}^{\mathbf{1/2}}\mathbf{V}^{\mathbf{T}}(\mathbf{U}\mathbf{\Lambda}^{\mathbf{1/2}}\mathbf{V}^{\mathbf{T}})^{\mathbf{T}} = \mathbf{U}\mathbf{\Lambda}\mathbf{U}^{\mathbf{T}}$. That is, $\mathbf{U}$ and $\mathbf{\Lambda}$ are the eigenvector and eigenvalue of $\mathbf{A}\mathbf{A}^{\mathbf{T}}$. Therefore, by SVD of $\mathbf{A}$ we can obtain the eigenvector of $\mathbf{A}\mathbf{A}^{\mathbf{T}}$.

Now we can calculate α in Eq. (5.19) because we know $\mathbf{H}_t^{+\frac{1}{2}} = \mathbf{U}\widehat{\Lambda}^{+\frac{1}{2}}\mathbf{U}^{\mathbf{T}}$ and $\mathbf{H}_t^{+\frac{1}{2}}\widetilde{\mathbf{M}}_b$. Though $\mathbf{H}_t^{+\frac{1}{2}}$ requires $n \times n$ matrix calculation, the proposed method can save the running time and the usage of memory to calculate α because $\mathbf{H}_t^{+\frac{1}{2}}\widetilde{\mathbf{M}}_b$ is $n \times c$ matrix calculation ($n >> c$). Given a sample $\mathbf{x} \in R^{l\times 1}$ and its mapped data $\Phi(\mathbf{x})$, the discriminant feature vector y is obtained by the following transformation

$$y = \mathbf{W}^{\mathbf{T}}\Phi(\mathbf{x}) = (\mathbf{Q}\alpha)^{\mathbf{T}}\Phi(\mathbf{x}) = \alpha^{\mathbf{T}}\mathbf{Q}^{\mathbf{T}}\Phi(\mathbf{x}) \tag{5.23}$$

$$= \quad \alpha^{\mathbf{T}}[k(\mathbf{x}_1, \mathbf{x}), \cdots, k(\mathbf{x}_n, \mathbf{x})]^{\mathbf{T}} \in R^{(c-1)\times 1}.$$

For a test sample $\mathbf{x}$, the predicted class is

$$\mathcal{C}(\mathbf{x}) = \text{argmin}_k \sum_{i=1}^{c-1} (\mathbf{W}_i^{\mathbf{T}}(\Phi(\mathbf{x}) - \mathbf{m}_k^{\Phi}))^2. \tag{5.24}$$

After mapping the mean vector of each class in the feature space and $\Phi(\mathbf{x})$ into the discriminant space, a class with the smallest distance between the mapped mean vector and the mapped $\Phi(\mathbf{x})$ in the discriminant space is chosen.

5.4 Experiments

5.4.1 The Dataset

The raw mass spectral data for Alzheimer's disease was downloaded from http://www.perkinelmer.com/biomarkerdata. The dataset consists of 276 samples, mild cognitive impairment (MCI:32), Alzheimer disease (AD:58) and normal (186), each processed in triplicate. In this study, one out of 3 separate sets was selected at random.

5.4.2 Classification Algorithms

FKDA was implemented in MATLAB 6.5. The performance of our method was compared with other algorithms, LDA, SVM, Random Forest, J48 and kNN with $k = 1$. In each classification algorithm, 10 cross validation (CV) was applied. That is, samples of each class are partitioned randomly into 10 folds consisting of 9 folds for training and one fold for testing. During 10-CV, all folds are used for testing. The 10-CV was repeated 30 times and the resulting measurements were averaged.

Table 5.1. The mean and standard deviation (in parenthesis) of accuracies in Alzheimer disease dataset. The dimensionality after mapping in FKDA and GLDA is $c-1$ regardless of the number of features used.

Methods / No. of features	FKDA (Gaussian)	FKDA (Polynomial)	GLDA	k NN (k=1)	RF	J48	SVM
500	82.07(0.92)	80.47(0.69)	74.84(1.89)	66.16(0.95)	73.80(2.18)	65.07(1.78)	75.07(1.29)
1000	86.01(0.74)	82.86(0.78)	82.30(0.54)	66.63(0.73)	73.22(1.14)	62.25(2.35)	75.14(0.86)
1500	86.83(0.70)	84.64(0.49)	84.73(0.68)	68.48(0.64)	72.83(1.70)	61.70(1.96)	73.01(1.03)
2000	87.07(0.50)	84.31(0.48)	84.89(0.62)	67.21(0.75)	72.72(0.71)	61.34(2.35)	73.15(1.10)
2500	85.74(0.63)	84.31(0.30)	85.18(0.57)	68.19(1.10)	71.96(1.52)	61.30(1.36)	72.61(0.95)
3000	85.83(0.64)	83.41(0.56)	84.35(0.64)	65.76(0.97)	71.63(1.38)	60.14(2.16)	75.22(0.86)
3500	85.80(0.57)	83.19(0.60)	84.00(0.71)	65.22(1.29)	71.63(1.82)	59.71(2.75)	73.66(0.65)
4000	84.69(0.52)	82.93(0.36)	83.66(0.48)	65.04(1.19)	70.14(1.72)	61.81(2.14)	71.96(1.27)
4500	84.29(0.44)	82.64(0.65)	83.22(0.53)	66.74(1.04)	71.20(1.65)	61.34(1.74)	72.79(0.75)
5000	83.35(0.68)	81.85(1.00)	82.64(0.55)	66.52(0.82)	69.38(1.65)	60.51(2.79)	70.00(0.96)

5.4.3 Feature Reduction

To reduce computational burden caused by using peaks in all the bins, we ranked peaks by a feature ranking method based on the ratio of between-group to within-group sums of squares and select the tractable size of features in our algorithm. By BW ratio, some of them were used in the experiments. The feature ranking method was proposed by Dudoit *et al.* for feature selection for multi-class problems [49]. For a peak j, the ratio is

$$\mathbf{BW}(j) = \frac{\sum_i \sum_k I(y_i = k)(\overline{x}_{kj} - \overline{x}_{.j})^2}{\sum_i \sum_k I(y_i = k)(\overline{x}_{ij} - \overline{x}_{kj})^2} \tag{5.25}$$

where $I(\cdot)$ is the indicator function. $\overline{x}_{.j}$ and $\overline{x}_{kj}$ denote the average intensity of peak j across all samples and across samples belong to class k. As the ratio for a peak is large, the peak is more likely relevant to class separation.

5.4.4 Experimental Results

Based on BW ratio, we extracted the top 500, 1000, and so forth up to the top 5000 peaks in all spectra. Note that no matter what the number of peaks is, the

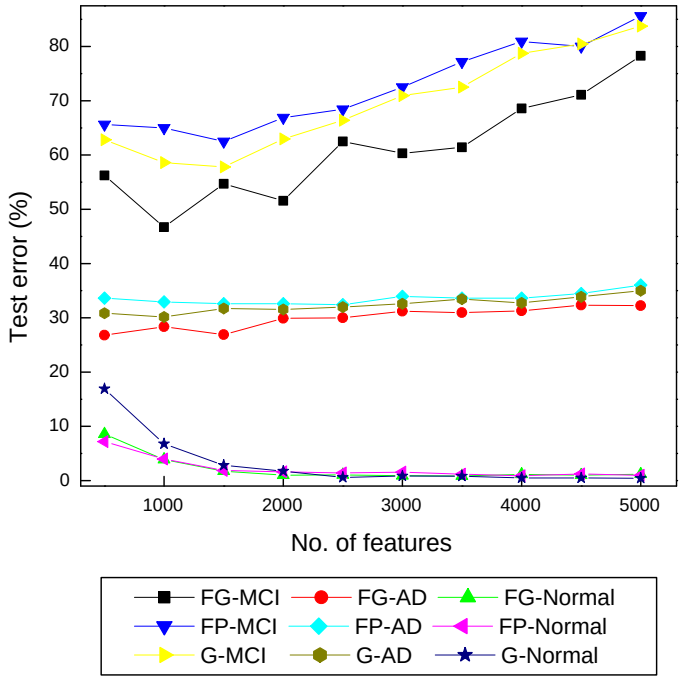

Figure 5.2. Error rates in test samples of each class. In labels, prefix FG, FP and G indicate FKDA with Gaussian kernel, FKDA with the second-order polynomial kernel and GLDA, respectively.

dimensionality after dimension reduction in FKDA and GLDA is $c-1$. With each selected feature subset, all classification algorithms mentioned in section 5.4.2 were carried out. For FKDA, two popular kernels were employed. One is Gaussian kernel $k(\mathbf{x},\mathbf{y}) = \exp(-||\mathbf{x}-\mathbf{y}||^2/\delta)$ and the other is the second-order polynomial kernel $k(\mathbf{x},\mathbf{y}) = (\mathbf{x}\cdot\mathbf{y}+1)^2$. Table 5.1 shows the averaged accuracies for all algorithms. As can be seen from the table, when the Gaussian kernel in FKDA was used, the best performance was achieved for all feature subsets. However, GLDA was superior to the polynomial kernel in FKDA. It should be noted that discriminant analysis methods (KFDA and GLDA) obtained the better performance compared to others.

Table 5.1 demonstrates overall accuracies for all the test sets. However, we are also interested in the accuracy for test samples of each class. In all classification methods, the accuracy rate to correctly classify MCI samples is low and the accuracy

rate for normal samples is high. It can be attributed to the fact that the distribution of samples used in this study is rather imbalanced. For example, the number of normal samples (186) is about 6 times as larger as MCI (32). In such a case, traditional classification algorithms are biased to the majority classes. According to the experimental results in this study, FKDA and GLDA are relatively strong in the situation (not shown in this paper). Fig. 5.2 illustrates the error rate for FKDA and GLDA in test samples of each class. FKDA with Gaussian kernel has the smallest error rate. We observed that when the number of features increases, the error rate in MCI also increases while the error rate in normal decreases. It is implied that if all features are used, the accuracy in MCI will dramatically get worse (not shown in this paper).

We compared the elapsed time to calculate α from FKDA and from the eigen-decomposition of $\mathbf{H}_t^+\mathbf{H}_b$ in Eq. (5.15). For test, values were generated uniformly between 0 and 1. Fig. 5.3 depicts the average running time after 10 runs to obtain α value when with 1000 fixed features the number of samples increases from 50 to 1000 by 50. As the number of samples increases, the elapsed time gap between two graphs grows larger. Since in our study the calculation of α is performed many times, after entire experiments the difference in the total accumulating running time will be considerably increased.

5.5 Conclusion

We proposed a fast kernel discriminant analysis technique, FKDA which was designed to aim to overcome some limitations of classical LDA: singularity and linearity. In experiments with mass spectral data for Alzheimer's disease, FKDA with Gaussian kernel outperformed other classification algorithms. Also, FKDA is faster in the calculation of the optimal discriminant vectors and strong in the imbalanced

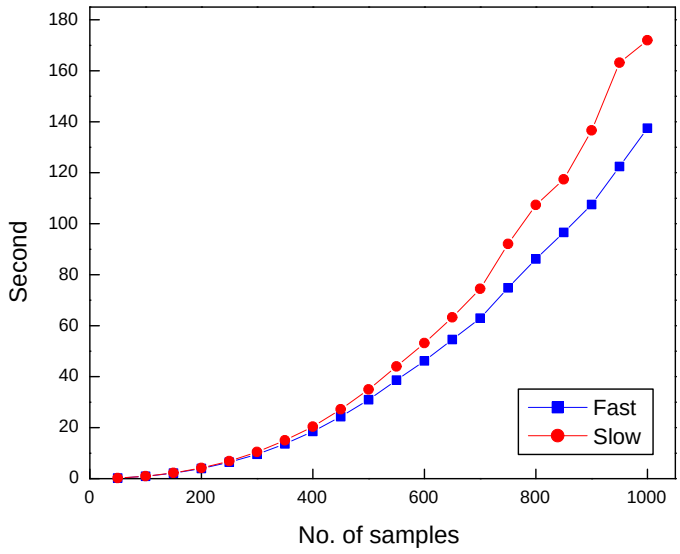

Figure 5.3. Averaged elapsed time in a run to calculate α. The label 'Fast' indicates our FKDA method and 'Slow' represents the method through the eigen-decomposition of $\mathbf{H}_t^+\mathbf{H}_b$ in Eq. (5.15).

dataset. Since diseases progress in multistage, the accurate diagnosis of the current stage is very important for treatment. It requires the fast and precise multi-class classification algorithm. FKDA can be applicable to such multi-class classification problems with nonlinearly structured data.

REFERENCES

[1] M. Anderle, S. Roy, H. Lin, C. Becker, and K. Joho, "Quantifying reproducibility for differential proteomics: noise analysis for protein liquid chromatography-mass spectrometry of human serum," *Bioinformatics*, vol. 20, pp. 3575–3582, 2004.

[2] J. Li, Z. Zhang, J. Rosenzweig, Y. Wang, and D. Chan, "Proteomics and bioinformatics approaches for identification of serum biomarkers to detect breast cancer," *Clin. Chem.*, vol. 48, pp. 1296–1304, 2002.

[3] K. Rosenblatt, P. Bryant-Greenwood, J. Killian, A. Mehta, D. Geho, V. Espina, E. Petricoin, and L. Liotta, "Serum proteomics in cancer diagnosis and management," *Annu. Rev. Med.*, vol. 55, pp. 97–112, 2004.

[4] P. Srinivas, S. Srivastava, S. Hanash, and G. Wright, "Proteomics in early detection of cancer," *Clin. Chem.*, vol. 47, pp. 1901–1911, 2001.

[5] J. Wulfkuhle, L. Liotta, and E. Petricoin, "Proteomic applications for the early detection of cancer," *Nat. Rev. Cancer*, vol. 3, pp. 267–275, 2003.

[6] E. Petricoin, A. Ardekani, B. Hitt, P. Levine, V. Fusaro, S. Steinberg, G. Mills, C. Simone, D. Fishman, E. Kohn, and L. Liotta, "Use of proteomic patterns in serum to identify ovarian cancer," *Lancet*, vol. 359, pp. 572–577, 2002.

[7] Y. Qu, B. Adam, Y. Yasui, M. Ward, L. Cazares, P. Schellhammer, Z. Feng, O. Semmes, and G. Wright, "Boosted decision tree analysis of surface-enhanced laser desorption/ionization mass spectral serum profiles discriminates prostate cancer from noncancer patients," *Clin. Chem.*, vol. 48, pp. 1835–1843, 2002.

[8] R. Lilien, H. Farid, and B. Donald, "Probabilistic disease classification of expression-dependent proteomic data from mass spectrometry of human serum," *J. Comput. Biol.*, vol. 10, pp. 925–946, 2003.

[9] M. Hilario, A. Kalousis, M. Muller, and C. Pellegrini, "Machine learning approaches to lung cancer prediction from mass-spectra," *Proteomics*, vol. 3, pp. 1716–1719, 2003.

[10] M. Lopez, A. Mikulskis, S. Kuzdzal, and *et al.*, "High-resolution serum proteomic profiling of alzheimer disease samples reveals disease-specific, carrier-protein-bound mass signatures," *Clin. Chem.*, vol. 51, no. 10, pp. 1946–1954, 2005.

[11] A. Metha, S. Ross, M. Lowenthal, and *et al.*, "Biomarker amplification by serum carrier protein binding," *Dis. Markers*, vol. 19, pp. 1–10, 2003.

[12] L. Li, D. Umbach, P. Terry, and J. Taylor, "Application of the ga/knn method to seldi proteomics data," *Bioinformatics*, vol. 20, pp. 1638–1640, 2004.

[13] B. Adam, Y. Qu, J. Davis, M. Ward, M. Clements, L. Cazares, O. Semmes, P. Schellhammer, Y. Yasui, Z. Feng, and G. Wright, "Serum protein fingerprinting coupled with a pattern-matching algorithm distinguishes prostate cancer from benign prostate hyperplasia and healthy men," *Cancer Res.*, vol. 62, pp. 3609–3614, 2002.

[14] A. Vlahou, J. Schorge, B. Gregory, and R. Coleman, "Diagnosis of ovarian cancer using decision tree classification of mass spectral data," *J. Biomed. Biotechnol.*, vol. 5, pp. 308–314, 2003.

[15] G. Ball, S. Mian, F. Holding, R. Allibone, J. Lowe, S. Ali, G. Li, S. McCardle, I. Ellis, C. Creaser, and R. Rees, "An integrated approach utilizing artificial neural networks and seldi mass spectrometry for the classification of human tu-

mours and rapid identification of potential biomarkers," *Bioinformatics*, vol. 18, pp. 395–404, 2002.

[16] H. Ressom, R. Varghese, M. Abdel-Hamid, S. Eissa, D. Saha, L. Goldman, E. Petricoin, T. Conrads, T. Veenstra, C. Loffredo, and R. Goldman, "Analysis of mass spectral serum profiles for biomarker selection," *Bioinformatics*, vol. 21, pp. 4039–4045, 2005.

[17] B. Wu, T. Abbott, D. Fishman, W. McMurray, G. Mor, K. Stone, D. Ward, K. Williams, and H. Zhao, "Comparison of statistical methods for classification of ovarian cancer using mass spectrometry data," *Bioinformatics*, vol. 19, pp. 1636–1643, 2003.

[18] R. Bast, "Status of tumor markers in ovarian cancer screening," *J. Clin.Oncol.*, vol. 21, pp. 200–205, 2003.

[19] L. Knowles, A. Nandi, P. Gurnani, D. Miller, S. Mok, K. Rosenblatt, and J. Schorge, "Serum proteomic profiling to predict early relapse in ovarian cancer," *Gynecol. Oncol.*, vol. 96, p. 926, 2005.

[20] M. Parmar, J. Ledermann, N. Colombo, and *et al.*, "Paclitaxel plus platinum-based chemotherapy versus conventional platinum-based chemotherapy in women with relapsed ovarian cancer: the icon4/ago-ovar-2.2 trial," *Lancet*, vol. 361, pp. 2099–2106, 2003.

[21] M. Bern, D. Goldberg, W. McDonald, and J. Yates, "Automatic quality assessment of peptide tandem mass spectra," *Bioinformatics*, vol. 20, pp. i49–i54, 2004.

[22] J. Pearl, *Probabilistic Reasoning in Intelligent Systems: Networks of Plausible Inference*. San Mateo, CA: Morgan Kaufmann, 1988.

[23] D. Koller and M. Sahami, "Toward optimal feature selection," in *Proc. of 13th Int. Conference on Machine Learning*. Morgan Kaufmann, 1996, pp. 284–292.

[24] E. Xing and R. Karp, "Cliff: clustering of high-dimensional microarray data via iterative feature filtering using normalized cuts," *Bioinformatics*, vol. 17, pp. S306–S315, 2001.

[25] U. Fayyad and K. Irani, "Multi-interval discretization of continuous-valued attributes for classification learning," in *Proc. of 13th Int. Joint Conference on AI*, 1993, pp. 1022–1029.

[26] T. Knijnenburg, M. Reinders, and L. Wessels, "Artifacts of markov blanket filtering based on discretized features in small sample size applications," *Pattern Recognition Letters*, vol. 27, no. 7, pp. 709–714, 2006.

[27] C. Burges, "A tutorial on support vector machines for pattern recognition," *Data Mining and Knowledge Discovery*, vol. 2, pp. 121–167, 1998.

[28] I. Guyon, J. Weston, S. Barnhill, and V. Vapnik, "Gene selection for cancer classification using support vector machines," *Machine Learning*, vol. 46, pp. 389–422, 2002.

[29] C. Chang and C. Lin, *LIBSVM: A Library for Support Vector Machines*, 2001, software available at http://www.csie.ntu.edu.tw/~cjlin/libsvm. [Online]. Available: http://www.csie.ntu.edu.tw/ cjlin/libsvm

[30] I. Witten and E. Frank, *Data Mining: Practical Machine Learning Tools and Techniques*, 2nd ed. San Francisco: Morgan Kaufmann, 2005.

[31] Y. Yasui, D. McLerran, B. Adam, M. Winget, M. Thornquist, and Z. Feng, "An automated peak identification/calibration procedure for high-dimensional protein measures from mass spectrometers," *J. Biomed. Biotechnol*, vol. 4, pp. 242–248, 2003.

[32] W. Zhu, X. Wang, Y. Ma, M. Rao, J. Glimm, and J. Kovach, "Detection of cancer-specific markers amid mas-. sive mass spectral data," *Proc. Nat. Acad. Sci.*, vol. 100, pp. 14 666–14 671, 2003.

[33] J. Sorace and M. Zhan, "A data review and re-assessment of ovarian cancer serum proteomic profiling," *BMC Bioinformatics*, vol. 4, p. 24, 2003.

[34] J. Yu, S. Ongarello, R. Fiedler, X. Chen, G. Toffolo, C. Cobelli, and Z. Trajanoski, "Ovarian cancer identification based on dimensionality reduction for high-throughput mass spectrometry data," *Bioinformatics*, vol. 21, pp. 2200–2209, 2005.

[35] J. Yu and X. Chen, "Bayesian neural network approaches to ovarian cnancer identification from high-resolution mass spectrometry data," *Bioinformatics*, vol. 21, pp. i487–i494, 2005.

[36] H. Ressom, R. Varghese, S. Drake, G. Hortin, M. Abdel-Hamid, C. Loffredo, and R. Goldman, "Peak selection from maldi-tof mass spectra using ant colony optimization," *Bioinformatics*, vol. 23, no. 5, pp. 619–626, 2007.

[37] C. Hsu and C. Lin, "A comparison of methods for multi-class support vector machines," *IEEE Trans. Neural Networks*, vol. 13, pp. 415–425, 2002.

[38] B. Fei and J. Liu, "Binary tree of svm: a new fast multiclass training and classification algorithm," *IEEE Trans. Neural Networks*, vol. 17, pp. 696–704, 2006.

[39] E. Ie, J. Weston, W. Noble, and C. Leslie, "Multi-class protein fold recognition using adaptive codes," in *Proc. International Conference on Machine Learning*, 2005, pp. 329–336.

[40] E. Allwein, R. Schapire, and Y. Singer, "Reducing multiclass to binary: a unifying approach for margin classifiers," *Journal of Machine Learning Research*, vol. 1, pp. 113–141, 2002.

[41] T. Dietterich and G. Bakiri, "Solving multiclass learning problems via error-correcting output codes," *Journal of Artificial Intelligence Research*, vol. 2, pp. 263–286, 1995.

[42] K. Crammer and Y. Singer, "On the learnability and design of output codes for multiclass problems," *Machine Learning*, vol. 47, pp. 201–233, 2002.

[43] O. Pujol, P. Radeva, and J. Vitria, "Discriminant ecoc: a heuristic method for application dependent design of error correcting output codes," *IEEE Trans. pattern analysis and machine intelligence*, vol. 28, pp. 1007–1012, 2006.

[44] R. Smith and T. Windeatt, "Decoding rules for error correcting output code ensembles," in *Proc. Internaltional Workshop on Multiple Classifer Systems*, 2005, pp. 53–63.

[45] A. Passerini, M. Pontil, and P. Frasconi, "New results on error correcting output codes of kernel machines," *IEEE Trans. Neural Networks*, vol. 15, pp. 45–54, 2004.

[46] L. Kuncheva and C. Whitaker, "Measures of diversity in classifier ensembles," *Mach. Learn.*, vol. 51, pp. 181–207, 2003.

[47] V. Guruswami and A. Sahai, "Multiclass learning, boosting, and error-correcting codes," in *Proc. Workshop on Computational Learning Theory*, 1999, pp. 145–155.

[48] R. Schapire, "Using output codes to boost multiclass learning problems," in *Proc. 14th Intl. Conf. on Machine Learning*, 1997, pp. 313–321.

[49] S. Dudoit, J. Fridlyand, and T. Speed, "Comparison of discriminant methods for the classification of tumors using gene expression data," *J. Am. Stat. Assoc*, vol. 97, pp. 77–87, 2002.

[50] T. Wu, C. Lin, and R. Weng, "Probability estimates for multi-class classification by pairwise coupling," *Journal of Machine Learning Research*, vol. 5, pp. 975–1005, 2004.

[51] D. Price, S. Knerr, L. Personnaz, and G. Dreyfus, "Pairwise nerual network classifiers with probabilistic outputs," *Neural Information Processing Systems*, vol. 7, pp. 1109–1116, 1995.

[52] J. Platt, *Advances in Large Margin Classifiers.* MIT Press, 1999, ch. Probabilistic outputs for SVMs and comparisons to regularized likelihood methods.

[53] V. Danick, T. Addona, K. Clauser, J. Vath, and P. Pevzner, "De novo peptide sequencing via tandem mass spectrometry," *J. Comput. Biol.*, vol. 6, pp. 327–342, 1999.

[54] B. Lu and T. Chen, "A suboptimal algorithm for de novo peptide sequencing via tandem mass spectrometry," *J. Comput. Biol.*, vol. 10, pp. 1–12, 2003.

[55] B. Ma, K. Zhang, C. Hendrie, C. Liang, M. Li, A. Doherty-Kirby, and G. Lajoie, "Peaks: powerful software for peptide de novo sequencing by ms/ms," *Rapid Communications in Mass Spectrometry*, vol. 17, pp. 2337–2342, 2003.

[56] N. Zhang, R. Aebersold, and B. Schwikowski, "Probid: A probabilistic algorithm to identify peptides through sequence database searching using tandem mass spectral data," *Proteomics*, vol. 2, pp. 1406–1412, 2002.

[57] B. Ma, K. Zhang, and C. Liang, "An effective algorithm for the peptide de novo sequencing from ms/ms spectrum," in *CPM03*, 2003, pp. 266–278.

[58] Y. Fu, Q. Yang, R. Sun, D. Li, R. Zeng, C. Ling, and W. Gao, "Exploiting the kernel trick to correlate fragment ions for peptide identification via tandem mass spectrometry," *Bioinformatics*, vol. 20, pp. 1948–1954, 2004.

[59] V. Bafna and N. Edwards, "Scope: a probabilistic model for scoring tandem mass spectra against a peptide database," *Bioinformatics*, vol. 17, pp. S13–S21, 2001.

[60] J. Eng, A. McCormack, and J. Yates, "An approach to correlate tandem mass spectral data of peptides with amino acid sequences in a protein database," *J. Am. Soc. Mass Spectrom*, vol. 5, pp. 976–989, 1994.

[61] B. Lu and T. Chen, "A suffix tree approach to the interpretation of tandem mass spectra: applications to peptides of non-specific digestion and post-translational modifications," *Bioinformatics*, vol. 19, pp. ii113–ii121, 2003.

[62] J. Taylor and R. Johnson, "Sequence database searches via de novo peptide sequencing by tandem mass spectrometr," *Rapid Communications in Mass Spectrometry*, vol. 11, pp. 1067–1075, 1997.

[63] B. Clauser, P. Baker, and A. Burlingame, "Role of accurate mass measurement (+/- 10ppm) in protein identification strategies employing ms or ms/ms," *Analytical Chem.*, vol. 71, pp. 2871–2882, 1999.

[64] D. Perkins, D. Pappin, D. Creagy, and J. Cottrell, "Probability-based protein indentification by searching sequence databases using mass spectrometry data," *Electrophoresis*, vol. 20, pp. 3551–3567, 1999.

[65] J. Taylor and R. Johnson, "Implementation and uses of automated de novo peptide sequencing by tandem mass spectrometry," *Anal. Chem.*, vol. 73, pp. 2594–2604, 2001.

[66] B. Yan, C. Pan, V. Olman, R. Hettich, and Y. Xu, "A graph-theoretic approach to separation of b and y ions in tandem mass spectra," *Bioinformatics*, vol. 21, pp. 563–574, 2005.

[67] K. Jarman, W. Cannon, K. Jarman, and A. Heredia-Langner, "A model of random sequences for de novo peptide sequencing," in *Proceedings of IEEE Symposium on Bioinformatics and Bioengineering*, 2003, pp. 206–213.

[68] A. Frank and P. Pevzner, "Pepnovo: De novo peptide sequencing via probabilistic network modeling," *Analytical Chemistry*, vol. 77, pp. 964–973, 2005.

[69] E. Petricoin and L. Liotta, "Seldi-tof-based serum proteomic pattern diagnostics for early detection of cancer," *Current Opinion in Biotechnology*, vol. 15, pp. 24–30, 2004.

[70] C. Tan, A. Ploner, A. Quandt, J. Lehtio, and Y. Pawitan, "Finding regions of significance in seldi measurements for identifying protein biomarkers," *Bioinformatics*, vol. 22, pp. 1515–1523, 2006.

[71] S. Pan, J. Rush, E. Peskind, D. Galasko, K. Chung, J. Quinn, J. Jankovic, J. Leverenz, C. Zabetian, C. Pan, Y. Wang, J. Oh, J. Gao, J. Zhang, T. Montine, and J. Zhang, "Application of targeted quantitative proteomics analysis in human cerebrospinal fluid using an lc maldi tof/tof platform," *J. Proteome Res.*, vol. 7, pp. 720–730, 2008.

[72] X. Zhang and Y. Jia, "A linear discriminant analysis framework based on random subspace for face recognition," *Pattern Recognition*, vol. 40, pp. 2585–2591, 2007.

[73] Y. Guo, S. Li, J. Yang, T. Shu, and L. Wu, "A generalized foley-sammon transform based on generalized fisher discriminant criterion and its application to face recognition," *Pattern Recognition Letters*, vol. 24, pp. 147–158, 2003.

[74] J. Ye, T. Li, T. Xiong, and R. Janardan, "Using uncorrelated discriminant analysis for tissue classification with gene expression data," *IEEE/ACM Trans. Comput. Biology Bioinform.*, vol. 1, pp. 181–190, 2004.

[75] P. Howland, M. Jeon, and H. Park, "Structure preserving dimension reduction for clustered text data based on the generalized singular value decomposition," *SIAM. J. Matrix Anal. Appl.*, vol. 25, pp. 165–179, 2003.

[76] P. Howland and H. Park, "Generalizing discriminant analysis using the generalized singular value decomposition," *IEEE Trans. Pattern Analysis and Machine Intelligence*, vol. 26, pp. 995–1006, 2004.

[77] H. Li, K. Zhang, and T. Jiang, "Robust and accurate cancer classification with gene expression profiling," in *Proceedings of IEEE Computational Systems Bioinformatics Conference*, 2005, pp. 310–321.

[78] Z. Liang and P. Shi, "An efficient and effective method to solve kernel fisher discriminant analysis," *Neurocomputing*, vol. 61, pp. 485–493, 2004.

[79] G. Baudat and F. Anouar, "Generalized discriminant analysis using a kernel approach," *Neural computation*, vol. 12, pp. 2385–2404, 2000.

[80] S. Mika, G. Ratsch, J. Weston, B. Scholkopf, and K. Muller, "Fisher discriminant analysis with kernels," in *Proceedings of IEEE Neural Netwo. Processing Workshop*, 1999, pp. 41–48.

BIOGRAPHICAL STATEMENT

Jung Hun Oh received his BS and MS degrees in Computer Science from Soongsil University, South Korea, in 1995 and 1997, respectively, and the PhD degree in Department of Computer Science and Engineering at the University of Texas at Arlington in 2008. His research interests include bioinformatics, machine learning, and data mining. His recent work has focused on biomarker selection, multi-class classification, and quantitative proteomics.